c.1

RAINFALL ESTIMATION FROM SATELLITE IMAGES

by

DIANE VERNA INGRAHAM

B.Sc. (Physics), Dalhousie University, Halifax, 1974

S.M. (Civil Engineering - Water Resources), Massachusetts Institute of Technology, Cambridge, U.S.A. 1976

A THESIS SUBMITTED IN PARTIAL FULFILMENT
OF THE REQUIREMENTS FOR THE DEGREE OF

DOCTOR OF PHILOSOPHY

in

THE FACULTY OF GRADUATE STUDIES
DEPARTMENT OF CIVIL ENGINEERING

We accept this thesis as conforming to
the required standard

THE UNIVERSITY OF BRITISH COLUMBIA

October 1980

© Diane Verna Ingraham, 1980

In presenting this thesis in partial fulfilment of the requirements for an advanced degree at the University of British Columbia, I agree that the Library shall make it freely available for reference and study. I further agree that permission for extensive copying of this thesis for scholarly purposes may be granted by the Head of my Department or by his representatives. It is understood that copying or publication of this thesis for financial gain shall not be allowed without my written permission.

Department of Civil Engineering
The University of British Columbia
2075 Wesbrook Place
Vancouver, Canada
V6T 1W5

Date October 17, 1980

RAINFALL ESTIMATION FROM SATELLITE IMAGES

ABSTRACT

The design, management and operation (as well as the associated costs) of major water resource projects are directly related to the assessment of the anticipated volumes of runoff to be handled by the project. In remote or sparsely gauged regions it is often very difficult to determine these volumes due to a lack of data. The meteorological satellites, and in particular, the Geostationary Operational Environmental Satellites (GOES) can provide good areal coverage of the Earth and its weather systems potentially every half hour day and night.

Since the first meteorological satellite images were transmitted, many attempts have been made to estimate rainfall using the images to identify specific cloud characteristics and correlating these with expected rainfall. However, these methods have been limited to convective rainfall in the tropics or near tropics.

A method is presented here for estimating half-hourly rainfall which relates the vertical updraft velocities and hence, the moisture flux into the cloud, to the rate of vertical and horizontal growth of the cloud top as revealed in the GOES infrared images. The method performs well in estimating

rainfall from widespread frontal systems common over British Columbia.

A number of computational difficulties which arose during the research were resolved. One was to ascertain cloud top temperature contours for those GOES infrared images which were not enhanced. This involved the use of a video camera-special effects generator-video monitor system. The second was one of bookkeeping to "keep track of" the individual cloud cells. This was taken care of through the use of computer routines which directed the input and output of data, accounted for the growth and movement of the storm cells over the region and interpolated for rainfall at those locations which fell between adjacent precipitation contours.

The method was used to estimate rainfall for a number of test storms occurring over British Columbia. The results were remarkably successful although there were some local inadequacies. An updating procedure was developed in which the satellite estimated values of rainfall were improved by taking into consideration the information provided by concurrent rainfall observations. Furthermore, the parameters of the updating model (determined for gauged locations) can be used to update rainfall estimates for ungauged locations.

In the light of present raingauge installation and operating costs and the limitations of radar in mountainous areas, the satellite rainfall estimation procedure provides an economical operational supplement to existing conventional precipitation data collection.

TABLE OF CONTENTS

ABSTRACT ii

TABLE OF CONTENTS v

LIST OF TABLES ix

LIST OF FIGURES xi

NOTATIONS USED xvi

ACKNOWLEDGEMENTS xix

CHAPTER

I INTRODUCTION . . . . . 1.

1.1 Study Objectives . . . . . 3.

1.2 Outline of the Following Chapters . . . . . 5.

II METEOROLOGICAL SATELLITES: BACKGROUND . . . . . 7.

2.1 Some Satellite Systems and Sensors . . . . . 7.

2.2 The GOES System . . . . . 13.

2.3 GOES Image Formation and Enhancement Schemes . 16.

2.4 Other Sources of Satellite Information . . . . 26.

III A REVIEW OF SATELLITE IMAGE PRECIPITATION ESTIMATION 28.

3.1 GOES Rainfall Estimation Techniques . . . . . 30.

3.1.1 The NHEML Technique . . . . . 30.

3.1.2 The UW Technique . . . . . 31.

3.1.3 The Scofield/Oliver Technique . . . . . 32.

3.2 Summary . . . . . 37.

IV THE MODEL USED TO DESCRIBE PRECIPITATING CLOUDS . . . . 39.

4.1 Precipitation in British Columbia . . . . . 39.

4.2 The Model . . . . . 41.

4.2.1 Rain-Producing Conditions . . . . . 42.

4.3 The Model Equations . . . . . 45.

4.3.1 The Atmospheric Thermodynamic Equations . . . 46.

4.3.2 The Momentum Equations . . . . . 47.

4.3.3 The Continuity Equation . . . . . 48.

4.4 The Continuity Equation Used to Estimate Rainfall . 48.

4.4.1 Estimating the Vertical Velocity w . . . . . 50.

4.4.2 Rewriting the Continuity Equation . . . . . 53.

4.5 Adaptations for Use with Satellite Images . . . . . 54.

4.5.1 Relation Between Average Divergence and Coldest Contour Divergence . . . . . 55.

4.5.2 One Proposed Divergence Function . . . . . 56.

4.5.3 The Rainfall Estimation Equations . . . . . 59.

4.6 Consequences of the Model . . . . . 60.

4.7 The Other Model Parameters . . . . . 61.

4.7.1 The Water Content wc . . . . . 61.

4.7.2 The Lapse Rate γ . . . . . 65.

4.7.3 Adjustment Factor e . . . . . 65.

4.8 Summary . . . . . 66.

V COMPUTATIONAL PROCEDURE FOR ESTIMATING RAINFALL FROM SATELLITE IMAGES . . . . . 68.

5.1 Conceptual Procedure . . . . . 68.

5.1.1 Movement of Storm Cells Near A Station . . 77.

5.2 Computer Routine Sequence . . . . . 82.

VI ESTIMATES OF PRECIPITATION USING SATELLITE IMAGES . . 86.

6.1 Test Storms . . . . . 86.

6.2 The October 31, 1978 Rainfall Estimates . . . . . 89.

6.2.1 Storm Description . . . . . 89.

6.2.2 Results . . . . . 92.

6.2.3 Comparison of Streamflow and Rainfall Volumes . . . . . 93.

6.3 The December 17, 1979 Rainfall Estimates . . . . 98.

6.3.1 Storm Description . . . . . 98.

6.3.2 Results . . . . . 101.

6.3.2a Point Estimates . . . . . 101.

6.3.2b Areal Rainfall Distribution . . . . 109.

6.4 The June 4, 1977 Rainfall Estimates . . . . . 114.

6.4.1 Storm Description . . . . . 114.

6.4.2 Results . . . . . 114.

6.5 The November 20, 1979 Rainfall Estimates . . . . 117.

6.5.1 Storm Description . . . . . 117.

6.5.2 Results . . . . . 120.

6.6 The December 5, 1979 Rainfall Estimates . . . . . 123.
6.6.1 Storm Description . . . . . 123.
6.6.2 Results . . . . . 123.
6.7 Comparison of Observed and Estimated Precipitation for All Storms . . . . . 128.

VII AN UPDATING PROCEDURE USING OBSERVED DATA . . . . . 130.
7.1 The Updating Model . . . . . 130.
7.2 Comparison of Updated and Observed Rainfall . . . 133.
7.2.1 The Updated October 31, 1978 Rainfall Estimates . . . . . 135.
7.2.2 The Updated December 17, 1979 Rainfall Estimates . . . . . 139.
7.3 Limitations on Transferring a and b . . . . . 141.
7.4 Summary . . . . . 145.

VIII SUMMARY AND CONCLUSIONS . . . . . 146.
8.1 Future Directions . . . . . 148.

BIBLIOGRAPHY . . . . . 151.

APPENDIX A . . . . . 159.
APPENDIX B . . . . . 161.

LIST OF TABLES

Table No.	Title	Page
2.1	Scales of Atmospheric Motions (from Holton 1972 and Knox, 1978)	8.
2.2	Major Atmospheric Windows Available for Spacecraft Remote Sensing (after Lintz and Simonett, 1976)	9.
2.3	Some Present and Proposed Satellites, their Sensors, and Characteristics. Additional information is available from WMO (1976), NESS (1976), Kodaira and Murayama (1976), *NOAA* (1979), *Spaceflight* (1980), and Davis (1980).	11.
4.1	Average Efficiencies and Water Content	62.
4.2	Portion of Typical Output of TIROS-N (TUXN) Precipitable Water (PCW) and other Data for Various Levels in the Atmosphere (Received by the Pacific Weather Centre from the Satellite Data Services Division, NESS, Washington, D.C.).	64.
6.1	Comparison of Observed and Estimated Storm Totals for the Period 0045 GMT on October 31, 1980 to 2245 GMT on November 1, 1978.	94.
6.2	Comparison of Rainfall and Runoff Volumes in $m^3 x 10^6$.	99.
6.3	Comparison of Observed and Estimated Rainfall Totals for the 6-hour Segment 0000 GMT to 0600 GMT on December 17, 1979. Vancouver International Airport data was used to calibrate the adjustment parameter e.	105.
6.4	Comparison of Observed and Estimated Rainfall Totals for the 6-hour Segment 0000 GMT to 0600 GMT on December 17, 1979. For each station the empirical adjustment factor e has been determined from the observed data for that station.	107.
6.5	Comparison of Observed and Estimated Rainfall Totals for the storm of June 4, 1977.	118.
6.6	Comparison of Observed and Estimated Rainfall Totals for the Storm of November 20, 1979.	122.
6.7	Comparison of Observed and Estimated Rainfall Totals for the Storm of December 5, 1979.	126.

7.1 Variation of a and b for Terrace Airport and Gospel Point as Each New Pair of Observed and Estimated Rainfalls are Added Sequentially to the Updating Procedure. 138.

7.2 Comparison of a and b for Vancouver International Airport and Victoria International Airport for the Storm of December 17, 1979. 142.

LIST OF FIGURES

Figure No.	Caption	Page
1.1	Distribution of Stations in British Columbia Observing Rainfall on an Hourly Basis. The Projection is the same as on the Satellite Images. (Lambert Conformal Conic, Farley 1980).	2.
2.1	Five Geostationary Meteorological Satellites Provide Global Coverage of the Weather (after Corbell *et al.*, 1977 and *NOAA*, 1979).	14.
2.2	Assembly of a VISSR Image. Each Scan Line is composed of 8 Visible Sensor Lines V_i and 1 Infrared Sensor Line. One Scan Line Represents a West to East Scan of the Earth and Each is Positioned Sequentially in a North-South Manner (Adapted from McKowan 1977).	17.
2.3	Distribution of the GOES signal	19.
2.4	Sectors Received at the Pacific Weather Centre (after Corbell *et al.*, 1977).	20.
	Visible and Infrared Sectors	
	Sector / Centre Point (lat/long) / Resolution (km)	
	SA-1 / 36°N/118°W / 1	
	SA-2 / 45°N/116°W / 1	
	SB-6 / 42°N/124°W / 2	
	UC-2 / 28°N/135°W / 4	
2.5	A Typical Satellite Visible Image (SB6 Sector) from GOES-West.	22.
2.6	A Typical Satellite Infrared Image (SB6 Sector) from GOES-West.	23.
2.7	A Typical Satellite Enhanced Infrared Image (SB6 Sector, "EC" Enhancement Scheme) from GOES-West.	24.
2.8	The "EC" Enhancement Scheme which Relates Temperatures to Specific Grey Shades (after Haering 1978).	25.

Segment No.	Temperature Range °C	Reason for Segment Enhancement
1	+56.8 to +37.3	No significant data
2	+36.3 to +20.8	Land and water
3	+20.3 to -13.2	Water and low clouds
4	-13.7 to -15.7	Benchmark between low and medium level clouds
5	-16.2 to -50.2	Medium and high clouds (cool season precipitation)
6	-51.2 to -60.2	Convective cloud tops
7	-61.2 to -70.2	Convective cloud tops
8	-71.2 to -110.2	Coldest cloud tops and space

3.1 Flowchart for the Estimation of Point Rainfall from GOES Images using the Scofield/Oliver Technique (After Ingraham, *et al.*, 1977). 36.

4.1 A Column of Air Between the Levels z and z+dz at Times t and t+dt. 44.

4.2 Schematic Diagram of Air Circulation During a Major Storm. 52.

5.1 Explanation of the Various Terms used to DescribeGOES Infrared Cloud Images.
CELL - The Coldest Self-Contained Cloud Top Contour and its Immediately Surrounding Warmer Contours.
STORM- The Cloudy Area on the Satellite Image which Brings Rain into an Area. A is Usually Made up of One or More Cells. 69.

5.2 Steps Followed to Make Estimates of Rainfall from GOES Satellite Images. 70.

5.3 The Tektronix Digitizing Tablet - Remote Computer Terminal Arrangement. The Infrared Satellite Image is Placed on the Tablet and the Temperature Contours are Traced using the Stylus. 72.

5.4 The Panasonic WJ-4500 Special Effects Generator Used to Determine Temperature Contours from Unenhanced Infrared Satellite Images. 74.

5.5 The top photo shows the satellite image as seen on the video monitor before the special effects generator is engaged. The second photo shows the satellite image as seen on the video monitor after

	the special effects generator is engaged. Those clouds warmer than T°C on the temperature-grey scale have been shown as black areas while those colder than T°C are shown as lighter areas. The boundary between the two is the T°C contour.	75.
5.6	The Video Camera - Special Effects Generator - Video Monitor Arrangement Used to Determine Temperature Contours from GOES Unenhanced Infrared Images.	76.
5.7	A Schematic Representation of One Storm Cell Contour as it Moves Over 3 Rainfall Stations Between Times t_1 and t_2. The Displacement of the Centre of Gravity During This Time is from c_1 to c_2. From These "Snap-Shot" Views, Station 1 Appears Not to Have Received Any Rainfall.	78.
5.8	The Cell's Position at Time t_2 is Shifted Back Half the Displacement so that Its Centre of Gravity is at Position c.	79.
5.9	Two Cells Affecting Rainfall at a Station. Both Are Shifted so that Their Centres of Gravity are Now at the Midpoints of Their Respective Total Displacements, c_1 and c_2. The Shifted Cells are shown by the Dashed Curves.	81.
5.10	Sequence of Computer Routines Used.	83.
6.1	Map of the Terrace Area with Isohyets (mm) for the Period October 29 to November 2, 1978 (After Schaefer 1979a, b).	90.
6.2	Areal Extent of the October 31, 1978 Storm at 0115 GMT as Viewed from GOES-West.	91.
6.3	Estimated and Observed Precipitation at Gospel Point and Terrace Airport.	95.
6.4	Location of Grid Points Used to Construct Satellite Estimated Isohyets for the October 31, 1978 Storm.	96.
6.5	Isohyets of Satellite Estimated Rainfall (mm) for the October 31, 1978 Storm Based on the Grid Points Shown in Figure 6.4.	97.
6.6	Map of the Vancouver Island - Lower Mainland Area with Isohyets (mm) for the 7-Day Period from December 12 to 18) 1979. (After Schaefer, 1980).	100.

6.7 Areal Extent of December 17, 1979 Storm at 0715 GMT as Viewed from GOES-West. 102.

6.8 Location of Stations Used in the December 17, 1979 Storm Analysis. 103.

1 Blue River
2 Bull Harbour
3 Burns Lake
4 Castlegar Airport
5 Cranbrook Airport
6 Dease Lake
7 Hope Airport
8 Kamloops Airport
9 Kelowna Airport
10 Langara
11 Lytton
12 Penticton Airport
13 Port Hardy Airport
14 Prince George Airport
15 Prince Rupert Airport
16 Quesnel Airport
17 Revelstoke Airport
18 Salmon Arm
19 Sandspit Airport
20 Terrace Airport
21 Tofino Airport
22 Vancouver International Airport
23 Victoria International Airport
24 Williams Lake Airport
25 Banff
26 Calgary

6.9 Estimated and Observed Precipitation for the December 17, 1979 Storm. (For each station the empirical adjustment factor e has been determined from the observed data for that station.) 108.

6.10 Storm Cell Rainfall "Maps" for 2 Hours During the December 17, 1979 Storm. 110.

6.11 Location of Grid Points Used to Construct Satellite Estimated Isohyets for the December 17, 1979 Storm. 111.

Observed rainfalls (mm) for:

Bull Harbour	8.9
Port Hardy	6.8
Tofino	22.6
Vancouver	10.6
Victoria	6.8

6.12 Evolution of Isohyets of Rainfall (mm) for the December 17, 1979 Storm Estimated for the Grid Points Shown in Figure 6.11. 112.

6.13 Location of Stations Used in the June 4, 1977 Storm Analysis: 115.

1 Duncan Lake Dam
2 Revelstoke Airport
3 Mica Dam
4 Castlegar Airport
5 Elko
6 Cranbrook Airport
7 Blue River

6.14	Areal Extent of June 4, 1977 Storm at 0245 GMT as Viewed from GOES-West.	116.
6.15	Estimated and Observed Precipitation for the June 4, 1977 Storm.	119.
6.16	Areal Extent of November 20, 1979 Storm at 1115 GMT as Viewed from GOES-West,	121.
6.17	Areal Extent of December 5, 1979 Storm at 1015 GMT as Viewed from GOES-West,	124.
6.18	Estimated and Observed Precipitation for the December 5, 1979 Storm.	127.
6.19	Estimated and Observed Precipitation for All Five Test Storms.	129.
7.1	The Behaviour of the Weights $W_i=W_1^{(n-i)}$ for n=50 and 3 values of W_1.	134.
7.2	Comparison of Updated Satellite Estimated Rainfall and Observed Rainfall for Gospel Point and Terrace Airport. Typical Values of a, b for Each Station are Given in Table 7.1 (W_1=0.8).	137.
7.3	Schematic of a river basin with 4 stations (A,B,C,D) where the areal rainfall distribution is of interest but where only one of the stations (A) has a raingauge. Satellite estimates of rainfall are available for all 4 stations throughout the duration of the storm. By updating the estimated series for A with the observed data measured there, values of a and b can be determined for each time interval. These values of a and b can be used to update the estimated rainfall at the other ungauged stations (B,C,D).	140.
7.4	Comparison of Updated Satellite Estimated Rainfall and Observed Rainfall for Gospel Point. This is similar to Figure 7.2 except that in this case the satellite estimated rainfalls for Gospel Point were updated using the a and b values determined at Terrace Airport.	143.
7.5	Evolution of Isohyets (mm) Constructed for the December 17, 1979 Storm Updated Satellite Rainfall Estimates for the Grid Points Shown in Figure 6.11	144.

NOTATIONS USED

The following notations are frequently used.

a	radius of the earth
a	updating model parameter
a_o	constant in UW technique
a_1	constant in UW technique
A	cloud area
A_c	satellite (cloud) area in NHEML technique
A_e	radar echo area in NHEML technique
b	updating model parameter
c_p	specific heat of air at constant pressure=c_v+R
c_v	specific heat of air at constant volume
e	adjustment factor, efficiency
E	evaporation
f, f_1, f_2	constants in the divergence functions
Fx,Fy,Fz	eastward, northward, vertical components of friction, respectively
g	gravity
$\mathring{H}$	rate at which external heat is added per unit mass of air
i	index
I	rain rate per unit area in NHEML technique
K	divergence of the coldest contour
M	mass of a column of air
n	total number in a series
O	"order of magnitude of"
p	pressure

P	precipitation (mm)
r_1	volume rain rate in NHEML technique
R	gas constant
R	volume rain rate in UW technique
t	time
T	temperature
u	eastward component of velocity $\bar{V}$
v	northward component of velocity $\bar{V}$
$\bar{V}$	velocity vector
w	vertical component of velocity $\bar{V}$
wc	water content
W_i	i-th weight in updating model
W_1	weighting parameter in updating model
x	eastward horizontal component
x	estimated rainfall in updating model
y	northward horizontal component
y	observed or "true" rainfall in updating model
z	vertical component
α	specific volume
γ	lapse rate
γ_{env}	environmental lapse rate
γ_s	saturated adiabatic lapse rate
ρ	density
ϕ	latitude
Ω	angular velocity of the Earth

Acronyms:

AES	Atmospheric Environment Service
ATS-III	Applications Technology Satellite-III
CDA	Central Data Acquisition
CNR	Canadian National Railway
DMSP	Defense Meteorological Satellite Program
ESSA	Environmental Survey Satellite - Environmental Science Services Administration
GMS	Geosynchronous Meteorological Satellite (Japan)
GMT	Greenwich Mean Time (Subtract 8 hours from GMT to get PST)
GOES	Geostationary Operational Environmental Satellite
GOES-Tap	High quality telephone link for transmission of GOES images
IR	infrared (image)
METEOSAT	Meteorological Satellite (European Space Agency)
NESS	National Environmental Satellite Service
PST	Pacific Standard Time
PWC	Pacific Weather Centre, Vancouver, B.C.
SMS	Synchronous Meteorological Satellite
TIROS-1, TIROS-N	Television Infrared Observational Satellite -1, -N
VISSR	Visible and Infrared Spin-Scan Radiometer

ACKNOWLEDGEMENTS

I want to thank Dr. S.O. (Denis) Russell whose advice and guidance was invaluable throughout the course of the study and who supervised this thesis with interest and optimism. It certainly has been a pleasure to work with Dr. Russell. I would also thank Dr. W. Caselton, Department of Civil Engineering; Dr. M. Quick, Department of Civil Engineering; Dr. P. Murtha, Department of Forestry; and Dr. J. Hay, Department of Geography; for their comments and suggestions concerning this work.

Thanks go to Dr. J. Amorocho, University of California, Davis, and Dr. R. Scofield, NESS for introducing me to rainfall estimation from satellite images; and to NESS, Washington, D.C. for providing GOES satellite images and film loops. Thanks also go to Dr. P. Haering and Mr. J. Spagnol of the Pacific Weather Centre for their interest and advice as well as for making GOES-West satellite images and TIROS-N data available. Appreciation is extended to Mr. W. Kreuder, Water Survey of Canada for providing runoff data for Terrace-Kitimat area basins; to Mr. N. Penny of the AES and to Mr. B. Yorke of the Climatological Data Services, AES, for providing precipitation data; and to Dr. D.G. Schaefer for providing the results of his analysis of the October 31, 1978 and December 17, 1979 storms. Funding for this study came from the Natural Sciences and Engineering Research Council, and was greatly appreciated.

Thanks are extended to Mrs. Tilly Schreinders for the excellent typing of the manuscript, to Mr. Richard Brun for the drafting assistance and to Mr. J. Bonser for computer programming assistance.

I would also like to thank my family and friends for being there when I needed them.

CHAPTER I

INTRODUCTION

The growth of a region is directly related to the development of its natural resources with the quality of this growth dependent on the skillful exploitation and management of the resources. As a basis for the efficient planning, design, and operation of projects, a detailed and reliable description of the resource is required but this has usually been difficult to provide.

In British Columbia water is a major resource contributing directly and indirectly to the economy and well-being of the province. The amount of rain falling over the region is an important quantity in the water resource inventory. The measurement of the rainfall is hampered because the existing network of raingauges is generally inadequate and in some instances non-existent. Figure 1.1 shows the distribution of stations recording precipitation on an hourly basis throughout British Columbia. Most of these stations are grouped near centres of population or along transportation routes, both to facilitate installation and maintenance, and to keep costs to a minimum. There are, however, large areas which remain without gauges or which have gauges where data are not available for use on a real-time basis, such as in flood forecasting. The lack of detailed rainfall data from river basins has long been

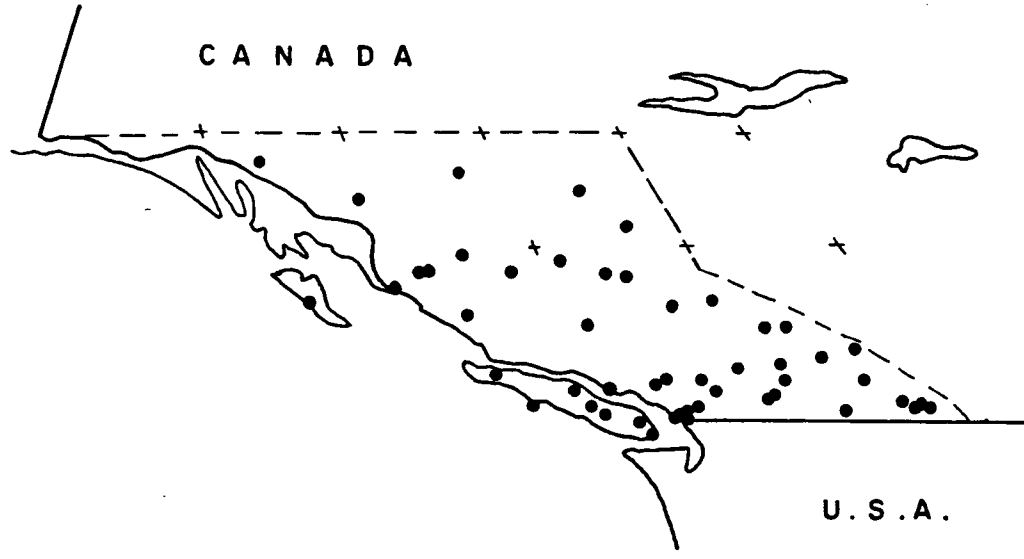

FIGURE 1.1

Distribution of Stations in British Columbia Observing Rainfall on an Hourly Basis. The Projection is the Same as on the Satellite Images, (Lambert Conformal Conic, Farley 1980).

a recognized problem among hydrologists but there appears to be little prospect of it being resolved by surface measurement techniques in the near future. This is particularly true in the more remote unpopulated regions where some of the largest water resource developments are now being engineered.

Meteorological satellites hold the promise of providing meteorologic information over large regions. The geostationary operational environmental satellites, GOES, record atmospheric conditions on the Earth around the clock and provide half-hourly images such as those shown on the television weather forecast. GOES images have been employed to estimate rainfall from large convective cells in tropical and sub-tropical areas by applying empirical relations specifically derived for this type of storm, (Scofield and Oliver, 1977a; Griffith *et al.*, 1978; Stout *et al.*, 1979). On the whole these approaches offer limited guidance for extending rainfall estimation using satellite images to other types of storms or geographic regions.

1.1 Study Objectives

The aims of the study described in the following chapters were to extend the satellite rainfall estimation procedure which would be applicable to frontal storms and other precipitation systems in the higher latitudes, to develop an applicable physical concept for the estimation procedure, and to test the procedure by applying it to actual storms.

The more successful methods for computing rainfall from satellite images all use the changes in the area of the cloud top temperature contours from one image to the next as input parameters to their computational procedures, as for example in Scofield and Oliver (1977a). In the course of the present study it was realized that the rate of change in the cloud top temperature contours provides a measure of the divergence, or the rate at which the ascending air is spreading out at the cloud top. By continuity this is in turn related to the rate at which air entering the cloud is rising. It has long been realized that the rainfall rate could be estimated from a knowledge of the rate at which an air mass was rising and its moisture content (Byers and Braham, 1948), but it has never been possible to measure the vertical velocity of the ascending air. Now, as shown in the present study, the vertical velocity can be estimated from the divergence of the cloud top which can be determined from successive satellite images. This insight provided an explanation, with a sound physical basis, for the success of techniques such as that of Scofield and Oliver (1977a), and it also provided a solid foundation for extending these same fundamental concepts to the type of storms encountered in British Columbia. To apply the concept it was necessary to develop procedures for estimating the divergence from satellite images, to develop a method for updating these estimates in the light of actual recorded data, and to develop computer routines to help with the extens-

ive calculations. Such procedures were developed and tested on a number of major and minor storms which occurred over British Columbia and for which satellite images were available.

The emphasis throughout has been on developing a practical technique which can be used by hydrologists and meteorologists. Potential engineering applications of the data include providing real-time regional flood forecasts, reservoir inflows, as well as the study of previous large storms for design flood calculations.

1.2 Outline of the Following Chapters

Chapter II contains general background information on meteorological satellites, in particular GOES, which provided the images used in this study. Chapter III reviews other investigations into the application of satellite imagery for rainfall estimation. Chapter IV describes the model employed to relate cloud growth as observed in satellite images to the actual rainfall from the cloud. Chapter V discusses the conceptual and computer sequence followed to arrive at satellite estimates of rainfall, while Chapter VI presents the estimates of precipitation for a number of storms over British Columbia and compares them with the observed precipitation. The first part of Chapter VII discusses the updating procedure for incorporating the information contained in the observed rainfall series with that of the estimated series. The second part of Chapter VII contains the updated

precipitation estimates for two storms over British Columbia and compares them to the measured precipitation. Chapter VIII draws together the conclusions, recommendations and suggested directions for future research that have become apparent during the course of this study.

CHAPTER II

METEOROLOGICAL SATELLITES: BACKGROUND

With space flight came the opportunity for taking a closer look at conditions on Earth (like the weather) from a unique vantage point. Present meteorological satellites scan the Earth regularly at a level of resolution which allows observation of meso and macroscale (10^3 to 10^7 m) phenomena. (Atmospheric motions of various scales and types are summarized in Table 2.1). These satellites offer a potential solution to the problem of inadequate hydrologic information by providing economical and timely data on a spatial and temporal scale virtually unattainable by conventional ground based-networks.

2.1 Some Satellite Systems and Sensors

There are two considerations which have affected meteorological satellite systems and their sensors. One is the optical behaviour of the atmosphere at different wavebands and the other is the type of orbit the satellite can take above the Earth's surface.

The atmosphere has "windows" (i.e. is transparent to radiation of certain wavelengths) which are important for remote sensing, in the visible, near visible, infrared, and microwave bands. These are shown in Table 2.2. Consequently sensors,

TABLE 2.1 Scales of Atmospheric Motions (from Holton, 1972 and Knox, 1978)

TYPE OF MOTION	HORIZONTAL SCALE (m)
molecular mean free path	10^{-7}
minute turbulent eddies	10^{-2} to 10^{-1}
small eddies	10^{-1} to 1
dust devils	1 to 10
gusts	10 to 10^{2}
tornadoes	10^{2}
cumulonimbus clouds	10^{3}
fronts, squall lines	10^{4} to 10^{5}
hurricanes	10^{5}
synoptic cyclones	10^{6}
planetary waves	10^{7}

TABLE 2.2 Major Atmospheric Windows Available for Spacecraft Remote Sensing (after Lintz and Simonett, 1976)

WINDOW	WAVEBAND
ultraviolet and visible	0.30 to 0.75μ
	0.77 to 0.91
near infrared	1.0 to 1.12
	1.19 to 1.34
	1.55 to 1.75
	2.05 to 2.4
mid-infrared	3.5 to 4.16
	4.5 to 5.0
thermal infrared	8.0 to 9.2
	10.2 to 12.4
	17.0 to 22.0
microwave	2.06 to 2.22 mm
	3.0 to 3.75
	7.5 to 11.5
	20.0+

sensitive to radiation in these bands were developed. Table 2.3 lists some meteorological satellites along with their sensors. The two most popular wavebands for operational use are the visible and the thermal infrared bands.

In addition to observing the Earth in several wavebands, the type of orbit the satellite assumes can also be controlled. Weather satellites generally have one of two orbital configurations: a polar orbit - the orbit of the satellite passes over both poles; or a geostationary orbit - the orbit of the satellite has a period of approximately 24 hours so that it remains "fixed" over one position on the Earth's surface. The advantage of polar orbiting satellites lies in the provision of images over the entire surface of the Earth. This is especially important for obtaining data for the polar regions. The width of the swath that polar satellites sweep out in their orbits is dependent in part on the type of sensor and the altitude of the spacecraft. The frequency of repeat coverage over any one location varies with the satellite used. (See Table 2.3). It is this repeat frequency which forms the principal disadvantage of polar orbiting satellites - it is usually too low to reveal rapidly changing weather features.

Geostationary satellites provide a "global view" of weather on a very frequent basis: one image as often as every half hour during regular operation and more often during severe

TABLE 2.3 Some Present and Proposed Satellites, their Sensors and Characteristics. Additional Information is Available from WMO (1976), NESS (1976), Kodaira and Murayama (1976), NOAA (1979), *Spaceflight* (1980), and Davis (1980).

SATELLITE	SENSOR	WAVEBAND	NOMINAL NADIR RESOLUTION (km)	REMARKS
Geostationary Satellites:				
SMS/GOES	Visible and Infrared Spin-Scan Radiometer (VISSR)	0.55-0.7 10.5-12.5	1 8	Repeat coverage every ½ hr, resolution double nadir value at latitudes >50°, polar coverage limited, GOES-B expected launch Aug. 1980.
GMS "Sunflower"	VISSR	0.5-0.75 10.5-12.5	1.25 5	Japanese satellite located at (0°N, 140°E).
METEOSAT	VISSR	0.7 11	1.25 5	European Space Agency Satellite (ESA=Belgium, Denmark, France, Germany, Italy, Sweden, Switzerland, and the United Kingdom). Satellite located at (0°N, 0°W); as of Nov. 24/79 on limited operation due to onboard overload problem.
	Water Vapor (WV)	6	5	
STORMSAT	Advanced Atmospheric Sounding and Imaging Radiometer (AASIR)	not available	not available	Prototype satellite, visible and infrared scanner; expected launch: mid 1980's.
Polar Satellites:				
NIMBUS 5	Electrically Scanning Microwave Radiometer (ESMR)	0.8 cm	32	Repeat coverage every 12 m.

TABLE 2.3 (continued)

SATELLITE	SENSOR	WAVEBAND	NOMINAL NADIR RESOLUTION (km)	REMARKS
NIMBUS 6	Temperature-Humidity-Infrared-Radiometer (THIR)	6.5-7.1 10.3-12.5	22 8	Repeat coverage every 12 hr.
NIMBUS G	THIR	(same as for NIMBUS 6)		
	Scanning Multifrequency Microwave Radiometer (SMMR)	4.55 cm 2.81 cm 1.67 cm 1.36 cm 0.81 cm	118 x 103 73 x 66 47 x 41 37 x 32 22 x 19	Repeat coverage every 36 hr., swath width 780 km.
NOAA 5,6	Scanning Radiometer (SR)	0.5-0.7 or 0.5-0.9 10.5-12.5	3.5 8	Repeat coverage every 12 hr, swath width 3000 km
	Very High Resolution Radiometer (VHRR)	0.6-0.7 10.5-12.5	1 1	
TIROS-N	Advanced VHRR (AVHRR)	0.55-0.9 0.72-1.1 3.55-3.93 10.5-11.5	1 - 4	Repeat coverage every 12 hr, swath width 2800 km, launched Oct. 31/78.

weather such as hurricanes and tornadoes. There is, however, a drawback: away from the equator the images become increasingly distorted due to the curvature of the Earth, becoming too distorted to be useful beyond about 60° latitude. Five geostationary satellites forming the World Wide Geosynchronous Satellite System are arranged around the Earth at altitudes of approximately 36,000 km, as shown in Figure 2.1. British Columbia receives satellite images from GOES-West which is located over the equator and 145° longitude.

2.2 The GOES System

The frequent, large areal coverage of a geostationary meteorological satellite makes it particularly attractive for observing the changes in weather conditions which are associated with rainfall as revealed by the growth and decay of cloud systems. (Images from the GOES-West satellite were used in this study for this reason, and, because these satellite images were readily available locally). The following briefly describes the GOES system which is generally similar to other geostationary satellites - the Geostationary Meteorological Satellite (GMS) of Japan and the Meteorological Satellite (METEOSAT) of the European Space Agency.

The GOES satellites are an outgrowth of earlier synchronous meteorological satellite (SMS) research and development. The primary aims of the SMS/GOES program are:

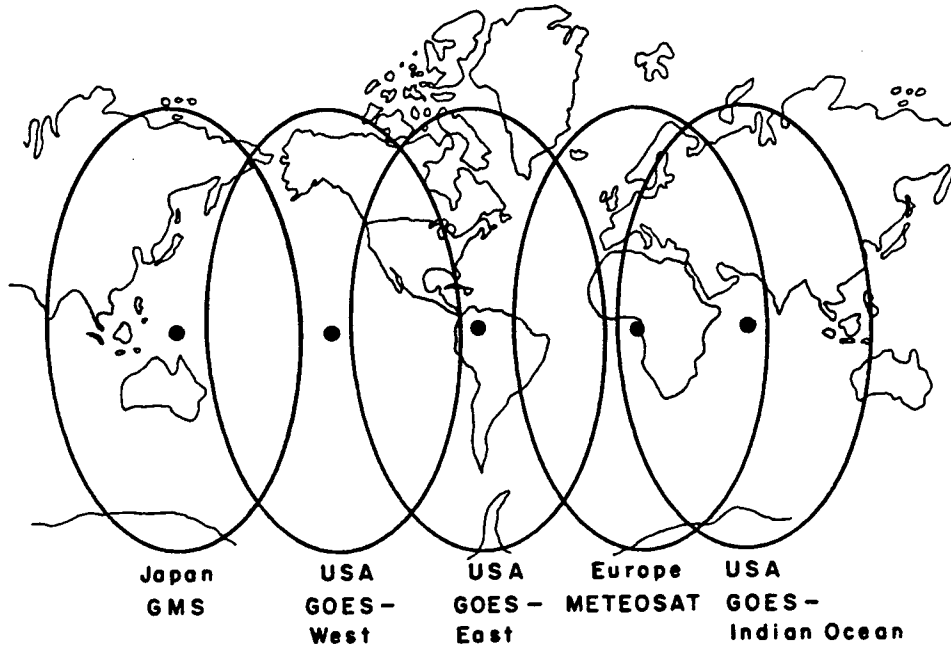

FIGURE 2.1

Five Geostationary Meteorological Satellites Provide Global Coverage of the Weather, (after Corbell *et al.*, 1977 and *NOAA*, 1979).

a - to increase the knowledge and understanding of atmospheric processes by observing the motions and lifecycles of storms and other phenomena,

b - to aid in the development of a domestic (U.S.) and international data network capable of collecting, processing, and distributing routine observations and early warnings in real time,

c - to increase the kind, quality and quantity of environmental parameter measurements.

These aims are achieved by combination of SMS/GOES satellites, ground stations and remote data collection platforms (DCP's). (McKowan, 1977).

The GOES satellite visible and infrared spin-scan radiometer (VISSR) senses conditions on the Earth using two wavebands - the visible (0.55 to 0.7μ) band which provides 1 km resolution images every hour during the daylight hours, and the thermal infrared (10.5 to 12.6μ) band which provides 8 km resolution images every half hour twenty-four hours a day. Under special stormy conditions the frequency of the images can be increased to provide, for example, images of the affected area every five minutes. This is controlled by the owner of the satellite.

The VISSR allows the mapping of cloud features both day and night using eight visible channels to give measurements of albedo from 0.5 to 100 percent, and two thermal infrared channels (one of which is redundant) which give radiance temperature measurements between -93 and 42°C. The European Space Agency's METEOSAT has an additional sensor for water vapor (in the 6μ band) (Davis, 1980), and slightly different resolution specifications, as does Japan's GMS, (Kodaira and Murayama, 1976). For these satellites the visible resolution is 1.25 km and the infrared resolution is 5 km. Both METEOSAT and GMS have redundant visible sensors as well.

2.3 GOES Image Formation and Enhancement Schemes

The formation of the GOES satellite image is a result of a combination of the satellite's spin motion (100 rpm) on its axis and the step action of its scanning optics. One line corresponding to the Earth's west-east axis is performed for each satellite rotation, while the scanner positions each line in a north-south manner. (METEOSAT scans from east to west and steps in a south-north manner). Once the full Earth disc has been sensed (a procedure which takes approximately 18 minutes for GOES and 25 minutes for GMS and METEOSAT), the scanner optics retrace to the original starting position (in approximately 2 minutes). See Figure 2.2.

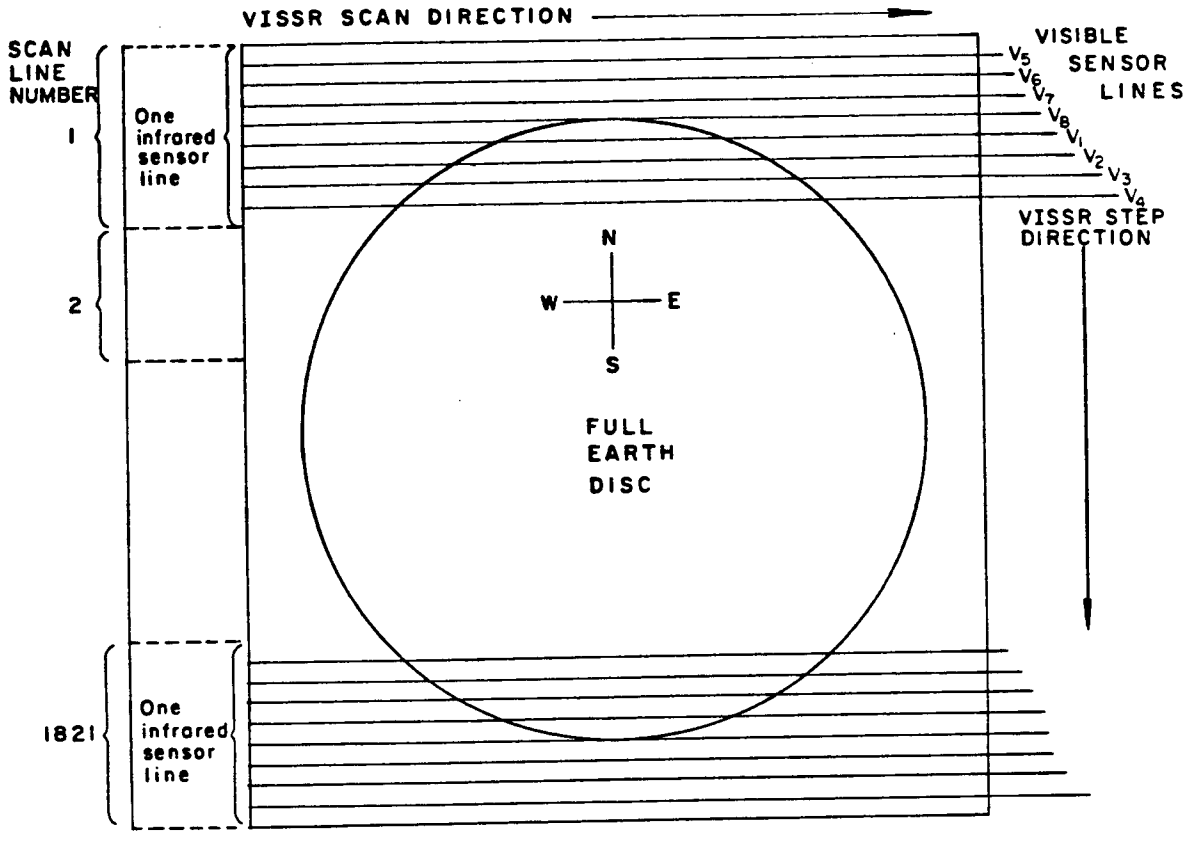

FIGURE 2.2

Assembly of a VISSR Image. Each scan line is composed of 8 visible sensor lines V_i and 1 infrared sensor line. One scan line represents a west to each scan of the earth and each is positioned sequentially in a north-south manner (Adapted from McKowan, 1977).

The signal from GOES-West is sent initially to the National Environmental Satellite Service (NESS) Central Data Acquisition (CDA) facility at Wallops Island, Virginia, where preliminary processing occurs including "stretching" the signal. (Since the information on the Earth takes up less than 5 percent of an entire VISSR scan line, that portion of the signal must be expanded before being assembled into a recognizable image). The signal is then transmitted back to the satellite for broadcast to the NESS Central Processing Facility in Washington, D.C. From here the information is sent by high quality telephone line to six major distribution centres (San Francisco, Kansas City, Washington, D.C., Miami, Honolulu, and Anchorage) for further distribution to other users under the GOES-Tap program. (For details on GOES-Tap see Appendix III of Corbell *et al.*, 1977). Figure 2.3 shows this distribution schematically.

The volume of data collected by the GOES satellites far exceeds the present capabilities for processing, storing and transmitting data. This has resulted in the selection of small subareas of the full Earth disc image for analysis and subsequent transmission by landline to the users. These subareas are known as sectors and a few of the typical sectors received in Vancouver, B.C., are shown in Figure 2.4. Of course, with a receiving station located in the Vancouver areas (as is proposed

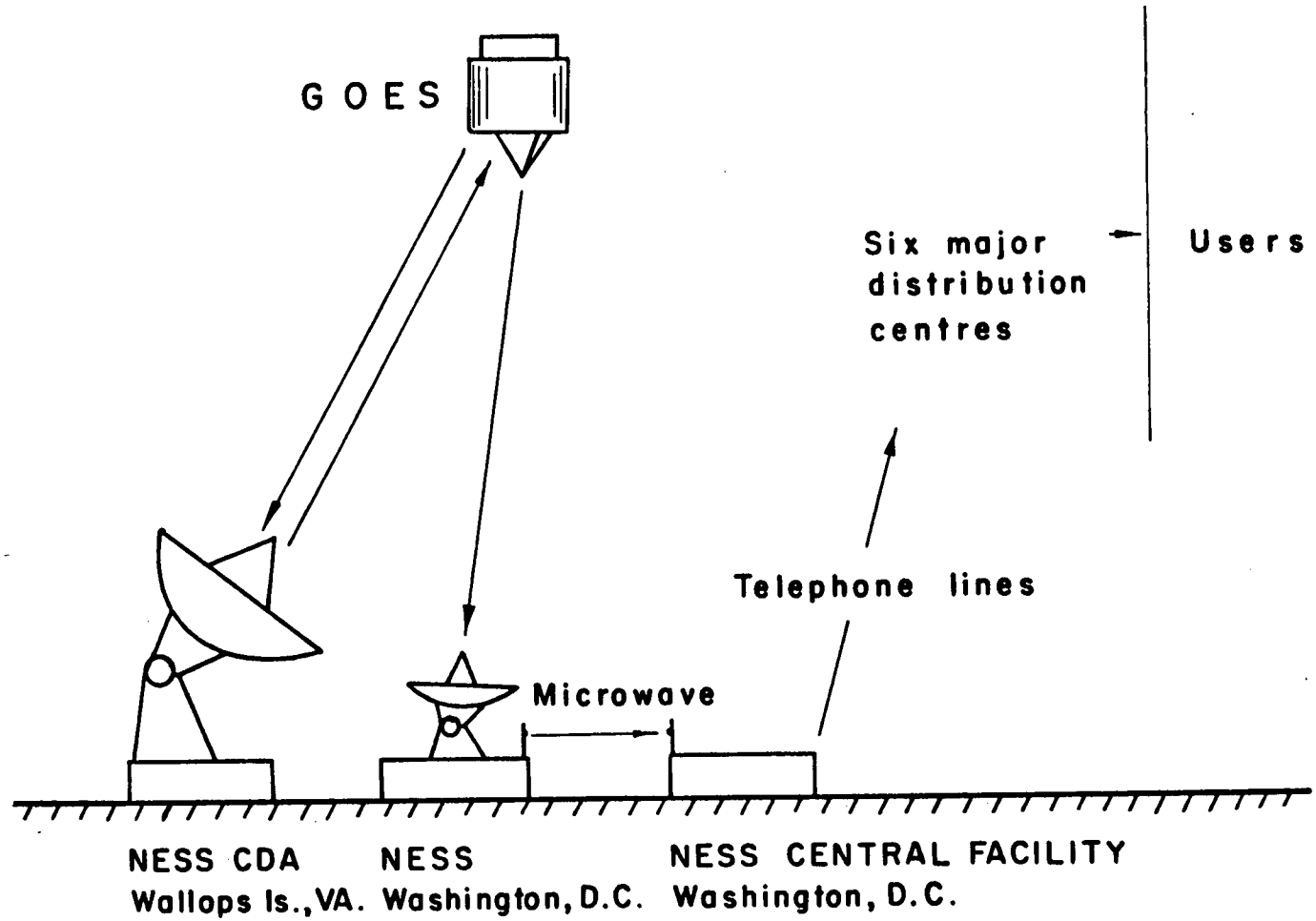

FIGURE 2.3 Distribution of the GOES Signal

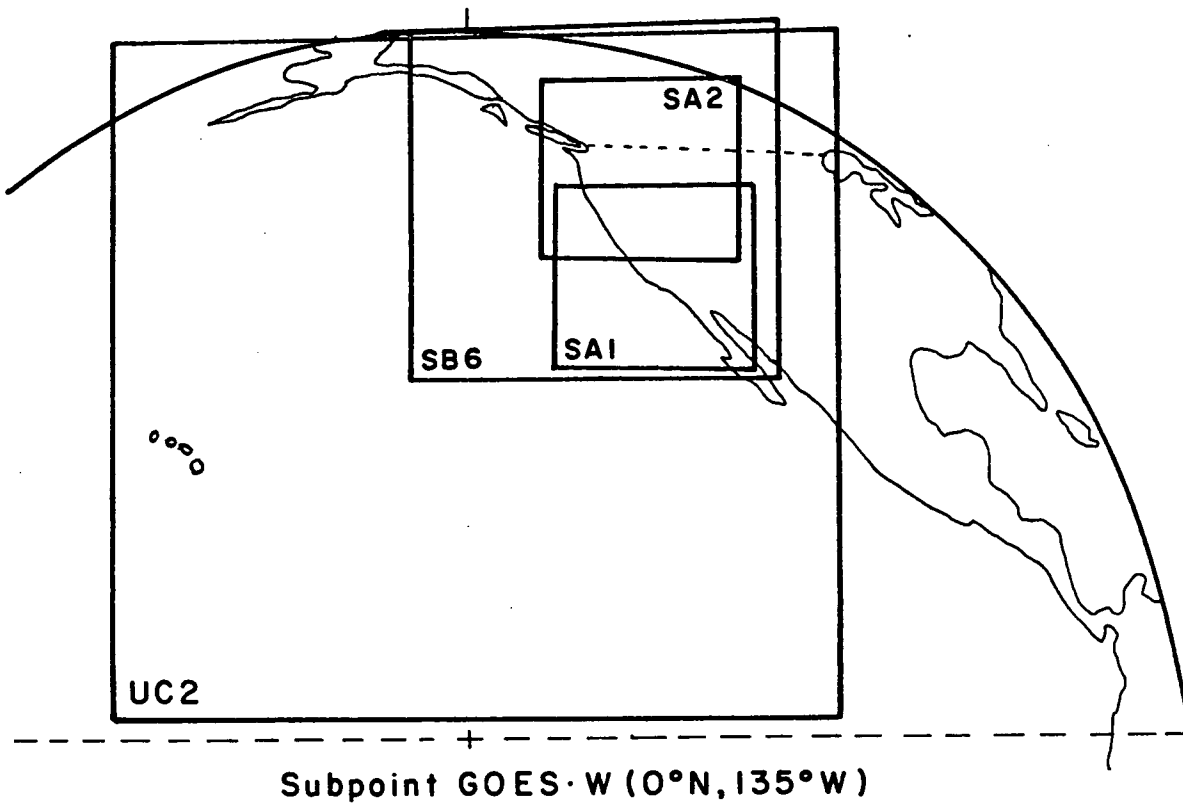

FIGURE 2.4

Sectors Received at the Pacific Weather Centre (after Corbell *et al.*, 1977)

Visible and Infrared Sectors:

Sector	Centre Point (lat./long.)	Resolution (km)
SA-1	$36^{o}N/118^{o}W$	1
SA-2	$45^{o}N/116^{o}W$	1
SB-6	$42^{o}N/124^{o}W$	2
UC-2	$28^{o}N/135^{o}W$	4

for 1981), other sectors of local interest could be chosen, including the full Earth disc for a global view of the weather, or "close-ups" of trouble areas within British Columbia. Popham and Rich (1975) describe a GOES VISSR ground station. Seymour *et al.* (1977) and MDA (1977) give details of a low-cost receiving, analyzing and distribution system for various environmental satellites including GOES and METEOSAT. The operational presentation of these satellite data is still in the form of hardcopy photographs of the half-hourly visible and infrared views of developing weather systems.

Both the visible and infrared satellite images have been used to identify precipitating clouds, although the emphasis in this study lies with the infrared images. Figure 2.5 shows an example of a visible image form GOES-West, while Figure 2.6 and 2.7 respectively, show typical unenhanced and enhanced infrared images. The enhancement scheme, that is, the relationship between temperature and the photo grey scale used to contour Figure 2.7, is given graphically in Figure 2.8. When temperature gradients detected by the VISSR are small it is difficult to recognize significant cloud and surface features (for example, fog, stratus and thunderstorm cloud tops) in the infrared image. Enhancing, then, increases the contrast between those features and their background. An ideal enhancement distinguishes a limited number of features and provides as much detail as possible without making the enhanced image too confusing. There are

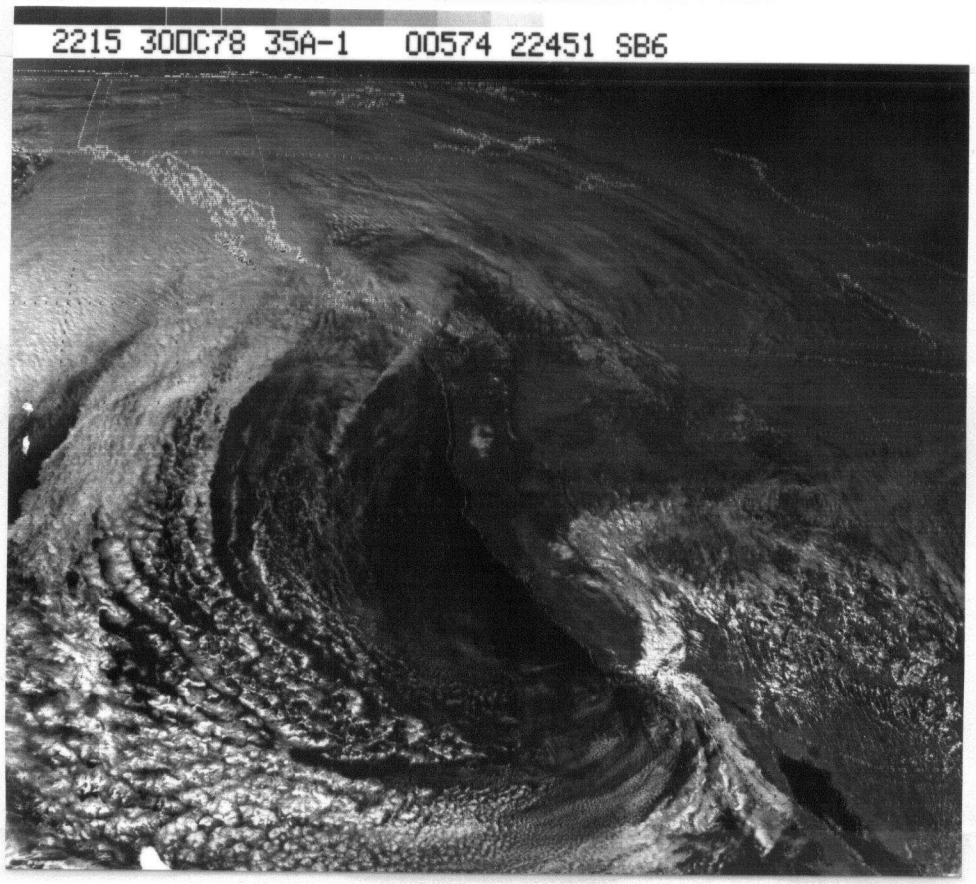

FIGURE 2.5

A Typical Satellite Visible Image (SB6 Sector) from GOES-West.

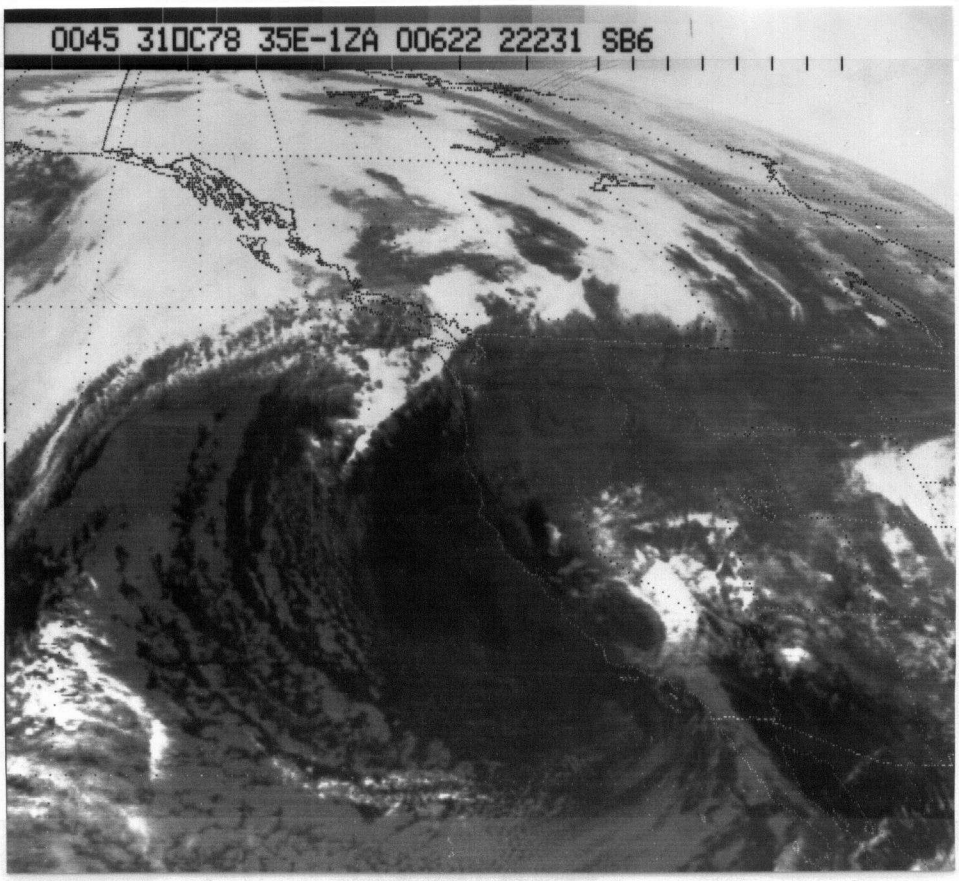

FIGURE 2.6

A Typical Satellite Infrared Image (SB6 Sector) from GOES-West.

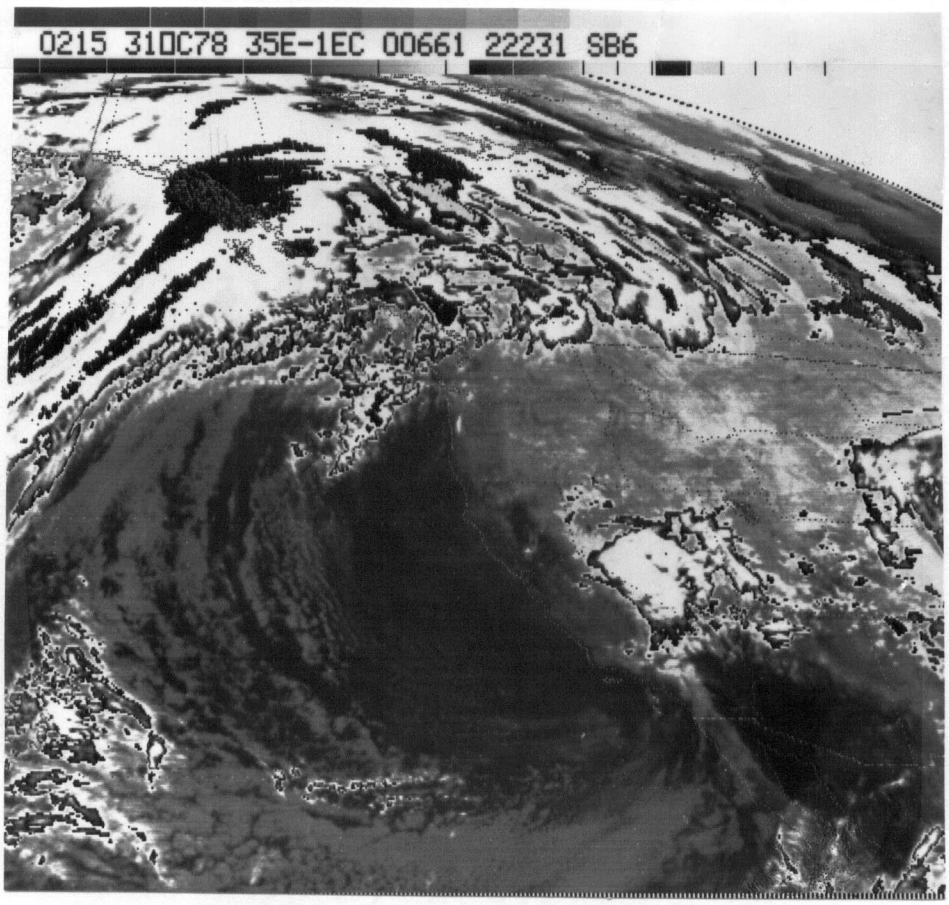

FIGURE 2.7

A Typical Satellite Enhanced Infrared Image (SB6 Sector, "EC" Enhancement Scheme) from GOES-West.

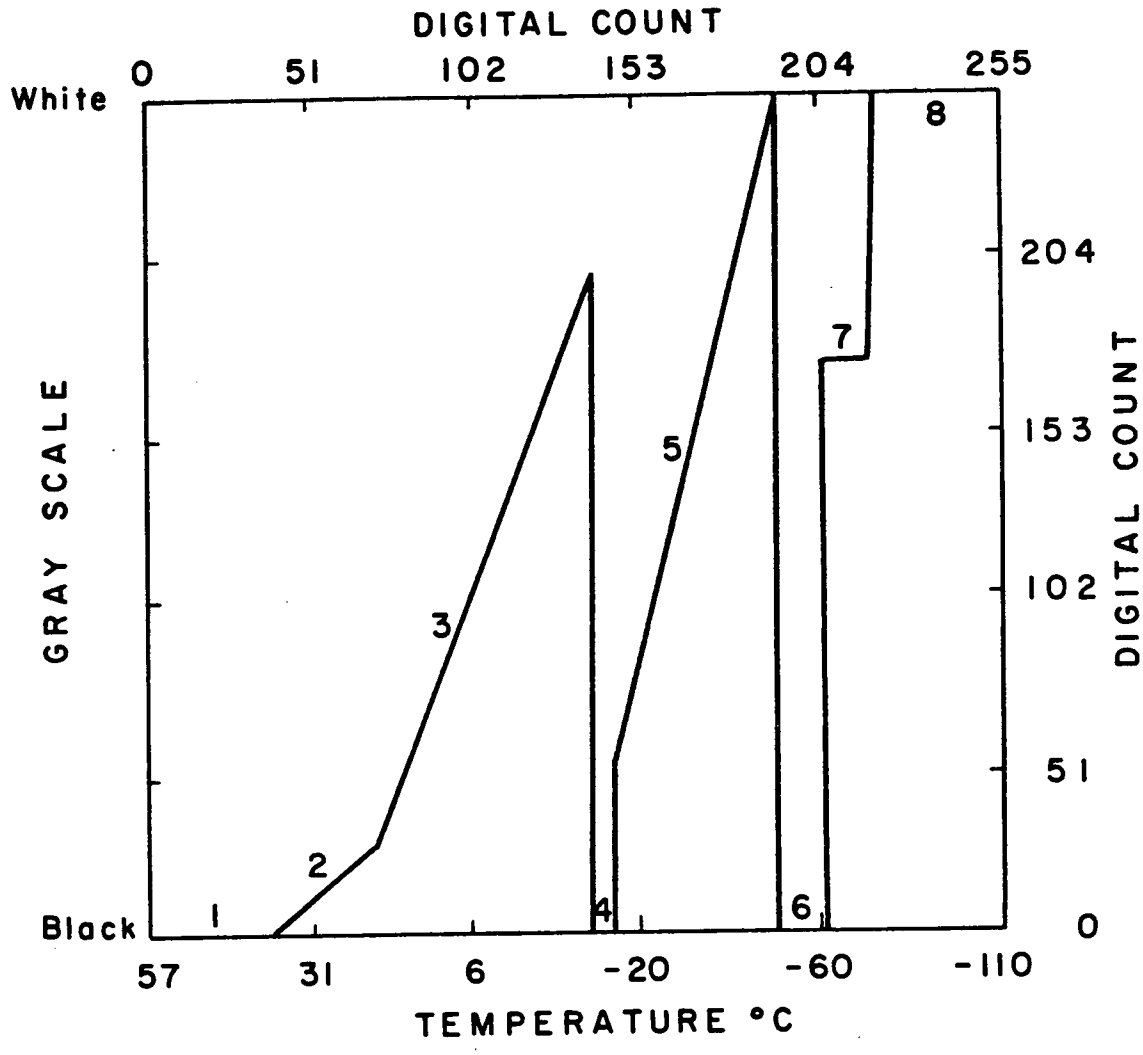

FIGURE 2.8

The "EC" Enhancement Scheme which Relates Temperature to Specific grey shades (after Haering, 1978)

Segment Number	Temperature Range (°C)	Reason for Segment Enhancement
1	+56.3 to +37.3	No significant data
2	+36.3 to +20.8	Land and Water
3	+20.3 to -13.2	Water and Low Clouds
4	+13.7 to -15.7	Benchmark between Low and Medium Level Clouds
5	-16.2 to -50.2	Medium and High Cloud (Cool Season Precipitation)
6	-51.2 to -60.2	Convective Cloud Tops
7	-61.2 to -70.2	Convective Cloud Tops
8	-71.2 to -110.2	Coldest Cloud Tops and Space

a large number of enhancement schemes available, although only a few of them are used operationally. These are described in detail in Corbell *et al.* (1977).

2.4 Other Sources of Satellite Information

A number of meteorological satellite systems have evolved each with a different combination of sensor and orbit. In the United States there are the NOAA, NIMBUS, TIROS, SMS/GOES, DMSP, and STORMSAT either operational or proposed. Parallel systems are being developed in other countries, notably the USSR, the European nations through ESA, and Japan. In the brief discussion of weather satellites here, microwave satellites have been omitted. Although they are promising in the determination of precipitation areas, they are of little use in real-time analyses at present because none are expected to exist in geostationary orbits until possibly 1985, (Lovejoy, 1978).

Additional information on the GOES system is contained in McKowan (1977), Corbell *et al.*, (1977) and Fordyce *et al.*, (1974). Lienesch *et al.*, (1975) discuss the accuracy and calibration of SMS infrared observations. Vesely and Botzong (1974) and Spangler (1974) describe the Defense Meteorological Satellite Program (DMSP). Fortuna and Hambrick (1974) discuss the NOAA polar-orbiting system, while Hussey (1977) describes the TIROS-N polar-orbiting system. Applications of weather satellite obser-

vations to water resources managers are discussed by McGinnis *et al.*, (1980), and to weather sensitive army operations by Miers (1976). Numerous authors (including Griffith *et al.*, 1977; Lovejoy and Austin; 1979; Lethbridge, 1967; Gurka 1976; Gantry *et al.*, 1976; Purdom, 1976; Clark *et al.*, 1980; and Maddox, 1980) have indicated the potential capabilities of geostationary satellites (GOES) for observing various meteorological parameters of use to hydrologists as well as meteorologists such as wind speeds, cloud cover, and albedo.

CHAPTER III

A REVIEW OF SATELLITE IMAGE PRECIPITATION ESTIMATION

Since the first pictures returned by TIROS-1 in 1960 scientists have been intrigued by the wealth of data contained in a single image. The images showed very clearly the organization and structure of cloud systems ranging from the large cyclonic systems of a thousand kilometers across to individual clouds of 1 kilometer or so in diameter. Other features could also be discerned such as the cloud features associated with, hurricanes, thunderstorms, squall lines, jet streams, mountain waves, and regions of strong wind shear. Analysis of a time sequence of these images indicates the development, decay and/or movement of weather through a region. The power of satellite images lies in the vast spatial information obtained on a 24-hour a day basis for remote, oceanic or other areas where observing networks may be too sparse to reveal these features by conventional means. Until recently, much of the information contained in satellite images has been of a qualitative nature and difficult to use directly. Anderson and Veltischchev (1973) discuss and illustrate the potential of satellite images in weather analysis and forecasting. In their work is a wealth of satellite images, including some of the very earliest weather satellite photographs, which serve as a catalogue of various weather conditions and cloud types as seen from a satellite's vantage point in space. It is an ideal reference for acquiring skill in cloud and weather identification using satellite images.

Development of rainfall estimation procedures involving satellite imagery has paralleled the evolution of satellite sensors, chiefly those which sense radiation in two major bands (visible and thermal infrared). Early work in extracting quantitative information from satellite imagery was based on finding relationships between infrared temperature and/or visible brightness and such parameters as precipitation. Martin and Scherer (1973) provide a brief overview of satellite estimation techniques up to 1973. Some studies, for example, Barrett (1970), investigated the areal statistics of cloud cover and cloud type with respect to rainfall probability and intensity on a monthly basis, while others correlated cloud top brightness and/or temperature with 24-hour rainfall (Gerrish, 1970, and Follansbee, 1973). Follansbee (1973) and Follansbee and Oliver (1975) adapted Barrett's method for estimating daily rainfall, concentrating solely on rain-producing cloud types (cumulonimbus, nimbostratus, and cumulus congestus). Davis and Serebreny (1972) have used a similar approach for estimating total precipitation including snowfall over mountainous regions of Montana using once-daily ESSA (Environmental Survey Satellite - Environmental Science Services Administration) satellite images.

Another approach evolved which used cloud brightness as a key variable in estimating convective precipitation (Sikdar and Suomi, 1971; Sikdar, 1972). In fact, Martin and Suomi (1971, 1972) tested brightness enhancement of ATS-III (Applications

Technology Satellite - III) images with radar images to isolate areas of intense convection. This is similar to an approach developed by Woodley and Sancho (1971) which was further developed by Woodley *et al.*, (1972) and Griffith *et al.*, (1976) for estimating rainfall in Florida.

In order to take advantage of the 24-hour availability of infrared imagery, Scherer and Hudlow (1971) developed a technique for transforming minimum cloud top areas into probable radar echo areas and hence, by a statistical model, to rainfall amounts.

3.1 GOES Rainfall Estimation Techniques

These initial studies formed the background for the emergence of three groups in the United States: Woodley/Griffith's group at the National Hurricane and Experimental Meteorology Laboratory (NHEML) in Florida, the University of Wisconsin (UW) group, and Scofield/Oliver's group in Washington, D.C., who have worked towards a rainfall estimation procedure using visible and infrared images from the GOES satellites. Each group's approach is discussed briefly in the following sections.

3.1.1 The NHEML Technique

The NHEML technique is based on the observation that areas of active deep convection and rainfall in the tropics appear brighter on visible images and colder on infrared images than

inactive areas. ATS-III and GOES images were calibrated with radar data from the south of Florida. The empirical relation NHEML developed is

$$r_v = IA_e \qquad 3.1$$

Where r_v is the volume rain rate (m^3/h), I is the rain rate per unit area ($(m^3/h)/km^2$) and is a function of the radar echo area growth trend), and A_e is the radar echo area (km^2) which is defined by a threshold rain rate of 1 mm/h. 'I' can be derived for any geographic area provided appropriate radar data are available (which limits its usefulness in mountainous terrain). The radar echo area, A_e, is determined on a cloud by cloud basis from empirical relations between satellite area A_c and radar echo area A_e. Testing of this technique has been carried out for a number of convective storms in Florida and Venezuela as well as for six hurricanes (Griffith *et al.*, 1978). Results were generally good although the authors noted that their accuracy varied with the total period of calculation and with the area of cloud cover examined. They anticipated increased accuracy with digital data and, in a paper by Waters *et al.*, (1977), present their first experimental results using digital geostationary data to assess the rainfall potential of selected hurricanes.

3.1.2 The UW Technique

Like the work of the NHEML group, the UW technique relates the volumetric rain rate to cloud area, $A(m^2)$ and radar echo

area (Stout *et al.*, 1977, 1979). In addition, the UW technique explicitly includes the rate of change of the cloud area ($\frac{dA}{dt}$ (m^2/s)) in the relation for the rainfall rate R:

$$R = a_0 A + a_1 \frac{dA}{dt} \qquad 3.2$$

the constants a_o (m/s) and a_1 (m) are determined by a least squares fit from pairs of satellite area and radar echo rain rate (determined at various reflectivity levels), and have slightly different values depending on whether visible or infrared images are being used.

This technique is a variant of the NHEML technique and as such was developed to provide estimates of rainfall from large precipitating cumulonimbus cells over the tropical North Atlantic. The authors suggest that these cells be identified by skilled meteorologists. They recognize the potential for errors in their technique if used outside the tropical North Atlantic, especially if convective cells are not the major contributors to the total rainfall and note that their coefficients, a_0, a_1, would need to be redefined.

3.1.3 The Scofield/Oliver Technique

Oliver and Scofield (1976) and Scofield and Oliver (1977a) have developed an operational technique which gives half-hourly or hourly rainfall estimates from GOES infrared and high resolution visible images. It is a decision hierarchical approach

based on the identification of certain cloud properties for deep convective precipitation systems occurring in tropical air masses with high (-80°C) tropopauses. The technique was essentially developed for the southern continental United States and papers describing its application in a number of varied cases (Scofield, 1976 a,b; 1978a,b; Scofield and Oliver, 1975, 1977b; Scofield and Weiss, 1976; Scofield *et al.*, 1980; and Scofield and Oliver, 1980) show the usefulness of the procedure. The Scofield/Oliver technique has been modified slightly and used to successfully estimate rainfall for a number of storm situations over Venezuela and Colombia (Ingraham *et al.*, 1977).

The Scofield/Oliver technique starts with the simple empirical relationship that the higher the top of the (cumulonimbus) cloud, the heavier the rainfall, and subsequently adds factors which improve this relationship. The two most important factors are the rate of growth of the anvil and the position of the cumulonimbus under the anvil. As well, a number of other characteristics of cumulonimbi are considered, such as the presence or absence of overshooting tops, the importance of merging cells, and merging convective cell lines, in order to improve the estimates of rainfall. These factors are arranged in a decision tree or flowchart which allows the user to determine the appropriate rainfall amount for a particular point. There are three major steps in the computation process:

A - Identification of the convective system and the determination of the active rain producing portion of the system,

B - The initial estimation of precipitation using the cloud top temperatures as given by the enhanced infrared imagery and empirical rainfall-temperature-cloud growth relations,

C - Correction of the initial precipitation estimates by the use of amplification factors based on the dynamic behaviour of the convective cloud system (for example, overshooting tops, merging cells, or merging convective cell lines).

The identification step is accomplished by following a set of diagnostic indices including:

1 - Identification of convection:

a) shape of the cloud (circular, oval, carrot-shaped) from the infrared and visible images

b) depth of convection - vertical development of the cloud, from the enhanced infrared images

2 - Identification of the active portion of the convective system.

a) area of steepest temperature gradient, from enhanced infrared images;

b) texture and brightness of the cloud top, from the visible images;

c) area of least downwind expansion aloft, from the enhanced infrared images;

d) location with respect to the upwind portion of the cloud anvil, from the visible images.

Figure 3.1 shows a streamlined version of the Scofield/Oliver flowchart, (Ingraham *et al.*, 1977).

There are a number of difficulties which become apparent after using the Scofield/Oliver technique. Irregularly shaped cloud cells cannot be adequately included. Clouds with local areas of subsidence ("holes") within their boundaries are also a problem. (It is thought that these "holes" within the cloud boundaries indicate the collapse of short-lived overshooting tops). Some of the factors which produce high rainfall rates depend upon access to the high (1 km) resolution visible images which are rarely available at the operational user's level (except if he has access to his own receiving station). The identification of the amplification parameters from the satellite images is very much dependent on the observer and his

FIGURE 3.1

Flowchart and Table for the Estimation of Point Rainfall from GOES Images Using the Scofield/Oliver Technique (after Ingraham *et al.*, 1977)

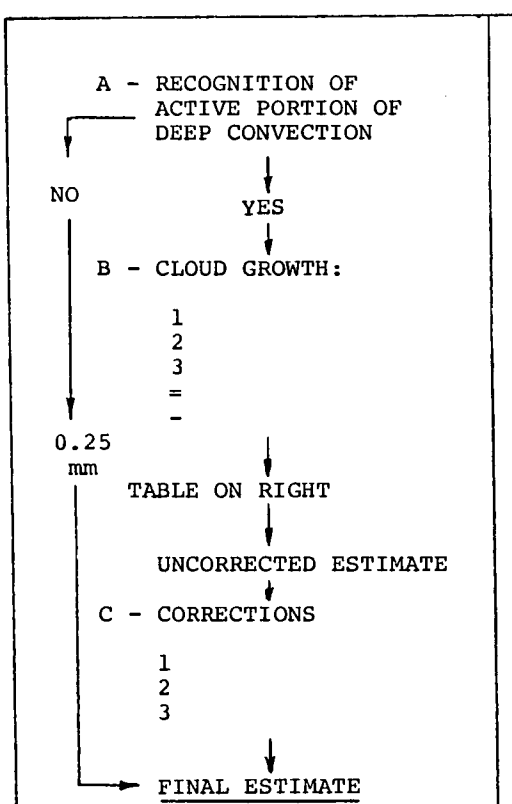

LEGEND:

REFER TO SECTION 3.1.3

GROWTH OF CLOUD IN A HALF HOUR IS SUCH THAT THE COLDEST CONTOUR DIAMETER

1 expands $>2/3^{o}$ lat.
2 expands $>1/3^{o}$ lat. but $\leq 2/3^{o}$ lat.
3 expands $\leq 1/3^{o}$ lat.
= remains the same
- contracts

CORRESTIONS FOR LOCAL OCCURRENCE OF

1 overshooting top
2 merging thunderstorms
3 convective cloud line mergers

FOR EACH OF THESE ADD 12.7 (mm) TO UNCORRECTED ESTIMATE TO GET FINAL ESTIMATE

TABLE:

PRECIPITATION ESTIMATES (mm)

CONTOUR COLOR	1	2	3	=	-
1975					
DARK GREY	12.7	3.1	3.8	2.5	0.3
LIGHT GREY	15.1	10.2	5.1	3.8	0.8
BLACK	25.4	15.2	7.6	5.1	1.3
WHITE	38.1	19.1	10.1	7.6	2.0
1976					
LIGHT GREY	10.1	5.1	3.8	2.5	0.3
DARK GREY	22.9	12.7	6.4	5.1	1.3
BLACK	27.9	17.8	10.2	7.6	2.0
WHITE	38.1	22.9	12.7	10.1	2.5

skill at satellite image interpretation. As well, this technique like the others discussed, does not explicitly allow for the movement of the storm cell over a region.

But, even more importantly, it is recognized that there would be great difficulty in transferring the use of this technique to more northerly latitudes with different rain-producing cloud regimes since it was derived empirically for deep convective cloud systems in tropical air masses. Nevertheless, the Scofield/Oliver technique does indicate which cloud top parameters are crucial to the estimation of rainfall, and this bespeaks the skill of these investigators in observing cumulonimbi and determining a workable empirical relationship.

3.2 Summary

All of these early precipitation estimation techniques focus on determining the rainfall from deep tropical convective systems. This is understandable because cumulonimbi are easy to identify and they are reasonably self-contained. Cheng and Rodenhius (1977) compare radar rain rates and satellite convective rainfall estimates based on visible cloud brightness or infrared temperature using relations such as those presented here. They note that although rainfall rates and satellite image brightness or coldness are related, quantitative differences in rainfall cannot be explained as being due to either bright or cold clouds. However, in suggesting that spatial and temporal

averaging would alleviate this, they missed the obvious deficiency common to these techniques: the need for a more physical basis relating the satellite image cloud characteristics (brightness, coldness, rate of growth) to the rainfall produced.

CHAPTER IV

THE MODEL USED TO DESCRIBE PRECIPITATING CLOUDS

Previous investigators (Scofield/Oliver, UW, and NHEML) identified in their techniques the crucial cloud top characteristics to be considered when estimating precipitation and they developed quantitative relationships for use with satellite images but their studies did not extend to what these characteristics were revealing about the dynamics of the cloud. Hence, there was no theoretical basis on which their techniques could be modified to encompass storm conditions over British Columbia.

4.1 Precipitation in British Columbia

There are three main types of air mass which bring rain to British Columbia. Warm, humid and relatively stable Maritime Tropical (mT) air with its origins in the tropics to the southwest occasionally reaches British Columbia in winter in the warm sector (or, more often in the upper levels of an occluded warm sector) of frontal waves and gives rise to major rainfalls. On the other hand, showery precipitation is often associated with Maritime Arctic (mA) air as it is warmed and moistened during its relatively short trip over the North Pacific from the Arctic landmasses of North America and Asia to British Columbia. Maritime Polar (mP) air has the same origins as mA air but with a longer trajectory over the ocean after which it reaches the coast from a more westerly direction. The charac-

teristics of precipitation within this air mass are intermediate between mT and mA air.

The mountain ranges of British Columbia are a formidable barrier to the eastward movement of air from the Pacific. The tendency of the air to produce rain is increased through lifting and the windward slopes receive among the world's largest annual amounts of precipitation. The climate along the coast is characterized by mild, humid winters and warm but not hot summers. The interior of British Columbia, which lies effectively in the rain shadow of the coastal mountains, is noted for hot and fairly dry summers punctuated by the occasional thunderstorm, and for cold winters with snow.

Weather systems affecting British Columbia, in general, originate to the west as depressions over the ocean and are usually in a mature state of development and well occluded before they reach the coast. Periods of showery weather within the mP air mass alternate with rainy spells along the fronts and occlusions. This prevails throughout the year, although during the summer months (June through August) the storms are fewer, less intense, and smaller in size. The actual centres of these disturbances generally do not cross the coast but rather fill and stagnate over the Aleutians or Alaska with only the associated fronts crossing the coast further south. The interior plateau region receives appreciable snowfall in winter

from these eastward moving fronts, while in summer much of the rainfall originates from thunderstorms. The fronts do not penetrate far into southern British Columbia leaving this region mainly clear and sunny. The annual pattern of precipitation in British Columbia is controlled chiefly by the position of the North Pacific sub-tropical anticyclone which migrates seasonally. During the summer months it is centered off the coast and deflects storm tracks northwards, while during the winter it shifts further south with the result that the storm tracks move southwards bringing more storms into the province.

In summary, precipitation in British Columbia falls almost exclusively from air of Pacific origin and annual precipitation is high along the coast diminishing towards the interior and deep valley floors increasing again along the windward slopes of the Rocky Mountains. Rain and snow fall chiefly in association with occlusions and fronts, except for summer thunderstorm contributions in the interior of the province. The distribution of this precipitation is highly subject to the local effects of relief. (Kendrew and Kerr, 1955; Hare, 1963; Hetherington, 1976).

4.2 The Model

A physical conceptual model used to estimate such rainfall from satellite images was developed by first considering the atmospheric conditions required for precipitation, and than examining the flux of water through a column of air in the atmosphere.

The expression for estimating the rainfall was derived to take advantage of the information about the motions and development of cloud systems provided by satellite images.

4.2.1 Rain-Producing Conditions

Mason (1971, 1975) in his work on cloud physics, discusses the conditions necessary for the formation of rain, which are: a source of moist air (like the mP air which flows into British Columbia), a mechanism for lifting (as provided by mountains or along fronts) and hence cooling the air so that condensation can occur, and a source of nuclei on which the moisture in the air can condense to form cloud droplets. If the droplets have enough time to reach a size where their terminal velocities exceed the lifting or updraft velocities in the cloud, then they will fall as rain and will reach the ground, provided they are not entirely evaporated during their descent.

Since the areal extent, intensity, and lifetime of a precipitating cloud system is controlled largely by the vertical air motions, rainfall can be distinguished as being one of two types depending on which lifting mechanism is dominant (Rogers, 1976). Widespread, continuous rainfall, of the type usually found on the coast of British Columbia, is associated with largescale ascent produced by fronts, topography, or large scale low level horizontal convergence. Localized showery pre-

cipitation, of the type usually occurring in the interior of British Columbia during the summer months, is associated with cumulus-scale convection in unstable air.

Regardless of the particular lifting mechanisms causing vertical motion, the air cannot continue to rise indefinitely. In the case of major storms, the tropopause acts as a limit to the upward movement of the air and at this level the air must spread out horizontally. The rising air is replaced by air converging at lower levels. By continuity the rate of air mass convergence at lower levels must equal the rate of rise which in turn must equal the rate of divergence (or spreading) at upper levels (for example, through the tops of clouds). The motion of air within a typical storm is shown schematically in Figure 4.1.

It has been generally noted that severe weather phenomena often occur with areas of upper level divergence (and associated lower level convergence), (Beebe and Bates, 1955; House, 1958; McNulty, 1977; and Schaefer, 1977). During the early 1950's several investigators (Cressman, 1954; Byers and Braham, 1948) tried to estimate the rainfall rate of thunderstorms by determining the vertical velocity from the horizontal near-surface winds (that is, the low level convergence of air into the base of the cloud). Danard (1975, 1978) used a similar approach to yield estimates of the 24-hour rainfall amounts for southern British Columbia. Although they were able to make reasonable estimates

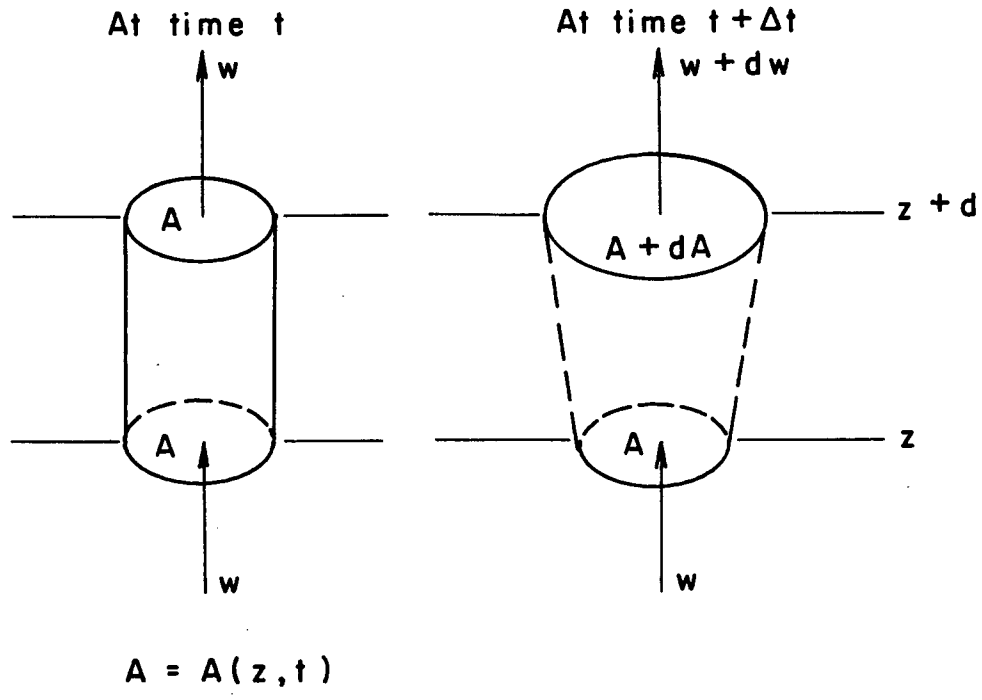

FIGURE 4.1

A Column of Air Between the Levels z and z+dz at Times t and t+dt

for a few storms, the technique was not considered feasible operationally due to the difficulty in measuring or estimating near-surface winds. It was also known that the vertical velocity could be determined if the horizontal winds at the top of the rising column could be measured. But that was even more difficult to do in practice. Now, however, horizontal divergence of the air mass can be estimated from successive images of cloud tops as sensed by geostationary meteorological satellites such as GOES. Adler and Fenn (1979a, b) have successfully used the approach to estimate the vertical velocities of thunderstorms although not to estimate the rainfalls from these storms. The theory for determining rainfall from the horizontal divergence of cloud tops as seen from GOES images is given below.

4.3 The Model Equations

Three sets of equations are needed to solve for the precipitation rate from a storm:

1 - the atmospheric thermodynamics equations

2 - the momentum equations

3 - the continuity equation.

The solution of the above three types of equations is difficult given the complex nature of atmospheric motions and the limited data available to describe these motions, unless various assumptions can be made to simplify the equations.

4.3.1 The Atmospheric Thermodynamics Equations

For an ideal gas the equation of state

$$p\alpha = RT \qquad 4.1$$

and the first law of thermodynamics

$$\mathring{H}\, dt = c_v dT + p d\alpha \qquad 4.2$$

relate the pressure p and specific volume α to the temperature T of the air. $\mathring{H}$ is the rate at which external heat is added per unit mass of air, and c_v is the specific heat of air at constant volume. The first law of thermodynamics, equation 4.2, states that the external heat added to the air from such processes as condensation, radiation and conduction is equal to the change in internal energy of the air mass ($c_v dT$) plus the work done by the air mass on its surroundings ($pd\alpha$). If no external heat is added, $\mathring{H} = 0$, then the motion of the air mass is said to be adiabatic. For midlatitude synoptic scale systems the external heating term $\mathring{H}\, dt$ is small in comparison with the other terms and hence the system motions are considered to be approximately adiabatic. The equation of state, equation 4.1, along with $c_p = c_v + R$, where c_p is the specific heat at constant pressure, can be used to rewrite the first law of thermodynamics as

$$\mathring{H}\, dt = c_p dT - \alpha dp \qquad 4.3$$

The change in temperature with pressure can then be given as

$$\frac{\dot{H}}{c_p}\frac{dt}{dp} + \frac{\alpha}{c_p} = \frac{dT}{dp} \qquad 4.4$$

This result will be used later to relate the change in temperature to the change in altitude.

4.3.2 The Momentum Equations

The changes in the velocity field with time are given by the momentum equations written in spherical coordinates using Holton's (1972, p28) notation

$$\frac{du}{dt} = \frac{uv\tan\phi}{a} - \frac{uw}{a} - \frac{1}{\rho}\frac{\partial p}{\partial x} + 2\Omega v\sin\phi - 2\Omega w\cos\phi + Fx \qquad 4.5$$

$$\frac{dv}{dt} = \frac{-u^2\tan\phi}{a} - \frac{vw}{a} - \frac{1}{\rho}\frac{\partial p}{\partial y} - 2\Omega u\sin\phi + Fy \qquad 4.6$$

$$\frac{dw}{dt} = \frac{u^2 + v^2}{a} - \frac{1}{\rho}\frac{\partial p}{\partial z} - g + 2\Omega u\cos\phi + Fz \qquad 4.7$$

where u, v, w are the eastward, northward and vertical components of the velocity, a is the radius of the Earth, ϕ is the latitude, ρ is the density, p is the pressure, Ω is the angular velocity of the Earth, and Fx, Fy and Fz are the eastward (x), northward (y), and vertical (z) components of friction. Holton (1972, chapter 2, section 4) uses scale analysis to reduce the above equations to those below by neglecting those terms with orders of magnitude less than 10^{-4} m/s^{-2}

$$\frac{du}{dt} \simeq 2\Omega v \sin\phi - \frac{1}{\rho}\frac{\partial p}{\partial x} \qquad 4.8$$

$$\frac{dv}{dt} \simeq -2\Omega u \sin\phi - \frac{1}{\rho}\frac{\partial p}{\partial y} \qquad 4.9$$

$$-\frac{1}{\rho}\frac{\partial p}{\partial z} \simeq +g \qquad 4.10$$

Equation 4.10 implies that motions in synoptic scale systems are approximately hydrostatic and that the vertical velocity cannot be determined directly from the vertical momentum equation. Since the vertical motion is of primary interest in the estimation of rainfall, it must be determined indirectly from the continuity equation.

4.3.3 The Continuity Equation

The continuity equation

$$\frac{1}{\rho}\frac{d\rho}{dt} + \nabla\cdot\vec{V} = 0 \qquad 4.11$$

states that the fractional increase in the density ρ following the motion is equal to minus the divergence of the velocity $\vec{V}$.

4.4 The Continuity Equation Used to Estimate Rainfall

During the exploratory development of the satellite rainfall estimation technique the equation of continuity in a form suggested by McIntosh and Thom (1973, chapters 5 and 8), and Wallace and Hobbs (1977, chapter 8) was considered to describe

the rainfall rate from cloud systems. A similar expression was proposed by Viezee *et al.*, (1980) for estimating the moisture budget of cyclones using microwave data.

The rate of precipiation $\frac{dP}{dt}$ is given by

$$\frac{dP}{dt} = wc \cdot w - E \qquad 4.12$$

where w is the vertical velocity of the air being lifted, wc is the water content of the air, and E is the evaporation rate. Wc•w represents the rate at which water enters the base of the cloud and is lifted. This minus losses due to evaporation yields the rainfall rate. Equation 4.12 assumes that all the water which enters a cloud either falls as rain or is evaporated. In practice, not all of the moisture entering a cloud is precipitated. Appreciable amounts are retained within the air mass as water vapor. A factor e can be introduced into equation 4.12 to allow for moisture retention. Rewriting equation 4.12 yields

$$\frac{dP}{dt} = e \cdot wc \cdot w - E \qquad 4.13$$

where e is the fraction of water which falls as rain. In some literature this fraction is taken as a measure of the efficiency of the storm. In equation 4.2, e represents an adjustment factor which can only be determined empirically on the basis of

experience. The water content wc (g/m^3) of the air mass can vary with temperature and location. On the basis of current spatial and temporal observations (such as those from TIROS-N) the water content, for a given air mass over a particular location, changes very gradually and may be assumed constant throughout a storm. The rate of evaporation E is negligible during a rainfall and can be neglected. Then equation 4.13 becomes

$$\frac{dP}{dt} = e \cdot wc \cdot w \qquad 4.14$$

4.4.1 Estimating the Vertical Velocity w

The following discussion focusses on estimating the vertical velocity w. The conservation of mass relates the vertical and horizontal motion fields and can be used to estimate the vertical velocity (Holton, 1972). The horizontal divergence of the cloud top as revealed by satellite images is directly related to the vertical velocity of air entering the cloud.

Consider a parcel of air within the cloud, with cross-sectional area which may be a function of altitude and time, ie. A=A(z,t), confined between the levels z and z+dz, and which has a density ρ. (See Figure 4.1). The mass of this air parcel is

$$M = \rho A dz \qquad 4.15$$

Although the shape of the parcel changes with time, the mass of the parcel is conserved following the motion of the parcel, that is $\frac{dM}{dt} = 0$. In other words

$$\frac{d}{dt}(\rho A dz) = 0 \qquad 4.16$$

The change in density of the air $\frac{1}{\rho}\frac{d}{dt}$ ($O \sim 10^{-6}$ S^{-1}) is generally small relative to the terms $\frac{1}{A}\frac{dA}{dt}$ ($O \sim 10^{-5}$ S^{-1}) and $\frac{dw}{dz}$ ($O \sim 10^{-5}$ S^{-1}), (Fleagle, 1946) and may be ignored. For a flow volume (Figure 4.1) which is hald constant in the z direction, so that net inflow is calculated as a function of z, but which is permitted to expand in the horizontal plane, so that no flow crosses the moving boundary, the equation of continuity can be written as:

$$\frac{1}{A}\frac{dA}{dt} + \frac{dw}{dz} = 0 \qquad 4.17$$

$\frac{1}{A}\frac{dA}{dt}$ is the definition of the horizontal divergence of the velocity $\nabla_H \cdot \vec{V}$. By rearranging and integrating equation 4.17 with respect to the altitude z gives the vertical velocity in terms of the horizontal divergence (or spreading).

$$\int_{z_2}^{z_3} dw = -\int_{z_2}^{z_3} \frac{1}{A}\frac{dA}{dt}\, dz \qquad 4.18$$

where z_2 and z_3 (see Figure 4.2) define the thickness of the diverging layer between the level of zero divergence z_2 and

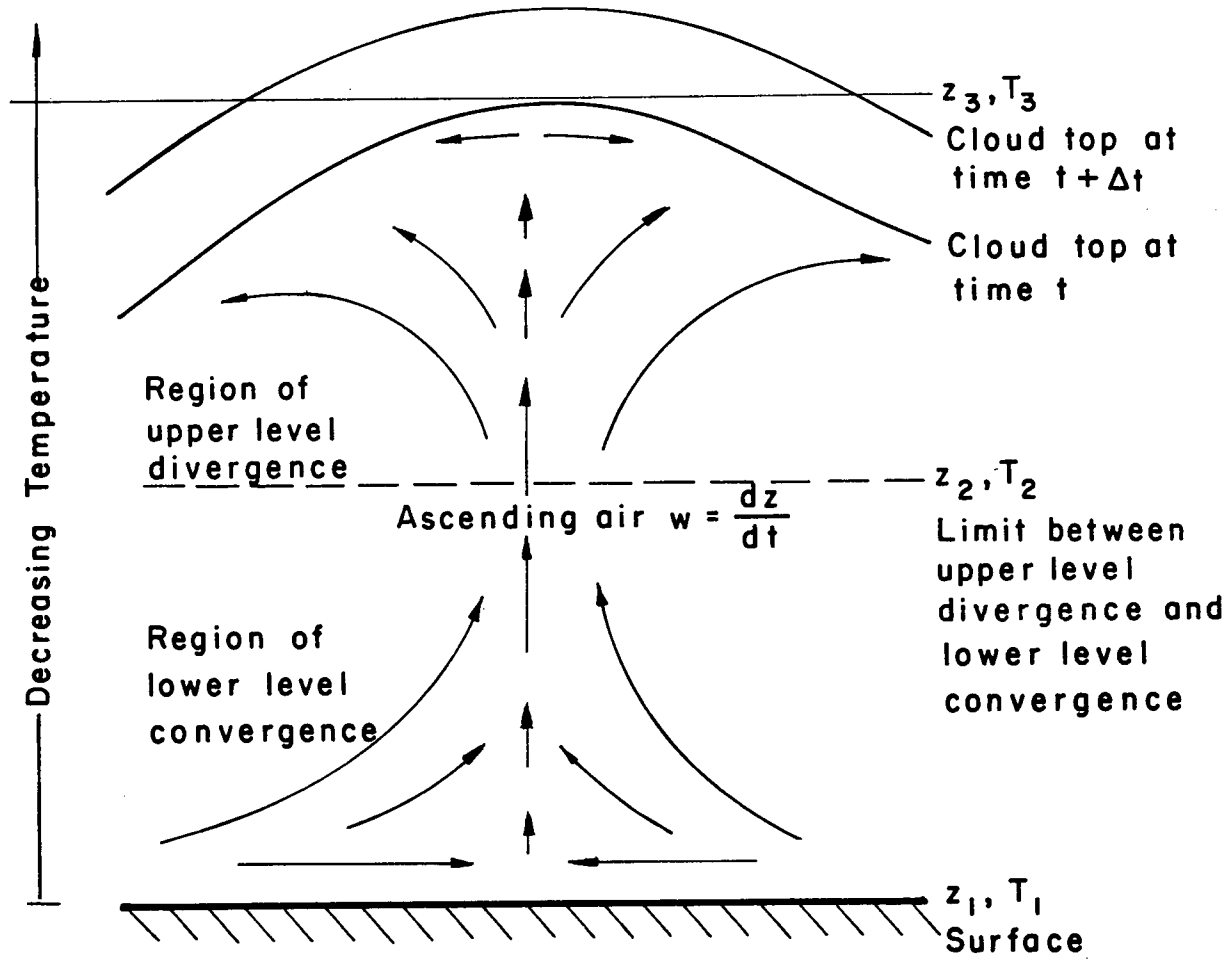

FIGURE 4.2

Schematic Diagram of Air Circulation During a Major Storm. (The horizontal scales of such storms are $O \sim 10^5 - 10^7$m , while the vertical scales are $O \sim 10^4$m.)

the tropopause or the top of the cloud, z_3. Equation 4.18 gives the change in the vertical velocity of the air between the tropopause or top of the cloud and the level of non-divergence. If the vertical velocity at the tropopause is considered zero then the velocity into the cloud at the level of non-divergence is

$$w(z_2) = \int_{z_2}^{z_3} \frac{1}{A} \frac{dA}{dt} \, dz \qquad 4.19$$

4.4.2 Rewriting the Continuity Equation

Substituting the expression for the vertical velocity (equation 4.20) into the equation for the rainfall rate (equation 4.14) yields

$$\frac{dP}{dt} = e \cdot wc \int_{z_2}^{z_3} \frac{1}{A} \frac{dA}{dt} \, dz \qquad 4.20$$

Equation 4.20 needs to be modified still further. The enhanced infrared satellite images contain the temperature of the cloud top as well as the areas of the temperature contours. Comparison of a succession of satellite images also gives the change in the cloud top area in time. It is a difficult matter to measure the altitudes of the cloud tops and to determine the level of zero divergence (the limits of integration in equation 4.20). Using the first law of thermodynamics (equation 4.4) and the assumption that the vertical motions are approximately

hydrostatic (equation 4.10), the decrease in temperature T with increasing height z can be written

$$-\frac{dT}{dz} = -\frac{\dot{H}}{Cp}\frac{dt}{dz} + \frac{\rho g \alpha}{Cp} \equiv \gamma \qquad 4.21$$

which is defined as the lapse rate γ.

Using equation 4.21 the limits of integration can be changed from altitudes z to temperatures T which can be immediately determined from the satellite imagery. So the rainfall rate (equation 4.21) can be written

$$\frac{dP}{dt} = \frac{e \cdot wc}{\gamma} \int_{T_2}^{T_3} \frac{1}{A}\frac{dA}{dt}\, dT \qquad 4.22$$

where T_3 is the temperature of the cloud top and T_2 is the temperature of the air at the level of zero divergence.

4.5 Adaptations for Use With Satellite Images

A number of modifications are made to equation 4.22 before estimates of rainfall can be made from satellite images. First of all, the temperature at the level of non-divergence is assumed to be reasonably constant throughout a storm.

The second adaptation involves the average divergence determined from the integral term $\int_{T_2}^{T_3} \frac{1}{A}\frac{dA}{dt}\, dT$, recalling that the area is a function of both temperature T and time t, A=A(T,t). In order to evaluate the integral it is necessary to

know how the cross-sectional area of the cloud changes at each temperature level T. In practice this is not known and likely varies from storm to storm depending on the energetics of the storm; however, the satellite images do show from one image to the next, the change in the cross-sectional area of the cloud at discrete temperature levels. Ideally, as the number of temperature levels contrasted by enhancement of the infrared images increases, the closer these discrete areas approximate the true (continuous) variation of the cloud cross-sectional area with temperature level T. Present enhancements, however, distinguish only a few temperature levels. For frontal systems in which the uplifting of one air mass over another is widespread and gradual, the coldest contour of the individual precipitating cells along the front may be the only one which is separable on the satellite infrared image, the warmer contours of the individual cells having all joined together. The rainfall rate, therefore, usually can only be estimated from the divergence determined at the coldest temperature level T_3 on the satellite image.

4.5.1 Relation Between Average Divergence and Coldest Contour Divergence

Reducing equation 4.22 to an expression for rainfall in terms of the average divergence in the layer between T_2 and T_3

$$\frac{dP}{dt} = - \frac{e \cdot wc}{\gamma} \overline{\frac{1}{A} \frac{dA}{dt}} (T_3 - T_2) \qquad 4.23$$

where the overbar denotes averaging with respect to temperature

T, allows the rainfall rate to be estimated from the divergence of the coldest contour. The divergence term can be taken outside the integral if it is similar, so that the process is essentially non-dimensional, in which case the mean, the maximum, or the divergence at any particular level can be used in place of the average divergence in eqaution 4.23.

The coldest contour divergence can now be shown to be a reasonable first approximation to the average divergence, given that only two pieces of information about the behaviour of the cross-sectional area are generally known and they are:

1 - at the level of non-divergence T_2 the divergence is by definition zero:

$$\frac{1}{A(T_2,t)} \quad \frac{dA(T_2,t)}{dt} = 0 \qquad 4.24$$

2 - at the cloud top level T_3 the divergence is

$$\frac{1}{A(T_3,t)} \quad \frac{dA(T_3,t)}{dt} = K \qquad 4.25$$

where K is the divergence measured from satellite infrared images.

4.5.2 <u>One Proposed Divergence Function</u>

One simple function relating the behaviour of the divergence $\frac{1}{A(T,t)} \frac{dA(T,t)}{dt}$ to the temperature level T can be shown to have an average value which is proportional to the divergence at the coldest contour level T_3. For example, consider the diver-

gence $\frac{1}{A(T,t)} \frac{dA(T,t)}{dt}$ as a function of temperature T of the form

$$\frac{1}{A(T,t)} \frac{dA(T,t)}{dt} = f_1 + f_2 T^n \qquad 4.26$$

where f_1 and f_2 are constants to be determined from the two boundary conditions above. This function can be shown to have a mean value

$$\overline{\frac{1}{A(T,t)} \frac{dA(T,t)}{dt}} =$$

$$K \frac{1}{(T_3-T_2)} \frac{1}{(n+1)} \frac{T_3^{n+1} - (n+1)T_2^n T_3 + nT_2^{n+1}}{T_3^n - T_2^n} \qquad 4.27$$

which is directly proportional to the divergence K at level T_3.

Assuming that the behaviour of the divergence with temperature can be approximated by the function suggested above, then the rainfall rate can be estimated satisfactorily using:

$$\frac{dP}{dt} \simeq -\frac{e \cdot wc}{\gamma} \frac{1}{A(T_3,t)} \frac{dA(T_3,t)}{dt} \int_{T_2}^{T_3} dT \qquad 4.28$$

or

$$\frac{dP}{dt} \simeq -\frac{e \cdot wc}{\gamma} \frac{1}{A(T_3,t)} \frac{dA(T_3,t)}{dt} \Delta T \qquad 4.29$$

where $\Delta T = T_3 - T_2$ is the temperature difference from the level of zero divergence to cloud top.

For ease in programming, equation 4.29 is integrated with respect to time to give the change in rainfall dP from time t to t+dt:

$$dP = -\frac{e \cdot wc}{\gamma} \int_{t}^{t+dt} \frac{1}{A(T_3,t)} \frac{dA(T_3,t)}{dt} \Delta T \, dt \qquad 4.30$$

$$= -\frac{e \cdot wc}{\gamma} \ln \left[\frac{A(T_3,t+dt)}{A(T_3,t)} \right] \Delta T \qquad 4.31$$

(Appendix B contains a brief sensitivity analysis of the rainfall estimation relation.)

4.5.3 The Rainfall Estimation Equations

The amount of rain ΔP falling in the time interval Δt can be estimated from the discrete series of satellite images using

$$\Delta P = -\frac{e \cdot wc}{\gamma} \Delta T \ln \left[\frac{A(T_3, t+\Delta t)}{A(T_3, t)} \right] \qquad 4.32$$

with $A(T_3, t) > 0$

In the case where the coldest cloud top contour is not present until the second satellite image, that is $A(T_3, t) = 0$, the expression in equation 4.31 is undefined. The discrete form of equation 4.29 is used to provide as estimate of the amount of precipitation ΔP falling in the first time interval Δt:

$$\Delta P = -\frac{e \cdot wc}{\gamma} \frac{A(T_3, t+\Delta t) - A(T_3, t)}{0.5(A(T_3, t+\Delta t) + A(T_3, t))} \Delta T \qquad 4.33$$

or

$$\Delta P = -\frac{e \cdot wc}{\gamma} 2 \Delta T \qquad 4.34$$

for $A(T_3, t) = 0$

Equations 4.32 and 4.34 form the basis of the computer routine which computes the precipitation amounts from satellite picture data.

4.6 Consequences of the Model

There are three consequences of the rainfall estimation model. First, it is postulated that rain falls from only those cloud cells which are actively growing in time as evidenced in the spreading of the coldest cloud top contour from one satellite image to the next. This is reasonable although some larger cells which are decaying often continue to deposit reducing amounts of rain. However, this rainfall is not considered to be a significant portion of the overall storm total.

The second consequence is that no rain falls for those clouds which are below the chosen level of zero divergence. This means that rainfall from some clouds below this level will not be accounted for in the analysis of the satellite images. This cannot be avoided at present due to the limitations of the enhancement schemes being used on the infrared images. The model is however, general enough to be useful for analyzing these lower level clouds when an appropriate enhancement scheme which contrasts the small temperature gradients of these clouds becomes available. It should be pointed out, however, that those cells which reach near tropopause heights of vertical development are likely to result in the heaviest rainfalls over an area.

The third consequence of the model lies in the manner in which the spatial distribution of rainfall from a storm cell is obtained. Because the average divergence of the cell has been

shown to be proportional to the divergence of the coldest contour for two general divergence functions, then the rainfall from a particular temperature contour T_i is proportional to the thickness ΔT of the diverging layer under that contour T_i which is $\Delta T=T_i-T_2$ (where T_2 is the level of non-divergence). For contours other than the coldest one, the rainfall is found using $\Delta T=T_i-T_2$ in the appropriate model equation (either 4.32 or 4.34).

4.7 The Other Model Parameters

The area and temperature parameters can be obtained from the satellite infrared pictures. That leaves the water content wc, the lapse rate γ, and the efficiency e to be determined. Ideally, the best choice of values for these parameters would be observed values. In practice, however, it may be necessary to rely on other sources of data. These are discussed below.

4.7.1 Water Content wc

The water content is the total amount of moisture in an air column that is available for precipitation. The literature shows a wide range of values of wc varying with the cloud type. Table 4.1 shows a summary of water content values obtained from published material. Water content can be determined from values of the precipitable water which are reported every six hours by the polar-orbiting satellite TIROS-N. Table 4.2 shows a sample printout of TIROS-N data. As well, water content can be determined from relative humidity observations at nearby upper air weather stations.

TABLE 4.1 Average Efficiencies and Water Content

Cloud Type	Efficiency e (as a fraction)	Water Content wc (g/m^3)
Seafog	---	0.10
Stratus	0.05	0.35
Orographic (Hawaii)	0.05-0.10	0.35
Small Cumulus	0.10	0.5-1.4
Cumulus Congestus	0.15	1.0
Cumuloniumbus	0.20-0.30	2.0-10.0

(from MASON, 1971, 1975; FLETCHER, 1962; ROGERS, 1976)

TABLE 4.2 Portion of Typical Output of TIROS-N (TUXN) Precipitable Water (PCW) and Other Data for Various Levels in the Atmosphere. (Received by the Pacific Weather Centre from NESS Satellite Data Services Division, Washington, D.C.)

RETRIEVAL OF TUXN DATA 3 HRS BFR AND AFT OOZ 05 DECEMBER (1979)
NOTE: % IS CONFIDENCE VALUE IN READINGS
AMOUNT OF CLOUD (CL) IN %, AVG CLOUD TOP (ACT) IN MB
THICKNESS (THKS) IN DECAMETERS
PRECIPITABLE WATER (PCW) IN MILLIMETERS
SURFACE TEMP(SFT), TROPOPAUSE TEMP (TRT)

DATM	LAT	LONG	850 MB	700 MB	500 MB	400 MB	300 MB	250 MB	CL	ACT	SFT	TRT
0500Z	28N	140W---							48	400		
90%:THKS	FM1000MB		136	294	558	724	928	052				
90%:PCW	FM1000MB			013	016		017					
											019	//
.												
.												
.												
0500Z	34N	136W---							93	294		
70%:THKS	FM1000MB		135	294	560	729	935	060				
70%:PCW	FM1000MB			016	022	024						
											017	//
0500Z	35N	132N---							19	300		
90%:THKS	FM1000MB		137	297	564	733	940	064				
90%:PCW	FM1000MB			017	021		022					
											018	//
.												
.												
.												

TABLE 4.2 (continued)

DATM	LAT	LONG	850 MB	700 MB	500 MB	400 MB	300 MB	250 MB	CL	ACT	SFT	TRT
0500Z	42N	137W---							10	441		
90%:THKS	FM1000MB		133	291	555	723	928	051				
90%:PCW	FM1000MB			008	009	010						
											011	//
0500Z	42N	130W---							09	306		
60%:THKS	FM1000MB		133	290	553	719	923	047				
60%:PCW	FM1000MB			007	008		009					
.											012	//
.												
.												
0500Z	45N	142@---							18	661		
70%:PCW	FM1000MB			011	014		015					
											005	//
0500Z	46N	136W---							29	750		
90%:PCW	FM1000MB			011	014		015					
.											009	//
.												
.												
0500Z	64N	144W---							42	506		
90%:PCW	FM920MB			002	003		004					
											M15	//
0422Z	62N	126W---							37	432		
90%:THKS	FM780MB			081	326	481	673	794				
90%:PCW	FM780MB			001	002		003					
											M15	//

4.7.2. The Lapse Rate γ

The lapse rate γ can be assumed equal to the saturated adiabatic lapse rate $\gamma = \gamma_s \simeq 5^{o}C/1000m$ which is a reasonable assumption during a rainfall. Alternately, the actual environmental lapse rate $\gamma = \gamma_{env}$ as recorded from radiosonde ascents can be used.

4.7.3. Adjustment Factor e

The parameter e is an empirical adjustment factor that some investigators have linked to the actual efficiency of a cloud in producing rain. The literature indicates a wide range of values for e depending on cloud type and varying significantly within each cloud type. Since various investigators have tended to define e and wc differently, values for these parameters often occur in pairs consistent with the definition employed.

Because in this model e is an empirical adjustment factor it can be used to take into account uncertainties in the other parameters. Consider the situation of a storm raining over a region which has a number of stations only one of which is able to provide values for the water content and the lapse rate, along with the observed precipitation ΔP_{obs} from the raingauge or radar located at this station. A calculation of the ratio

$$e = \frac{\Delta P_{obs}}{\frac{wc}{\gamma} \ln \left[\frac{A(T_3, t+\Delta t)}{A(T_3, t)} \right]} \qquad 4.35$$

yields a value for e which contains both the difficult to determine "efficiency" of the cloud, and the uncertainty in the other parameters. This value of the efficiency e could well serve as the best initial estimate of e for all of the stations in the region.

Once the efficiency e, water content wc and lapse rate γ have been chosen for each station they are assumed to remain constant throughout the storm. This is considered to be a reasonable assumption since the characteristics of the airmass over the station change very slowly during the storm. (The uncertainty in the precipitation that this assumption introduces is accounted for in the updating routine discussed in Chapter 7).

4.8 Summary

A brief discussion of the conditions necessary for precipitation to occur pointed towards a physical-conceptual model which considers the precipitation process in terms of the flux of water through an air column. The vertical velocity could be determined from the lower level convergence of air into the column - an approach that was used by several researchers to estimate rainfall but was never exploited operationally due to the difficulties involved in determining the lower level winds. Satellite images, however, provide the means for determining the upper level divergence which can be used as a basis for estimating the vertical velocity. The cloud itself is treated as a tracer of

the motions of the atmosphere of which it is a part. The model (equations 4.32 and 4.34) was developed keeping in mind the information satellite images provide.

CHAPTER V

COMPUTATIONAL PROCEDURE

FOR ESTIMATING RAINFALL FROM SATELLITE IMAGES

The analysis of rainfall events using GOES images involves a difficult exercise in bookkeeping to keep track of the essential image parameters describing the storm, especially if the storms are major ones containing many individual cells, which appear, grow and decay as they move over an area. Figure 5.1 defines the image terms used in this study. Computer routines to facilitate the calculations of the rainfall estimates were developed during the course of the analysis of the first major storm.

5.1 Conceptual Procedure

Estimating rainfall from GOES infrared images was accomplished through a computer-user interactive process which is flowcharted in Figure 5.2, with each of the steps discussed briefly below.

The first step in the process was to obtain the half-hourly GOES satellite images. These can be obtained either through a loan arrangement with the Atmospheric Environment Service, the Pacific Weather Centre (or local weather centre), via a GOES-Tap link, or through direct reception of the satellite signal. The

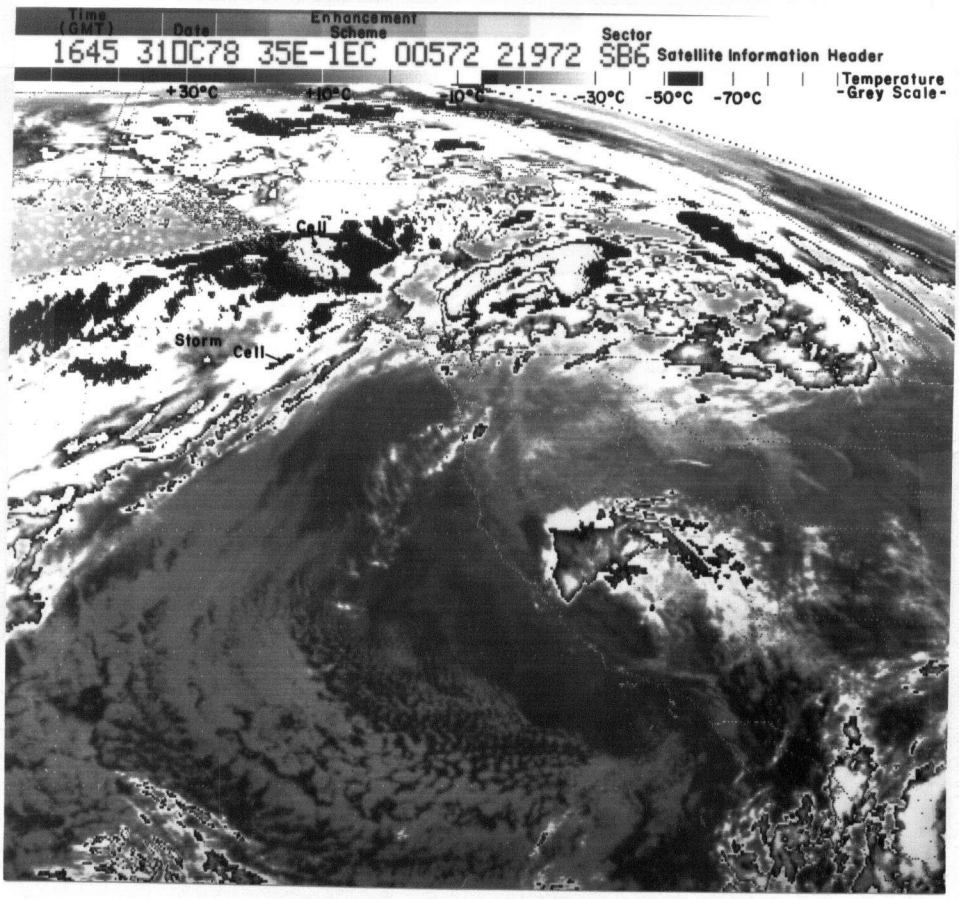

FIGURE 5.1

Explanation of the Various Terms used to Describe GOES Infrared Cloud Images:

CELL - The Coldest Self-Contained Cloud Top Contour and Its Immediately Surrounding Warmer Contours.

STORM - The Cloudy Area on the Satellite Image Which Brings Rain into an Area. It is usually made up of one or more cells.

FIGURE 5.2 Steps followed to make estimates of rainfall from GOES satellite images.

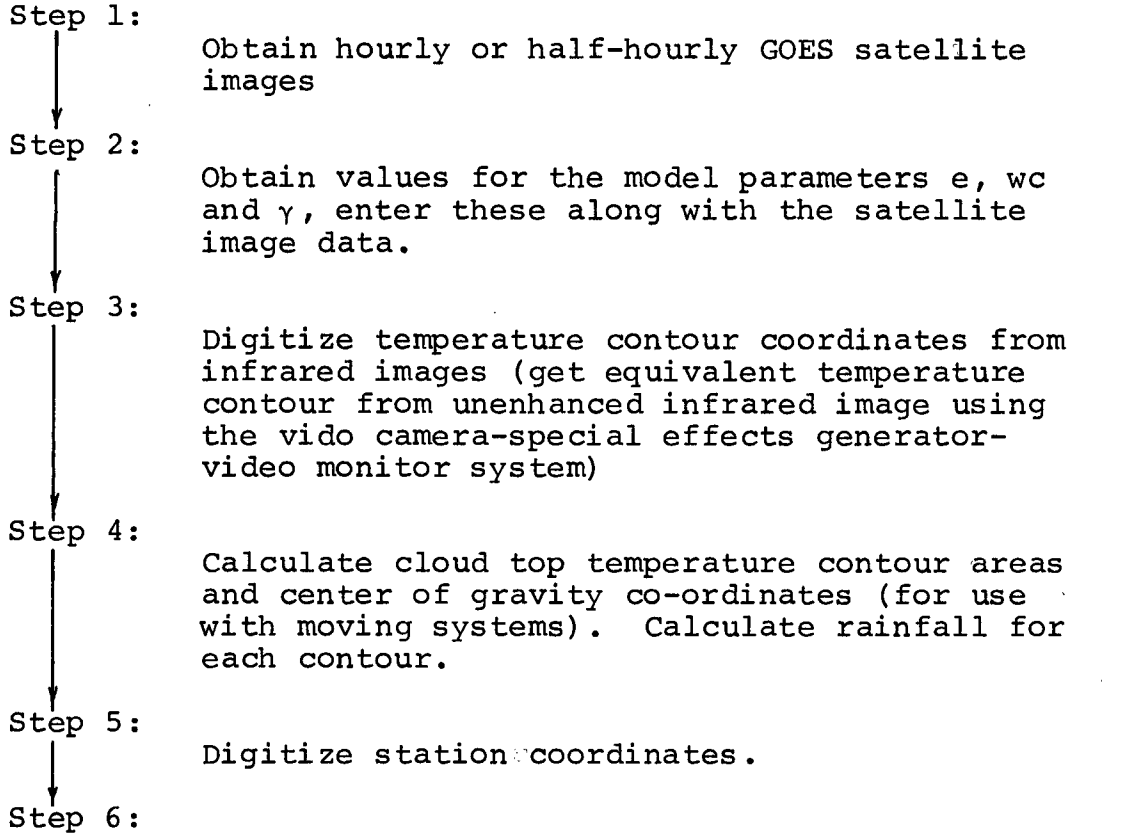

satellite images used in this study were provided by the Pacific Weather Centre in Vancouver, British Columbia.

The second step involved the choice of the rainfall estimation model parameters, the water content wc, the lapse rate γ , and the adjustment factor e, as discussed in section 4.7.

The next major step and the first involving the use of a computer routine, was to input the storm information including a storm cell identification number, the time the satellite image was taken, the enhancement scheme used, the sector used, and the temperature contour level, and then to digitize the individual cell cloud top temperature contours. A Tektronix digitizing tablet, Figure 5.3, linked by a time-sharing computer terminal to the University of British Columbia's Amdahl 470 V/6 model II computer system (Leigh and Duke, 1978) was used to digitize the perimeter of the cloud top temperature contours and store the coordinates for use in the subsequent steps. This was a straightforward procedure in those instances where the infrared image had been enhanced, that is, if the temperatures had been scaled in discrete grey scales making identifiable temperature contours. However, the availability of these enhanced images is intermittent especially when visible or unenhanced images are being received instead. There is an additional difficulty at times when more than one enhancement scheme is in use during the day. Direct reception and enhancement of the satellite image eliminates these problems, although, for most users this is not possible.

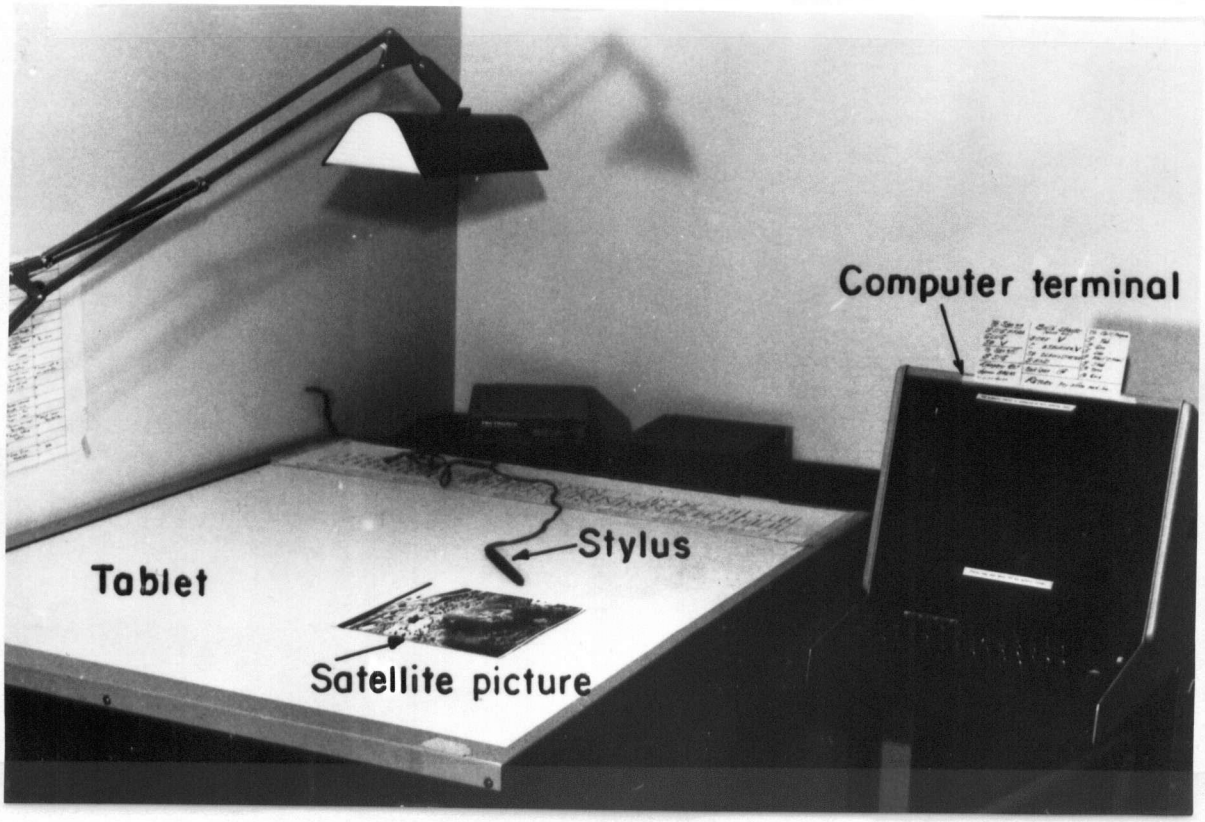

FIGURE 5.3

The Tektronix Digitizing Tablet - Remote Computer Terminal Arrangement. The Infrared Satellite Image is Placed on the Tablet and the Temperature Contours are Traced using the Stylus.

Therefore, to supplement the enhanced images and to fill in the gaps, unenhanced images were first analyzed using equipment within the Civil Engineering Department at the University of British Columbia which included a video camera, a special effects generator and a video monitor. The special effects generator, Figure 5.4, allowed blacking out the grey shades (representing different temperatures) below any particular level of brightness. By successively blacking out darker shades of grey, temperature contours could be shown on the video monitor screen, Figure 5.5. These were traced and digitized. Figure 5.6 shows the video camera-special effects generator-video monitor arrangement.

The digitized contours were used as input to the computer routine which calculated their areas, as well as their centre of gravity coordinates for use in estimating the precipitation that falls at a point from a moving cloud system. The centre of gravity of the coldest contour was also computed and used as an indicator of the movement of the cloud cell between successive satellite images. All of this information was written onto the computer files that served as input files for the next step in which the rainfall was estimated for each contour using the model equations 4.32 and 4.34. This allowed contours of rainfall from individual cells to be presented every half-hour if required.

In the next step the station locations of interest were mapped by the user onto a satellite image grid and then their

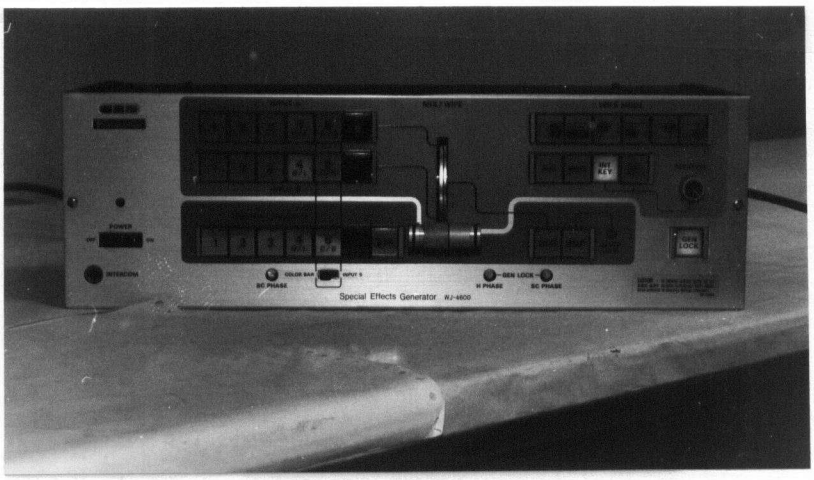

FIGURE 5.4

The Panasonic WJ-4500 Special Effects Generator Used to Determine Temperature Contours from Unenhanced Infrared Satellite Images.

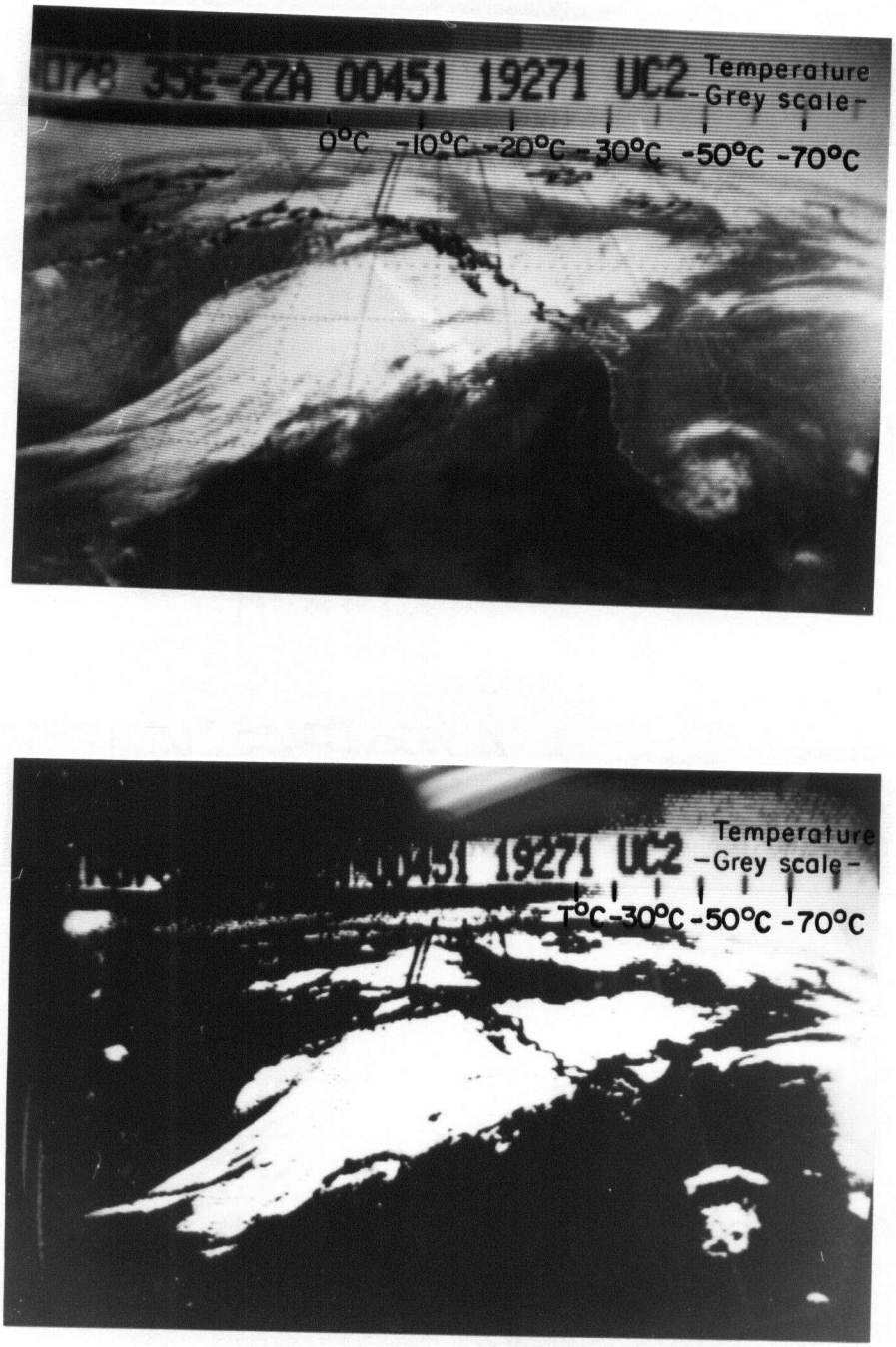

FIGURE 5.5

The top photo shows the satellite image as seen on the video monitor before the special effects generator is engaged. The second photo shows the satellite image as seen on the video monitor after the special effects generator is engaged. Those clouds warmer than $T^{\circ}C$ on the temperature-grey scale have been shown as black areas while those colder than $T^{\circ}C$ are shown as lighter areas. The boundary between the two is the $T^{\circ}C$ contour.

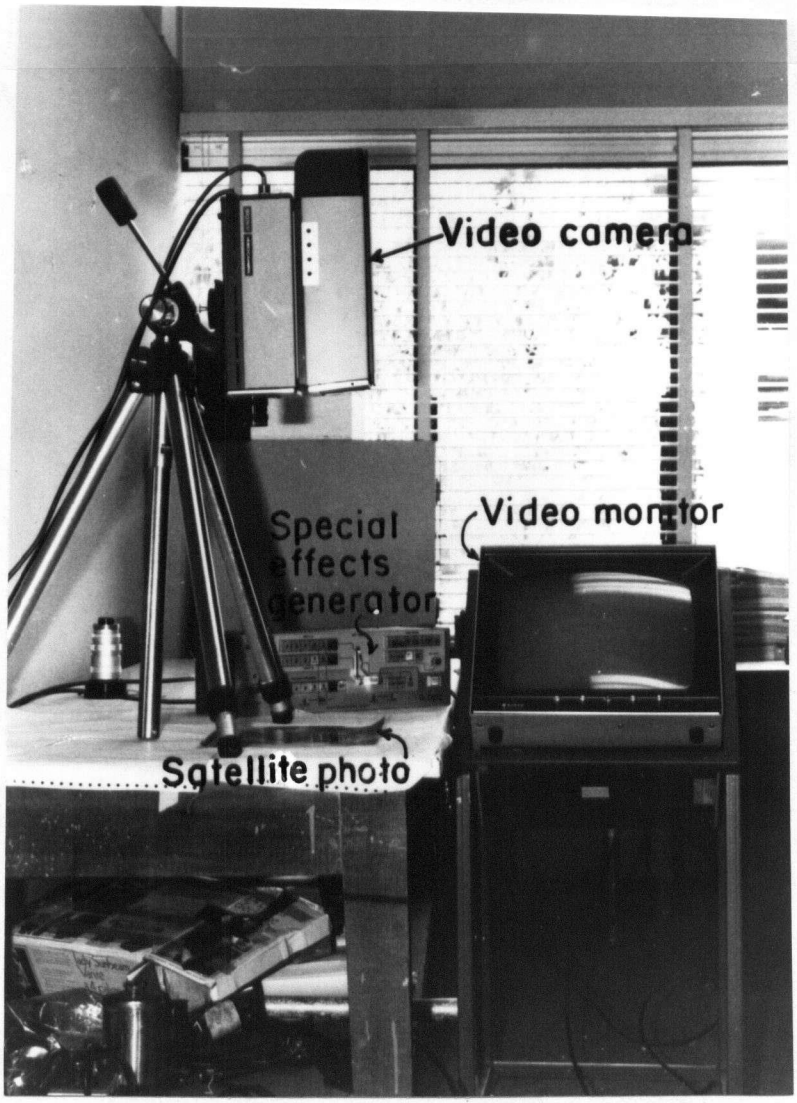

FIGURE 5.6

The Video Camera - Special Effects Generator-Video Monitor Arrangement used to Determine Temperature Contours from GOES Unenhanced Infrared Images.

coordinates were digitized using the digitizing tablet as before. This was a one time operation in preparation for calculating the rainfall at these stations. The coordinates were used by the computer routine which determined the movement of the storm cell or cells past the station and interpolated for rainfall should the station location lie between rainfall contours.

5.1.1 Movement of Storm Cells Near A Station

Since the satellite images form a series of "snap-shots" of a continuously changing process the effect on the rainfall due to the movement of storm cells near a station was handled in the following manner. Figure 5.7 shows a situation which represents the positions of a cloud top temperature contour as seen in two successive satellite images, separated by a time interval Δt. From this it would seem that Station 1 apparently does not receive any rainfall since it lies outside the cloud contour in both satellite images. However, it is clear that part of the storm cell passed over Station 1 leaving some rain as it did. To account for this effect caused by the movement of the cell, the centre of gravity of the cell at the second time is shifted back to the mid-point of the line which indicates the displacement of the centre of gravity so that the cell appears in the position shown in Figure 5.8.

If more than one cell passed near the station the procedure was essentially the same. The computer routine

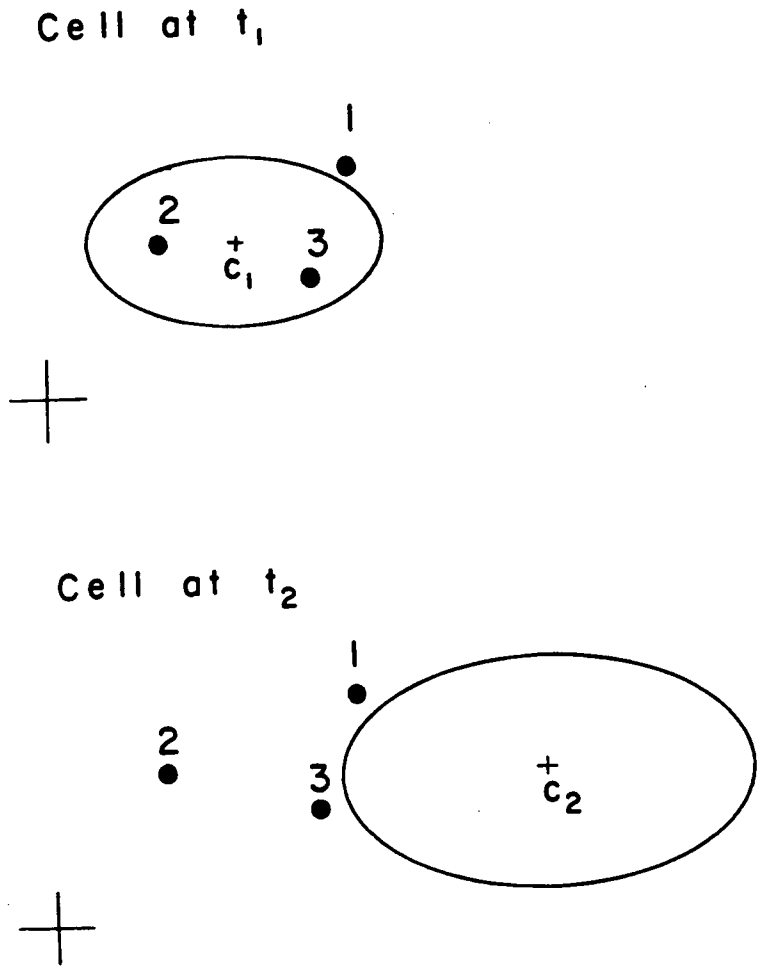

FIGURE 5.7

A Schematic Representation of One Storm Cell Contour as it Moves over 3 Rainfall Stations Between Times t_1 and t_2 . The Displacement of the Centre of Gravity during this Time is from C_1 to C_2. From these "Snap-Shot" views, Station 1 appears not to have received any Rainfall.

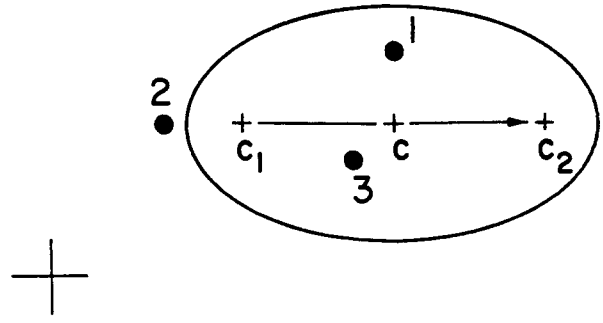

FIGURE 5.8

The Cell's Position at Time t_2 is Shifted Back Half the Displacement so that its Centre of Gravity is at Position C.

searched for those two cells whose centres of gravity were closest to the station and yet not to the east of the station on the first satellite image. Because of the generally eastward movement of the storms, those cells to the east of the station had already contributed to the station's rainfall in previous time intervals. Again the cells' centres of gravity were shifted back to the mid-point of the line joining their positions at the beginning and end of the time interval. This is illustrated schematically in Figure 5.9.

Should the station in its new position lie between contours, the interpolation for rainfall was performed by the University of British Columbia Computing Centre library routine XPAND.S (UBC Computing Centre, 1979) which was modified somewhat to suit the purpose at hand. This routine uses a heuristic algorithm to interpolate for intermediate values from an array of known values. Details of this algorithm are given in the UBC Computing Centre document: UBC Surface, (Mair, 1978b). The half-hourly estimates of the rainfall at each of the stations are then summed to yield cumulative rainfall estimates.

Details of the computer routine sequence are given in the next section.

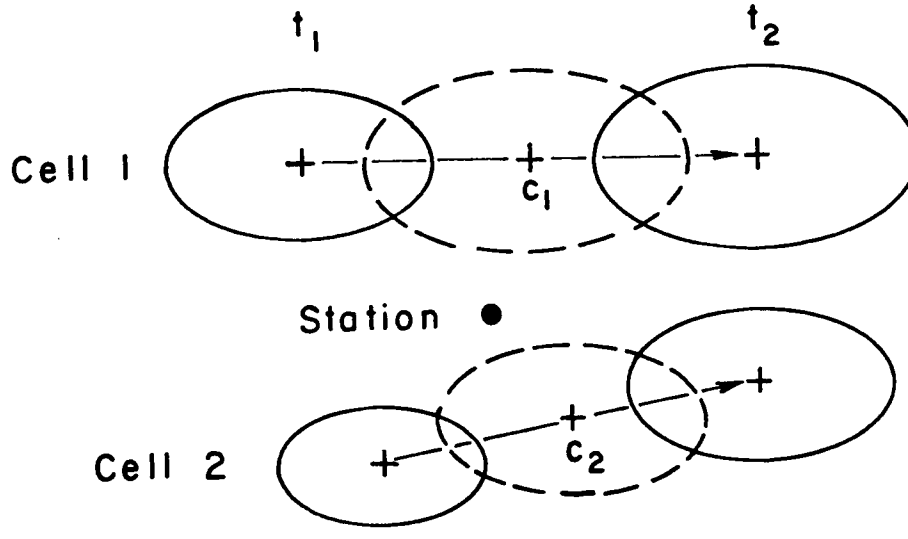

FIGURE 5.9

Two Cells Affecting Rainfall at a Station. Both are shifted so that their Centres of Gravity are now at the Midpoints of their respective total Displacements, c_1 and C_2. The shifted cells are shown by the dashed curves.

5.2 Computer Routine Sequence

Figure 5.10 graphically charts the sequence of computer routines developed during this study and used to make estimates of the rainfall from cloud top temperature contours taken from GOES infrared images. There are five major routines (DOG, STATION, RF, IN, UP) which perform various operations towards yielding a satellite rainfall estimate. All of these routines were programmed in Fortran for use on the UBC computer terminal system.

The first two routines, DOG and STATION, are digitizing routines enabling the user to input either satellite image parameters and temperature contours - DOG, or station names and locations - STATION, via the digitizing tablet. Both of these routines make use of the UBC Computing Centre Library program IG (Mair, 1978a) to control the actual input of the data points along with standardized x-y axes. The routine DOG also calculates the area (A) of each contour traced using

$$A = \sum_i \left[\frac{(x_{i+1} - x_i)}{2} \cdot \frac{(y_{i+1} - y_i)}{2} \right] \quad 5.1$$

where x_i, y_i are the coordinates of the i-th point digitized. The centre of gravity of each contour (xc, yc) is determined by the routine DOG using

FIGURE 5.10

Sequence of Computer Routines Used:

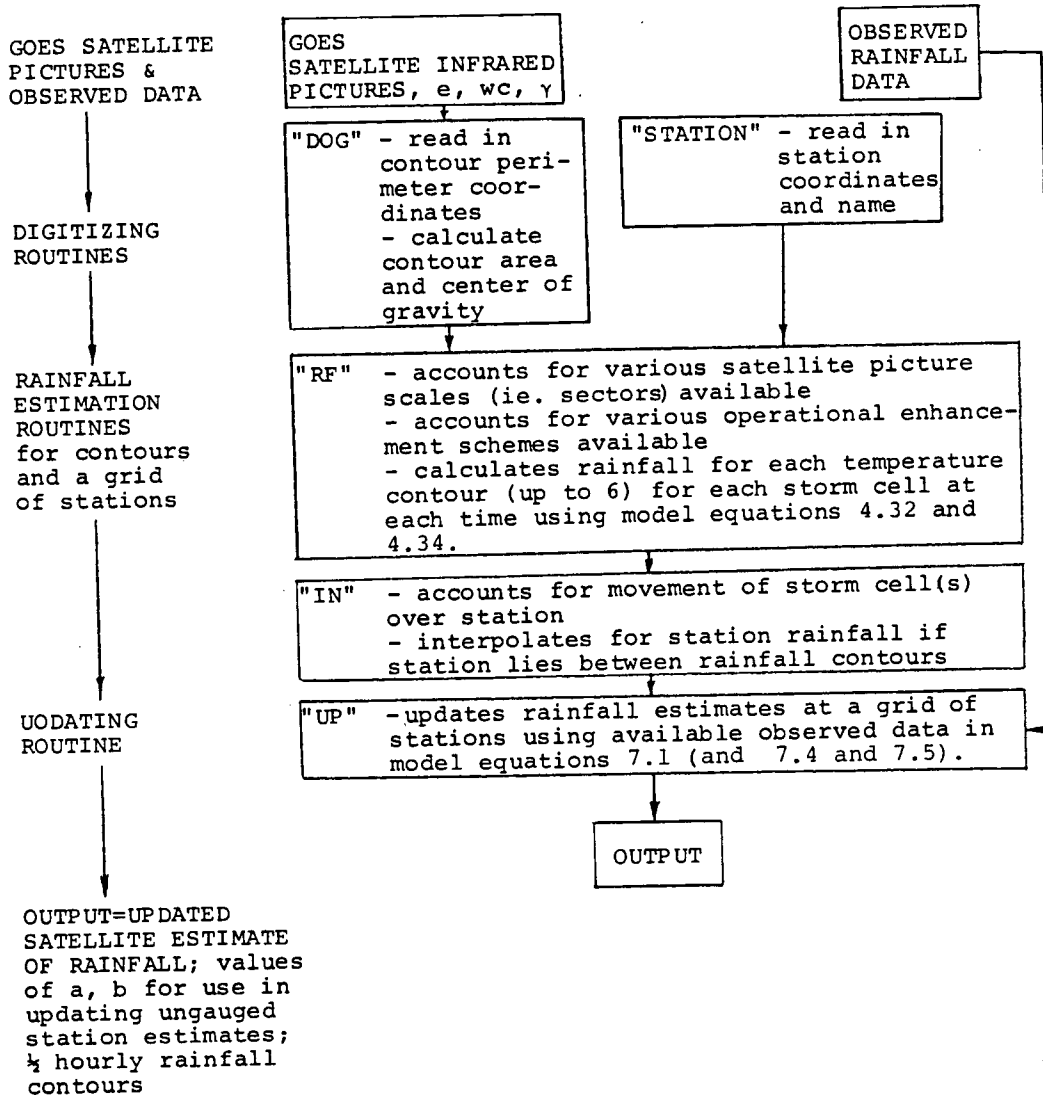

$$xc = \frac{1}{n}\sum_{i}^{n} x_i \qquad 5.2$$

$$yc = \frac{1}{n}\sum_{i}^{n} y_i \qquad 5.3$$

which essentially described the centre of gravity.

The second two routines, RF and IN, are the rainfall estimation routines. The first of these, RF, provides estimates of the rainfall for each temperature contour using the rainfall model equations 4.32 and 4.34. This is done after the routine scales all the satellite images to the size of the SB6 image sector. This is necessary because several sector scales are received operationally. The routine then must determine which of the various operational enhancement schemes is being used before proceeding to compute the rainfall for each of the temperature contours, up to a maximum of 6, for each storm cell since each of the various cells may be evolving at different rates, for the duration of the storm event.

The second of the rainfall estimation routines, IN, provides estimates of rainfall for those stations whose coordinates were stored using the routine STATION and the cell contour rain estimates obtained from the routine RF. The routine IN accounts for the movement of the storm and its cells over the station (as described in the previous section). The second part of the rou-

tine IN is to interpolate, using the modified XPAND.S, for the rainfall at the station after the movement of the storm has been taken care of. If the isohyets of the rainfall are required they are determined and plotted automatically using the UBC Computing Centre library grid contouring routine CNTOUR (Mair, 1978b).

The final major routine, the updating routine, UP is based on the updating procedure described in Chapter 7. This routine incorporates the observed rainfall for each station with the satellite estimates using the updating model, equations 7.1, 7.4 and 7.5, in addition to the updating model parameters, a and b, for use in updating rainfall estimates for ungauged locations.

The output from these routines includes point estimates of rainfall for various stations, contours of the estimated rainfall produced by each cell, and isohyets of estimated rainfall for a grid of points.

CHAPTER VI

ESTIMATES OF PRECIPITATION USING SATELLITE IMAGES

6.1 The Test Storms

As a test of the model under actual conditions, a number of storms which occurred over British Columbia were chosen for analysis using the available infrared GOES-West images received at the Pacific Weather Centre in Vancouver. Except for one of the test storm dates (June 4, 1977) satellite images were chosen for those dates and times during which rainfall was known (from news media or Pacific Weather Centre reports, or direct experience) to be falling over British Columbia. For the June 4, 1977 case it was assumed that rain was falling from those cells which had relatively cold cloud top temperatures ($<-40^{\circ}C$). The actual occurrence of rainfall for the June 4, 1977 storm was confirmed on examination of the hourly rainfall records for the affected station. The following criteria influenced the choice of test storms:

1 - The storm had to be sufficiently well-developed in the vertical to have cloud top temperatures which were within the stepwise range of the enhancement scheme used so that definite cloud top temperature contours were formed on the satellite infrared images.

2 - The storm had to be located over an area which had at least one raingauge to allow verification and/or calibration of the rainfall estimation model.

3 - Over regions with hourly records of rainfall, the storm had to exist on at least two successive satellite images to permit a calculation of the rainfall estimate. Over regions with only 6-hour or 12-hour records of rainfall, the storm had to exist for the entire 6-hour or 12-hour period.

During the analysis of the test storms several problems arose which required innovative solutions before the estimation procedure could be used operationally. The development of the computer routines, discussed in the previous chapter, to facilitate the analysis proceeded along with the examination of the initial storm which occurred on October 31, 1978.

The test storms included two examples of widespread and severe cyclonic systems occurring on October 31, 1978 and December 17, 1979, both of which were noteworthy. The first, which swept across the Queen Charlotte Islands and over the Terrace area was dubbed the Halloween Deluge by local meteorologists (Hammond, 1978). The second was a storm which followed an earlier event that caused extensive property damage from flooding and landslides in Port Moody on the outskirts of Vancouver, British Columbia. The other storms investigated were

storms of a more typical nature, including a summer storm, occurring on June 4, 1977, and two winter storms which occurred on November 20, 1979 and December 5, 1979.

For each of the test storms the temperature of the level of non-divergence was chosen as a constant T_2.

The effect of chosing an incorrect value T_2 for the temperature at the level of non-divergence when the correct temperature is T_T can be readily accounted for in the expression for rainfall by the addition of an adjustment ΔT^1 to the temperature thickness of the diverging layer ΔT in the rainfall estimation equations (4.32 and 4.34)

$$\Delta T^1 = \int_{T_T}^{T_2} dT = T_2 - T_T \qquad 6.1$$

where ΔT^1 is the temperature thickness between the true temperature level of non-divergence (T_T) and the temperature level actually chosen (T_2).

Following the steps outlined in the previous chapter, the rainfall was estimated from the available GOES infrared images. A description of each of the test storms as well as the results of the estimation procedure are discussed below.

6.2 The October 31, 1978 Rainfall Estimates

6.2.1 Storm Description

Between October 29 and November 2, 1978 a major storm occurred over the North Coast of British Columbia. During the storm, winds gusting to 125 kph and 5-day rainfall totals exceeding 400mm in some areas coincided with heavy snowmelt to cause flooding and damages well in excess of $10 million. Two CNR crew members were killed and two motorists were injured as a result of roadbed damage (*Chinook*, 1979). Schaefer (1979a, b) and Hammond (1978) describe the storm from a meteorological point of view. Figure 6.1 shows the isohyets estimated from the recorded rainfall amounts (from Schaefer, 1979a, b). It also shows the precipitation gauges and the location of several small basins where runoff volumes were also measured. The terrain in the area is extremely rugged with mountains rising to over 2000 m. It is sparsely inhabited and precipitation and discharge gauges are few and far between. Figure 6.2 shows the areal extent of this storm at 0115 GMT as viewed from GOES-West.

The aim of the analysis was to check the procedure for estimating rainfall with a major storm. Since the October 31, 1978 storm was the first rainfall event examined, most of the calculations apart from the digitizing of the cloud top temperature contours and the computation of the areas within these

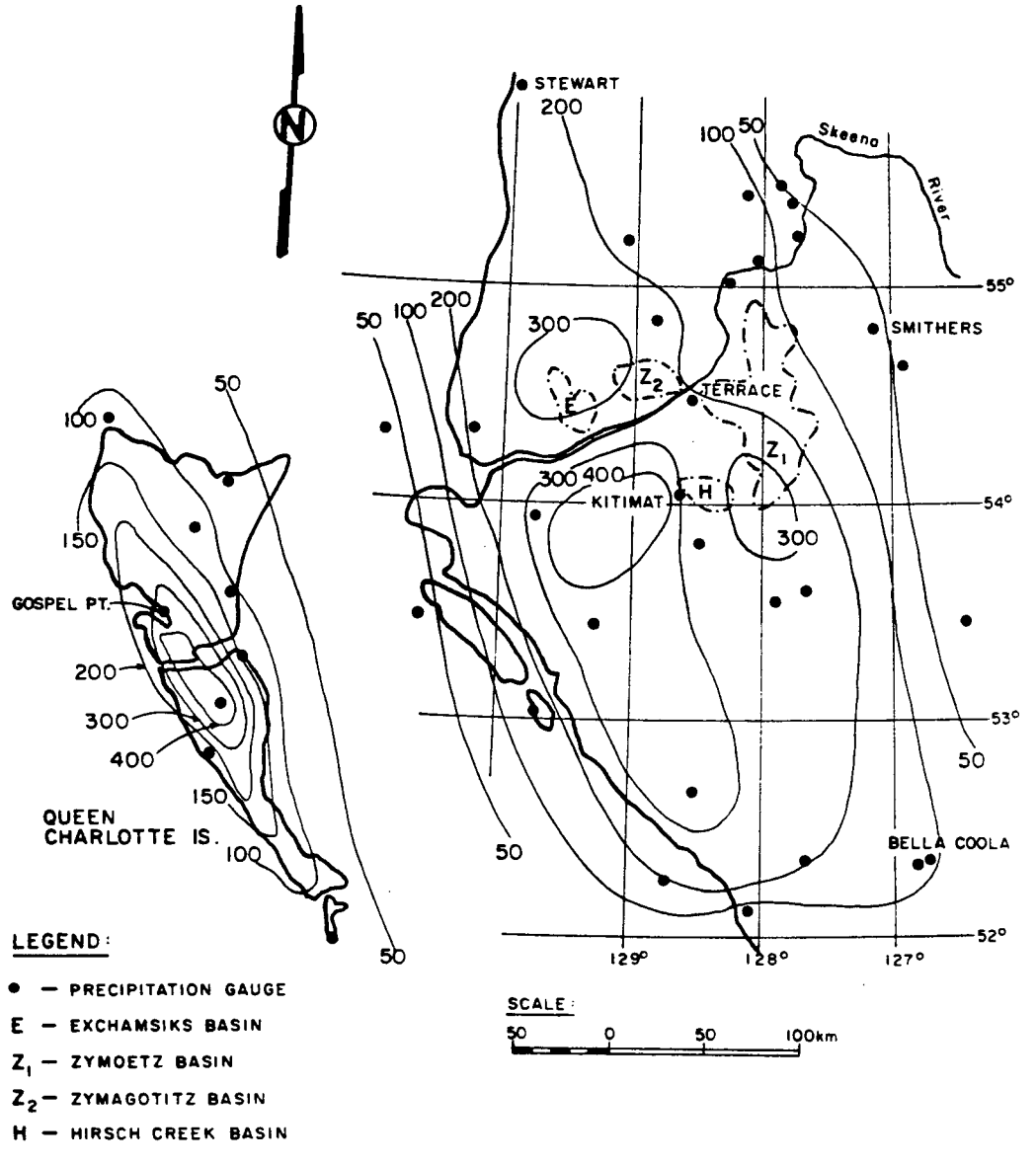

FIGURE 6.1

Map of the Terrace Area with Isohyets (mm) for the Period October 29 to November 2, 1978 (After Schaefer 1979a, b).

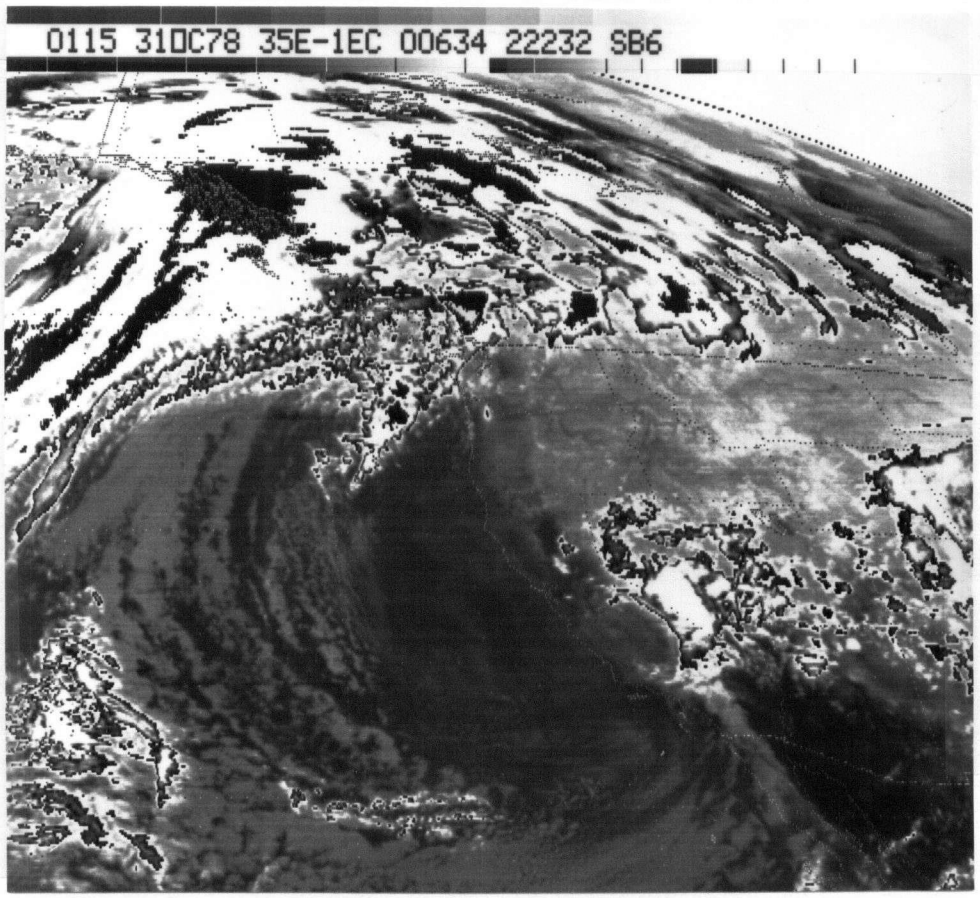

FIGURE 6.2

Areal Extent of the October 31, 1978 Storm at 0115 GMT as Viewed from GOES-West.

contours were carried out by hand. This exploratory exercise was necessary before developing the computer routines which were used in the rainfall estimation calculations in the subsequent test storm analyses.

6.2.2 Results

The analysis was limited to two stations for which the cumulative observed rainfalls were available - Terrace Airport, and Gospel Point on the Queen Charlotte Islands. The series of GOES-West images examined covered the time interval between 0045 GMT on October 31, 1978 and 2245 GMT on November 1, 1978. Of the 93 possible images, 29 were enhanced and could be used directly, 31 were unenhanced and had to first be processed through the video camera-special effects generator-video monitor system to extract the appropriate cloud top temperature contours, 16 were missing cloud information for British Columbia (for such reasons as poor signal quality, no transmitted signal, and the use of the satellite VISSR to scan another serious storm situation over the United States), and 17 were visible images. Although the visible images could not be used directly for the rainfall estimation, they were useful for determining the types of clouds present.

There were also 4 images for which the geographic grid, that is automatically superimposed on the image, was significantly displaced with respect to the actual geography. In these images the geographic grid was re-navigated by eye to

coincide within 20 km of the observed land-ocean boundaries.

The rainfall was calculated for both Terrace and Gospel Point with the model parameters chosen from the literature on the basis of cloud identification from the satellite images. The coldest clouds were tentatively identified as bands of cumulonimbus within layer clouds. Both the classical Norwegian model of fronts (Bjerknes, 1918; Bjerknes and Solberg, 1922) and the more recent mesoscale rainband models (Browning *et al.*, 1973; Harrold, 1973; House *et al.*, 1976; Hobbs and Locatelli, 1978; and Matejka *et al.*, 1980) anticipate this combination of clouds along an active frontal system. The estimated rainfall totals for Terrace Airport and Gospel Point are given in Table 6.1 and lie within 12% of the observed rainfall totals. The cumulative estimated rainfalls are compared graphically with the observed cumulative rainfalls in Figure 6.3. As can be seen the cumulative estimated rainfall curve generally behaves in the same manner as the observed cumulative rainfall curve.

6.2.3 Comparison of Streamflow And Rainfall Volumes

In addition to the raingauge measurements, streamflow records for four small basins in the Terrace-Kitimat area, including the Exchamsiks River basin, the Hirsch Creek basin, the Zymoetz River basin, and the Zymagotitz River basin, were available. Isohyets were constructed from the GOES images for the points shown in Figure 6.4. From the isohyets shown in Figure 6.5 the rainfall volume over each of the four basins was

TABLE 6.1 Comparison of Observed and Estimated Storm Totals for the Period 0045 GMT on October 31, 1978 to 2245 GMT on November 1, 1978.

STATION	OBSERVED RAINFALL (mm)	ESTIMATED RAINFALL (mm)	DIFFERENCE (mm)	DIFFERENCE (%)	e	wc g/mc^3	γ $^oC/1000m$
Terrace Airport	200	180	20	10	0.2	10	5
Gospel Point	250	220	30	12	0.2	10	5

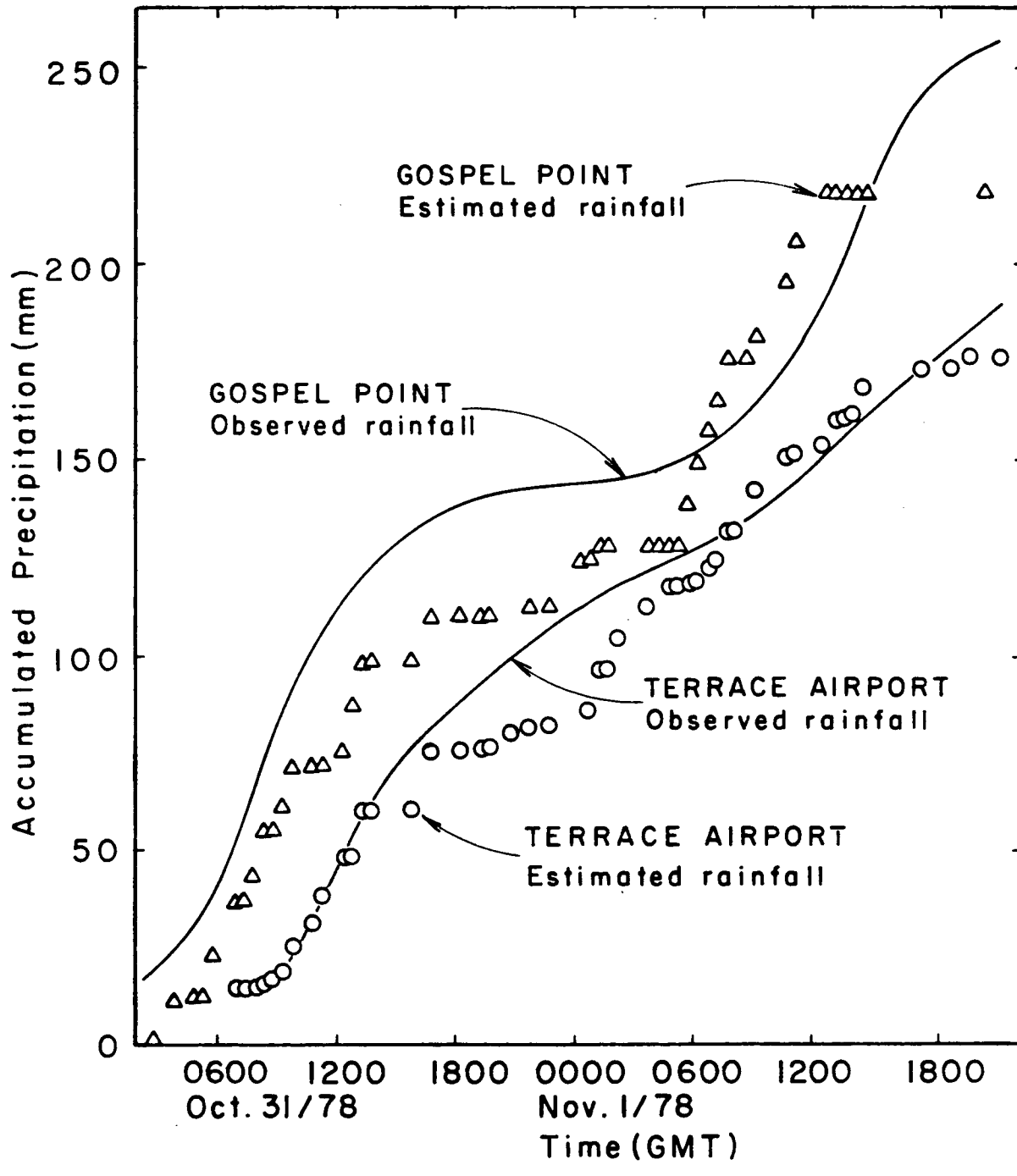

FIGURE 6.3

Estimated and Observed Precipitation at Gospel Point and Terrace Airport.

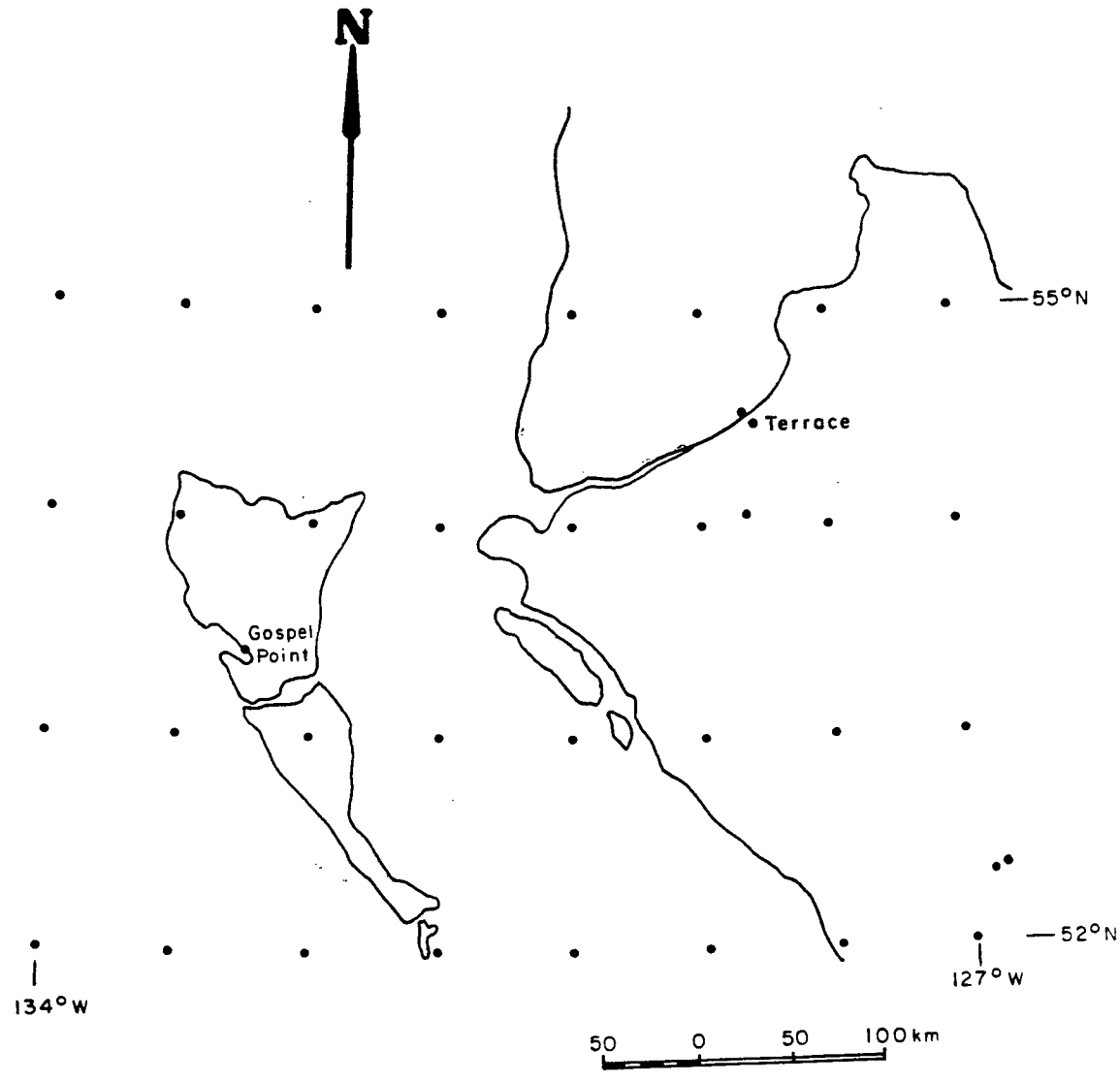

FIGURE 6.4

Location of Grid Points Used to Construct Satellite Estimated Isohyets for the October 31, 1978 Storm.

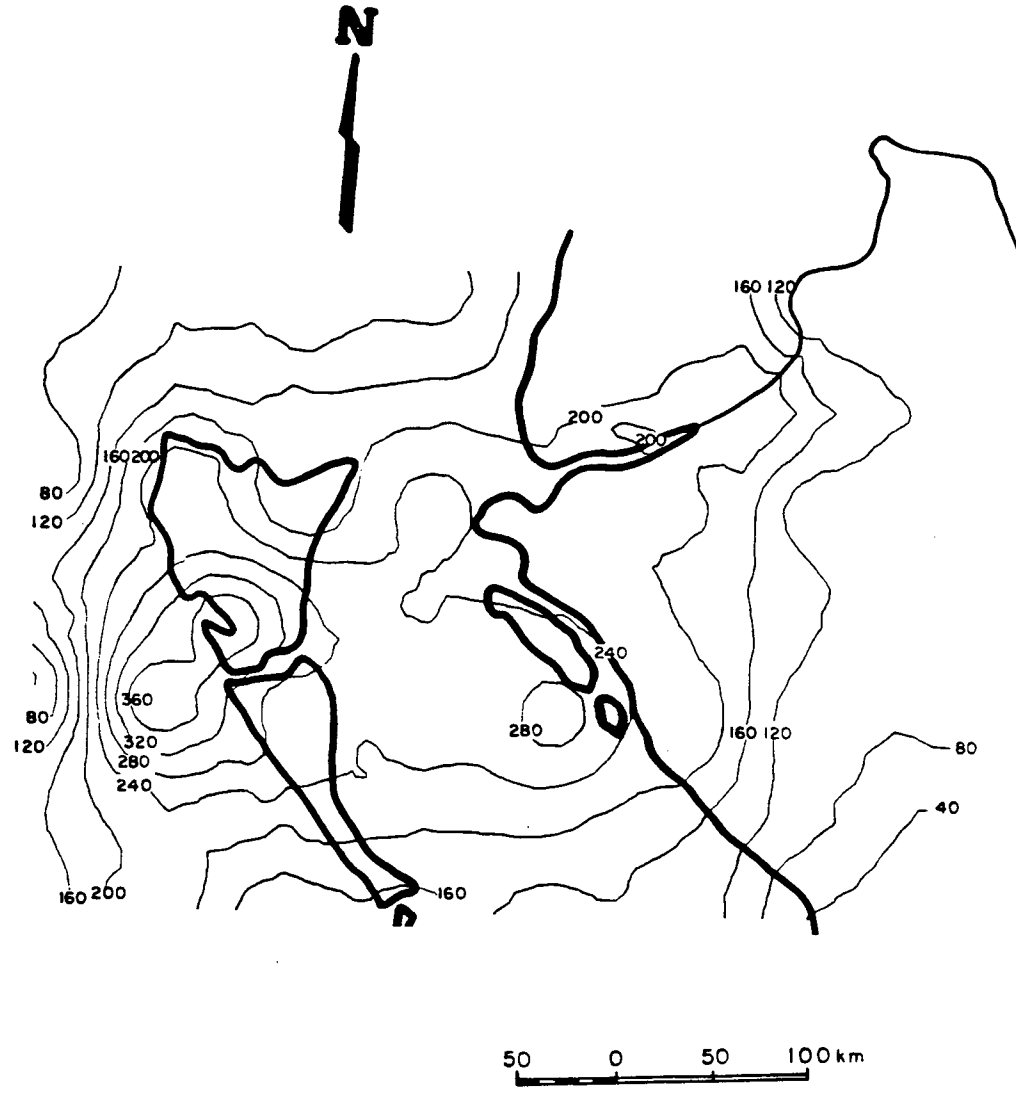

FIGURE 6.5

Isohyets of Satellite Estimated Rainfall (mm) for the October 31, 1978 Storm Based on the Grid Points Shown in Figure 6.4.

estimated and compared in Table 6.2 with the rainfall volume determined from Schaefer's isohyets (Figure 6.1), and the runoff volume recorded at the discharge gauges. The rainfall volumes estimated from the satellite images compare well with the conventional volume calculations and are within 20% of the observed runoff volumes. (Baseflow was subtracted.)

6.3 The December 17,1979 Rainfall Estimates

The December 17, 1979 storm was the second major event analyzed. Since the storm occurred over the southern portions of British Columbia and Alberta, an area in which the majority of the people in these provinces resides and hence, where many raingauges are located, it was an appropriate test of the ability of the procedure to make rainfall estimates at a number of stations.

6.3.1 Storm Description

The storm was the last of two events to move into the region within a 4-day period. In the Lower Mainland area of British Columbia, the first storm saturated soils leading to extensive property damage from flooding and mudslides especially in Port Moody near Vancouver. The second storm, that of December 17, 1979, added to the already high water table levels and there were many reports of flooded basements and washed out roads in and around Vancouver and Victoria. Figure 6.6 (from Schaefer, 1980) shows the combined observed isohyets for the 7-day period

TABLE 6.2 Comparison of Rainfall and Runoff Volumes in $m^3 \times 10^6$

(Baseflow has been subtracted from the streamflow.)

Basin:	Exchamsiks	Zymoetz	Zymagotitz	Hirsch
Area (km^2):	480	2950	350	330
Observed Runoff	116 (%)	281* (%)	58* (%)	88 (%)
Rainfall from Isohyets	121 (4)	388 (38)	65 (12)	81 (8)
Rainfall from satellite images	107 (8)	328 (17)	69 (19)	73 (17)

Key:

% = % Difference
* Included some estimated values

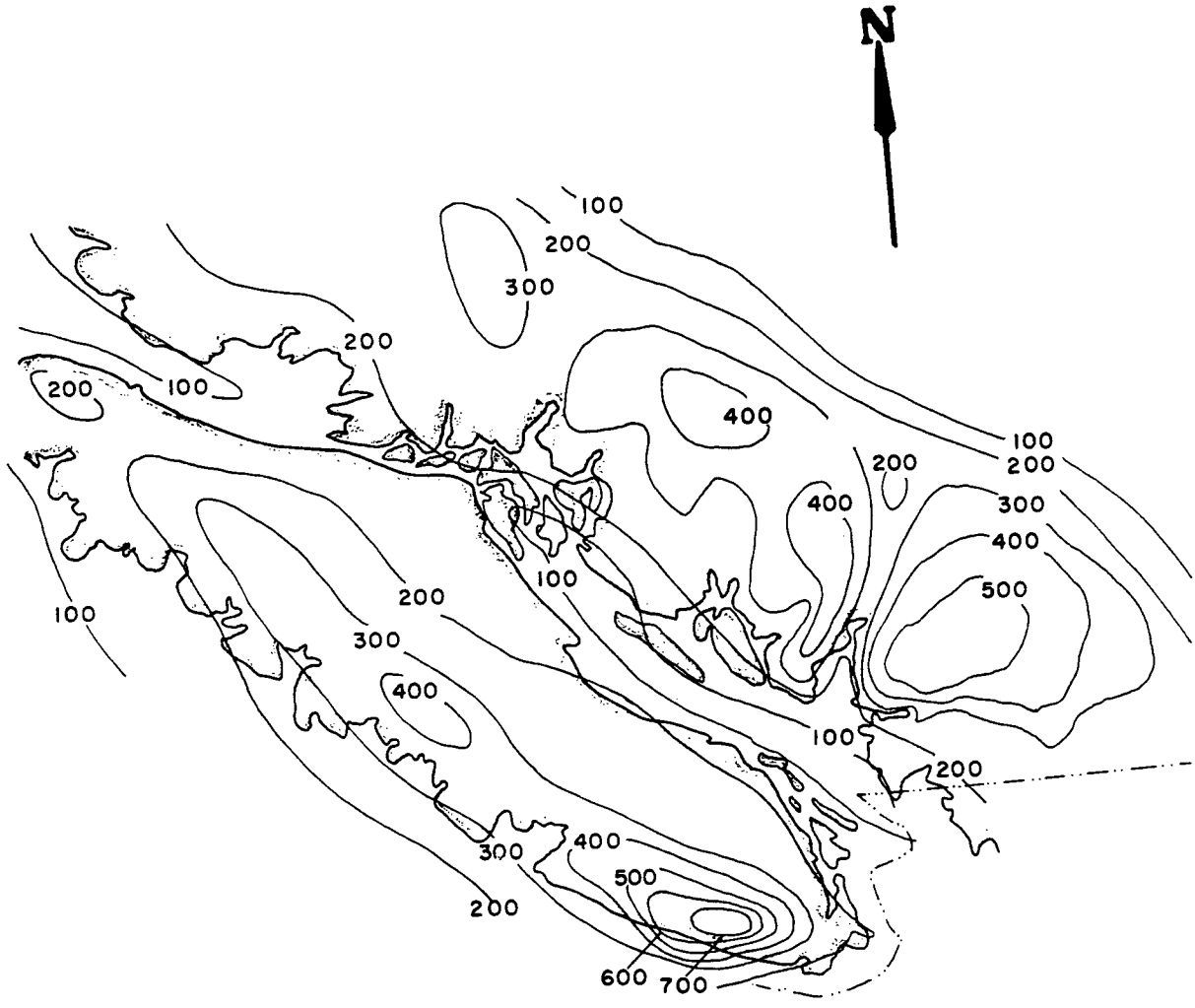

FIGURE 6.6

Map of the Vancouver Island - Lower Mainland Area with Isohyets (mm) for the 7-Day Period from December 12 to 18, 1979 (After Schaefer, 1980).

from December 12 to December 18, 1979, while Figure 6.7 shows the areal extent of the storm at 0715 GMT on December 17, 1979 as viewed from GOES-West.

6.3.2. Results

The satellite images for December 17, 1979 were analyzed and rainfall was estimated for 24 stations in British Columbia and 2 stations in Alberta. The locations of the stations are shown in Figure 6.8. Since the analysis proceeded in real time as the storm progressed, all of the stations were assumed to be receiving precipitation in the form of rain. Observed hourly rainfall data was available immediately for only three stations: Vancouver International Airport, Victoria International Airport, and Hope Airport. The actual type and amount of precipitation received at the other stations was not known until some time later (almost 4 months) when the observed data became available. Those other stations which normally report hourly rainfall amounts were, in general, receiving snow and hence only 6-hour snow amounts were available. The remaining stations reported precipitation on a 6- or 12-hourly basis.

6.3.2a Point Estimates

The series of GOES-West images examined covered the 6-hour interval from 0045 to 0645 GMT on December 17, 1979. This 6-hour segment was chosen for a number of reasons. Prior to 0045 GMT on December 17, 1979, the observed rainfall amounts were negligible and this was evident on the satellite images which recorded low

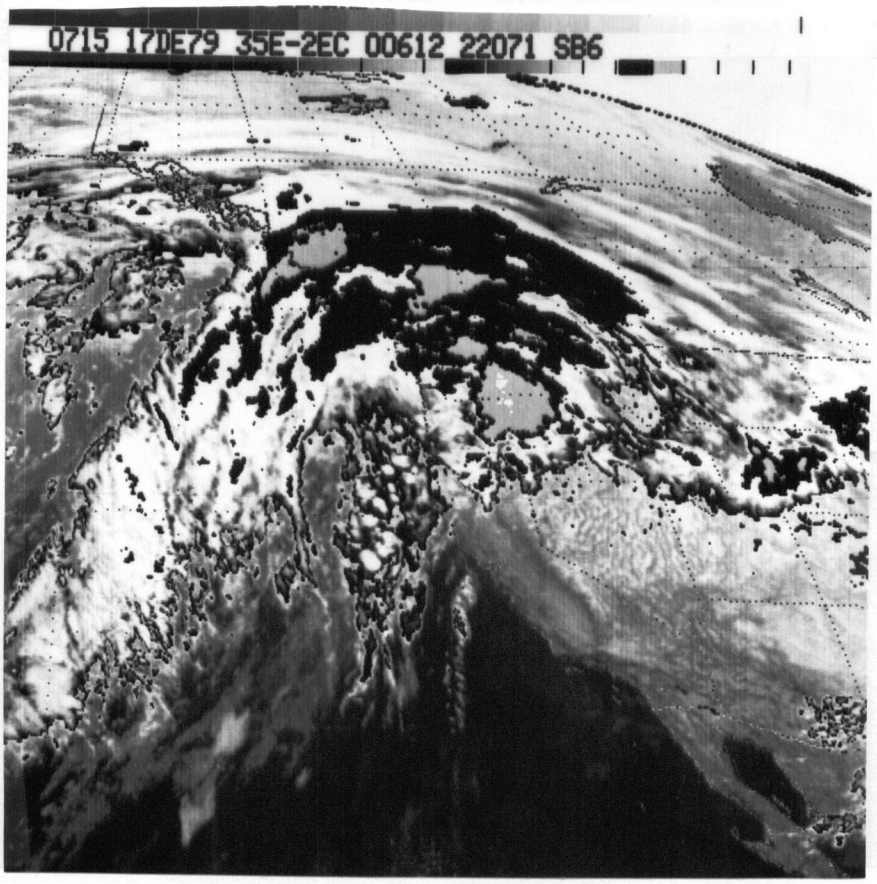

FIGURE 6.7

Areal Extent of December 17, 1979 Storm at 0715 GMT as Viewed from GOES-West.

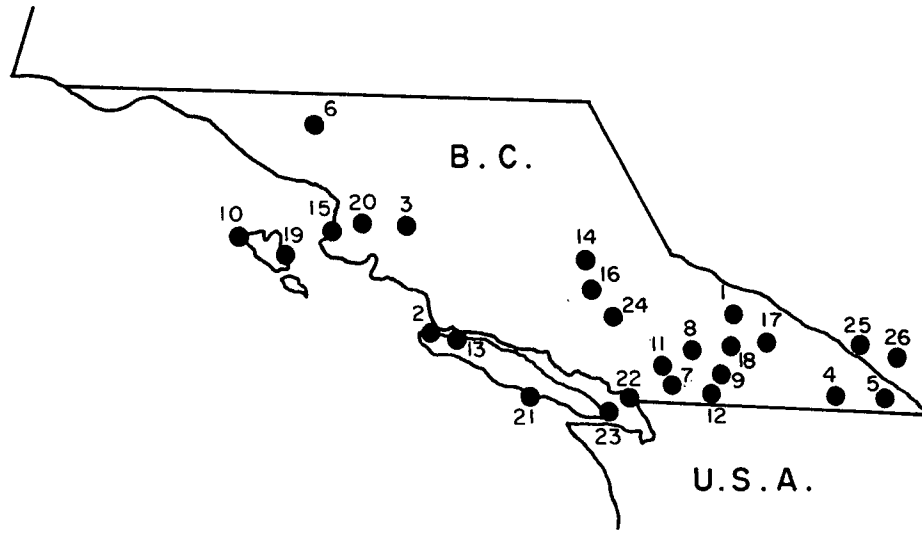

FIGURE 6.8

Location of Stations Used in the December 17, 1979 Storm Analysis.

1	Blue River	14	Prince George Airport
2	Bull Harbour	15	Prince Rupert Airport
3	Burns Lake	16	Quesnel Airport
4	Castlegar Airport	17	Revelstoke Airport
5	Cranbrook Airport	18	Salmon Arm
6	Dease Lake	19	Sandspit Airport
7	Hope Airport	20	Terrace Airport
8	Kamloops Airport	21	Tofino Airport
9	Kelowna Airport	22	Vancouver International Airport
10	Langara	23	Victoria International Airport
11	Lytton	24	Williams Lake Airport
12	Penticton Airport	25	Banff
13	Port Hardy Airport	26	Calgary

cloud but no expanding deep cold cloud over the region. During the 6-hour period all of the infrared images available were enhanced and as such could be used directly in the estimation procedure, thus eliminating the uncertainties introduced by using unenhanced infrared images. After 0645 GMT many of the infrared images were enhanced. In addition, this 6-hour period roughly corresponded to the first 6 hours of the climatological day and all of the stations reported 6-hour rainfall or snowfall (as rainfall equivalent) amounts which could be used to compare with the 6-hour cumulative rainfall estimates.

For this segment of the storm the water content wc was inferred from the TIROS-N data since it was readily available at the time of the storm and the lapse rate γ was assumed equal to the saturated adiabatic lapse rate $\gamma_s = 5^{\circ}C/1000m$. For Vancouver International Airport, Victoria International Airport, and Hope Airport the efficiency e was determined using equation 4.35. It was assumed that the efficiency e for Vancouver International Airport was representative of the efficiencies at all the other stations for which the observed data was not immediately available. With these values of the parameters, the 6-hour cumulative estimated rainfalls were calculated and then compared with the 6-hour cumulative observed rainfalls in Table 6.3. The percent difference between the observed 6-hour rainfall total and the estimated 6-hour rainfall total ranges from 0 to 2500% with the worst differences found for those stations that were later

TABLE 6.3 Comparison of Observed and Estimated Rainfall Totals for the 6-hour Segment 0000 GMT to 0600 GMT on December 17, 1979. Vancouver International Airport data was used to calibrate the adjustment parameter e.

STATION	OBSERVED RAINFALL (mm)	ESTIMATED RAINFALL (mm)	DIFFERENCE (mm)	DIFFERENCE (%)	e	wc (g/m^3)	γ ($^oC/1000m$)
Observed Data Precipitation Immediately Available:							
CALIBRATION STATION-							
VANCOUVER I.A.	10.6	9.5	1.1	10	0.2	10	5
VICTORIA I.A.	6.8	6.4	0.4	6	0.2	10	5
HOPE A.	0.0	2.5	2.5	-	0.2	5	5
Observed Precipitation Data Not Immediately Available:							
Blue River	6.2 S	9.1	2.9	47	0.2	5	5
Ball Harbour	8.9	9.2	0.3	3		10	
Burns Lake	M S	5.2	-	-		5	
Castlegar A.	2.4 S	3.6	1.2	50		5	
Cranbrook A.	1.6 S	3.0	1.4	88		5	
Dease Lake	0.8 S	0.03	0.77	96		5	
Kamloops A.	T S	3.2	-	-		2	
Kelowna A.	T S	2.2	-	-		2	
Langara	0.8 RS	0.2	0.6	75		13	
Lytton	1.6 S	7.8	6.2	388		2	
Penticton A.	0.0	1.7	1.7	-		2	
Port Hardy A.	6.8	7.4	0.6	9		10	
Prince George A.	2.0 S	1.5	0.5	25		10	
Prince Rupert A.	8.8 RS	1.0	7.8	89		13	
Quesnel A.	1.3 S	5.2	3.9	300		2	
Revelstoke A.	6.6 S	7.7	1.1	17		5	
Salmon Arm[1]	1.0 S	7.3	6.3	630		5	
	5.1 S	7.3	2.2	43		5	
Sandspit A.	5.0	0.3	4.7	94		13	
Terrace A.	1.6 S	0.7	0.9	56		13	
Tofino A.	22.6	15.6	7.0	31		13	
Williams Lake A.	0.2 S	5.2	5.0	2500		2	
Banff	0.3 S	2.6	2.3	767		2	
Calgary	0.0	0.0	0	0	0.2	2	5

Key:

A Airport
I.A. International Airport
M Missing
RS mixed rain and snow in mm rain equivalent
S snowfall in mm of rain equivalent
1 two separate observers

determined to be receiving snow or mixed rain and snow. The difficulty in estimating snowfall lies in the behaviour of the snowflakes as they fall, with their tendency to drift with the wind some distance from the cloud location, as well as, in the problem of measuring point snow accumulation. Estimates for the stations receiving only rain were within 10% of the observed 6-hour rainfall total except for Sandspit Airport which had a 94% or 4.7 (mm) difference between observed and estimated 6-hour rainfall totals. Sandspit Airport may have been receiving significant rainfall from "warm" or low level clouds which had cloud top temperatures warmer than the colder, stepwise enhanced, temperature range of the enhancement scheme used on the infrared images.

After the observed precipitation data were received, the actual efficiencies for each station were then determined from the observed data using equation 4.35. The estimated 6-hour total precipitation were recalculated and are shown in Table 6.4. The estimates are plotted with the observed data in Figure 6.9.

The estimates were determined using the computer routines developed during the course of the analysis of the first storm (that of October 31, 1978). The routines considerably eased the computations since for the 6-hour period analyzed there were 12 half-hourly infrared images with up to 41 cells per image and on the average of 2 temperature contours per cell to digitize, all

TABLE 6.4 Comparison of Observed and Estimated Rainfall Totals for the 6-hour Segment 0000GMT to 0600GMT on December 17,1979. For each station the empirical adjustment e has been determined using the observed data for that station.

STATION	OBSERVED RAINFALL (mm)	ESTIMATED RAINFALL (mm)	DIFFERENCE (mm)	DIFFERENCE (%)	e	wc (g/m^3)	γ ($^oC/1000m$)
Vancouver I.A.	10.6	9.5	1.1	10	0.2	10	5
Victoria I.A.	6.8	6.4	0.4	6	0.2	10	
Hope A.	0.0	2.5	2.5	-	0.2	10	
Blue River	6.2 S	9.1	2.9	47	0.2	5	
Bull Harbour	8.9	9.2	0.3	3	0.2	10	
Burns Lake	M S	5.2	-	-	0.2	5	
Castlegar A.	2.4 S	3.6	1.2	50	0.2	5	
Cranbrook A.	1.6 S	3.0	1.4	88	0.2	5	
Dease Lake	0.8 S	0.03	0.77	96	0.2	5	
Kamloops A.	T S	3.2	-	-	0.2	2	
Kelowna A.	T S	2.2	-	-	0.2	2	
Langara	0.8 RS	0.3	0.5	63	0.3	13	
Lytton	1.6 S	7.8	6.2	388	0.2	2	
Penticton A.	0.0	1.7	1.7	-	0.2	2	
Port Hardy A.	6.8	7.4	0.6	9	0.2	10	
Prince George A.	2.0 S	1.5	0.5	25	0.2	10	
Prince Rupert A.	8.8 RS	1.5	7.3	83	0.3	13	
Quesnel A.	1.3 S	5.2	3.9	300	0.2	2	
Revelstoke A.	6.6 S	7.7	1.1	17	0.2	5	
Salmon Arm[1]	1.0 S	7.3	6.3	630	0.2	5	
	5.1 S	7.3	2.2	43	0.2	5	
Sandspit A.	5.0	0.4	4.6	92	0.3	13	
Terrace A.	1.6 S	1.0	0.6	38	0.3	13	
Tofino A.	22.6	23.4	0.8	4	0.3	13	
Williams Lake A.	0.2 S	5.2	5.0	2500	0.2	2	
Banff	0.3 S	1.3	1.0	333	0.1	2	
Calgary	0.0	0.0	0	0	0.1	2	5

Key:

A Airport
I.A. International Airport
M Missing
RS Mixed rain and snow in mm rain equivalent
S Snowfall in mm rain equivalent
1 two separate observers

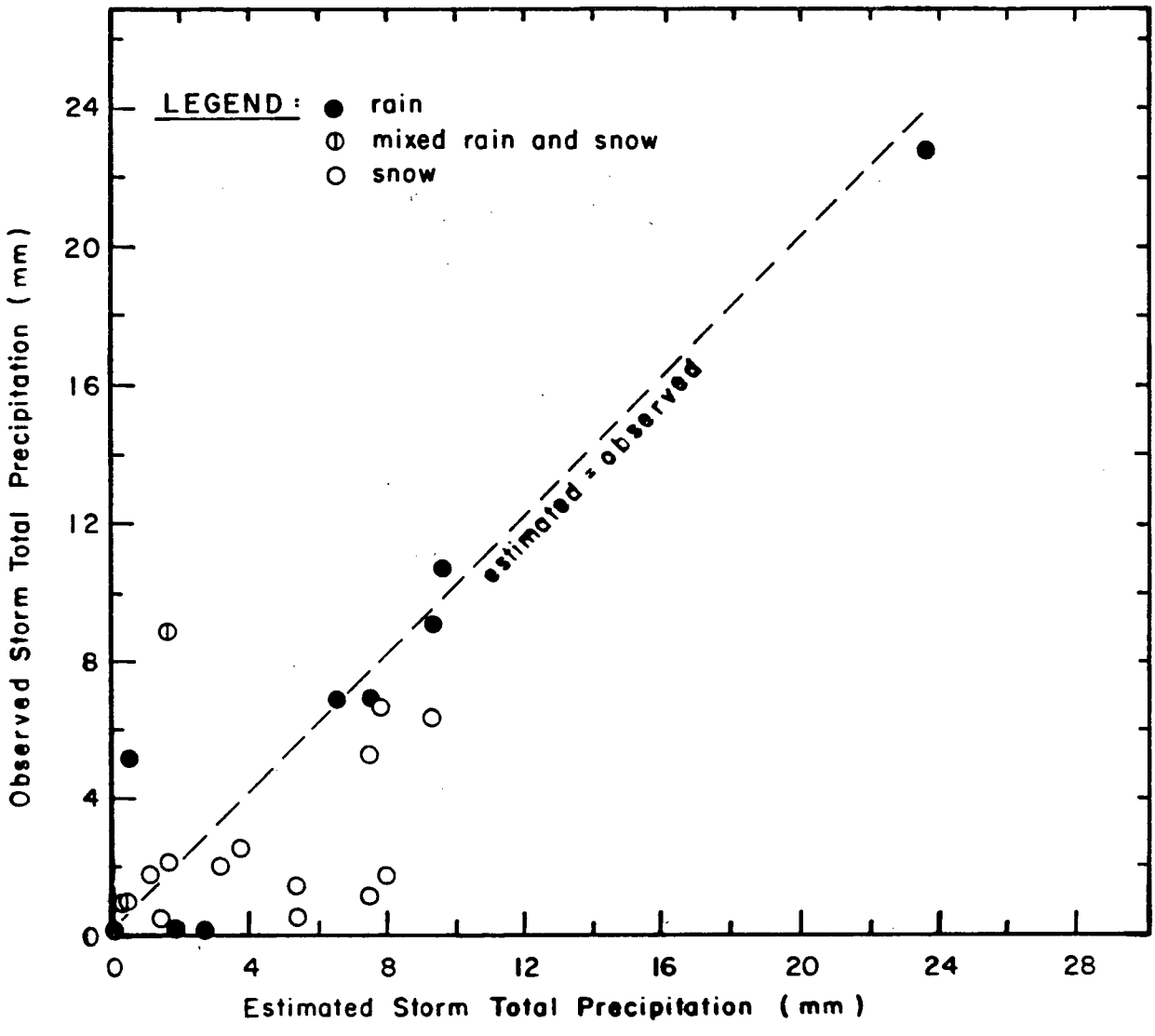

FIGURE 6.9

Estimated and Observed Precipitation for the December 17, 1979 Storm. (For each station the empirical adjustment e has been determined from the observed data for that station.)

of which had to be manipulated and "accounted for" to make rainfall estimates for each of the 26 stations. This would have been a tremendous task to do by hand.

6.3.2b Areal Rainfall Distribution

As well as providing point estimates for the specified stations, the computer routines also output rainfall amounts for each cell. In this way a series of satellite pictures becomes a sequence of cell rainfall "maps", for example Figure 6.10, showing the evolution of rainfall in time relative to the storm. Some cells can be seen to increase in size and release rainfall while others are decreasing and not releasing rainfall. Such sequences of cell rainfall "maps" are useful for the observation of large scale cloud system development and accompanying rainfall. However, in practice, a more detailed analysis of the developing storm and the areal distribution of rainfall over a smaller area is needed.

This is accomplished by estimating the rainfall for a grid of points and then constructing the isohyets. As an example, a grid of 150 points as shown in Figure 6.11 covering Vancouver Island and the Lower Mainland was chosen in order to construct satellite estimated isohyets over this area for the 6-hour period between 0045 and 0645 GMT. Figure 6.12 shows the evolution of the isohyets.

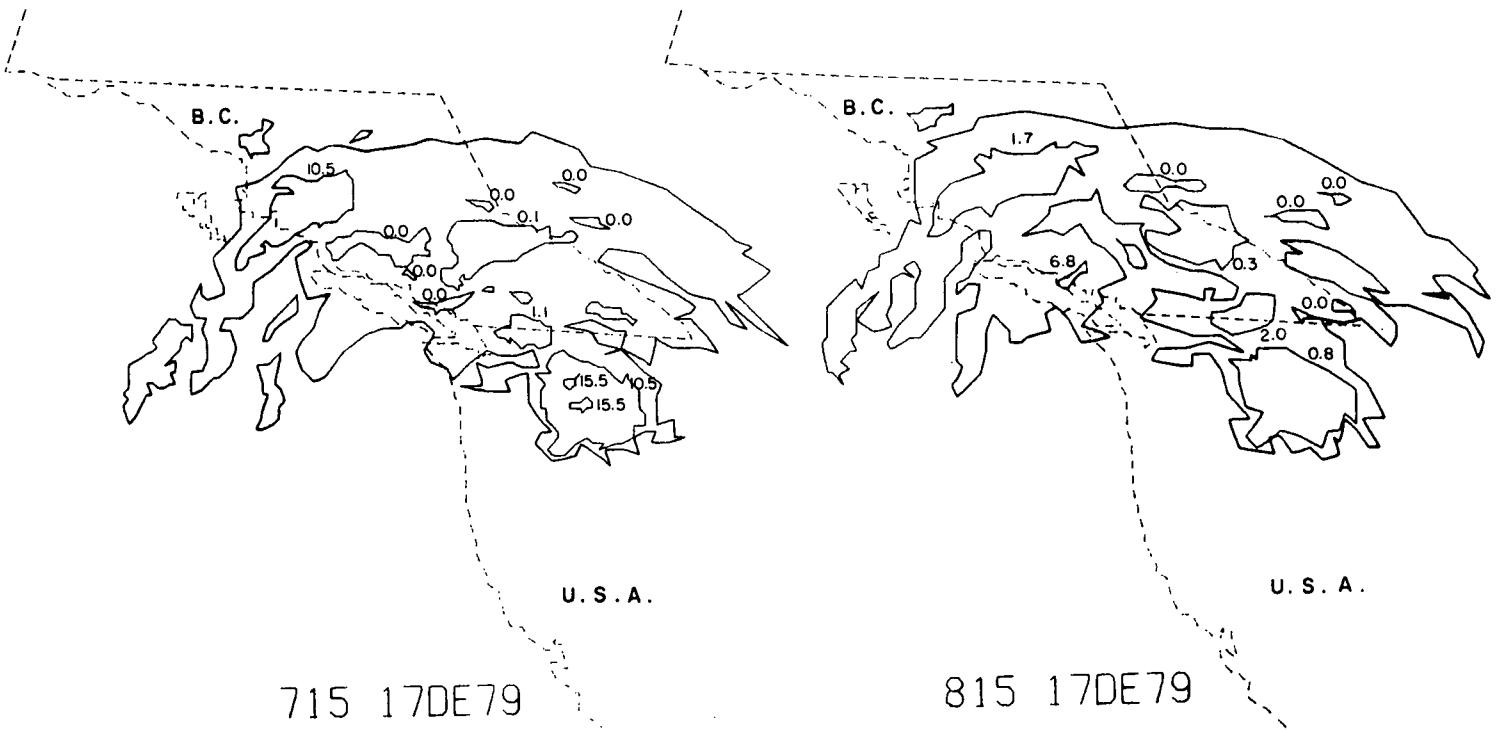

FIGURE 6.10

Storm Cell Rainfall "Maps" for 2 Hours During the December 17, 1979 Storm.

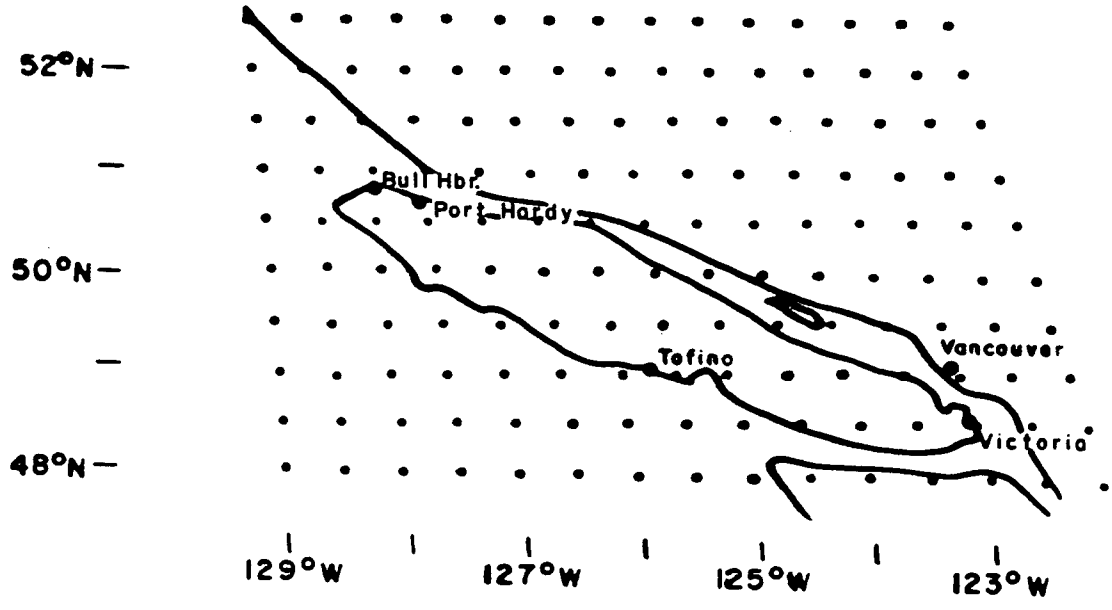

FIGURE 6.11

Location of Grid Points Used to Construct Satellite Estimated Isohyets for the December 17, 1979 Storm.

Observed rainfalls (mm) for:

Bull Harbour	8.9
Port Hardy	6.8
Tofino	22.6
Vancouver	10.6
Victoria	6.8

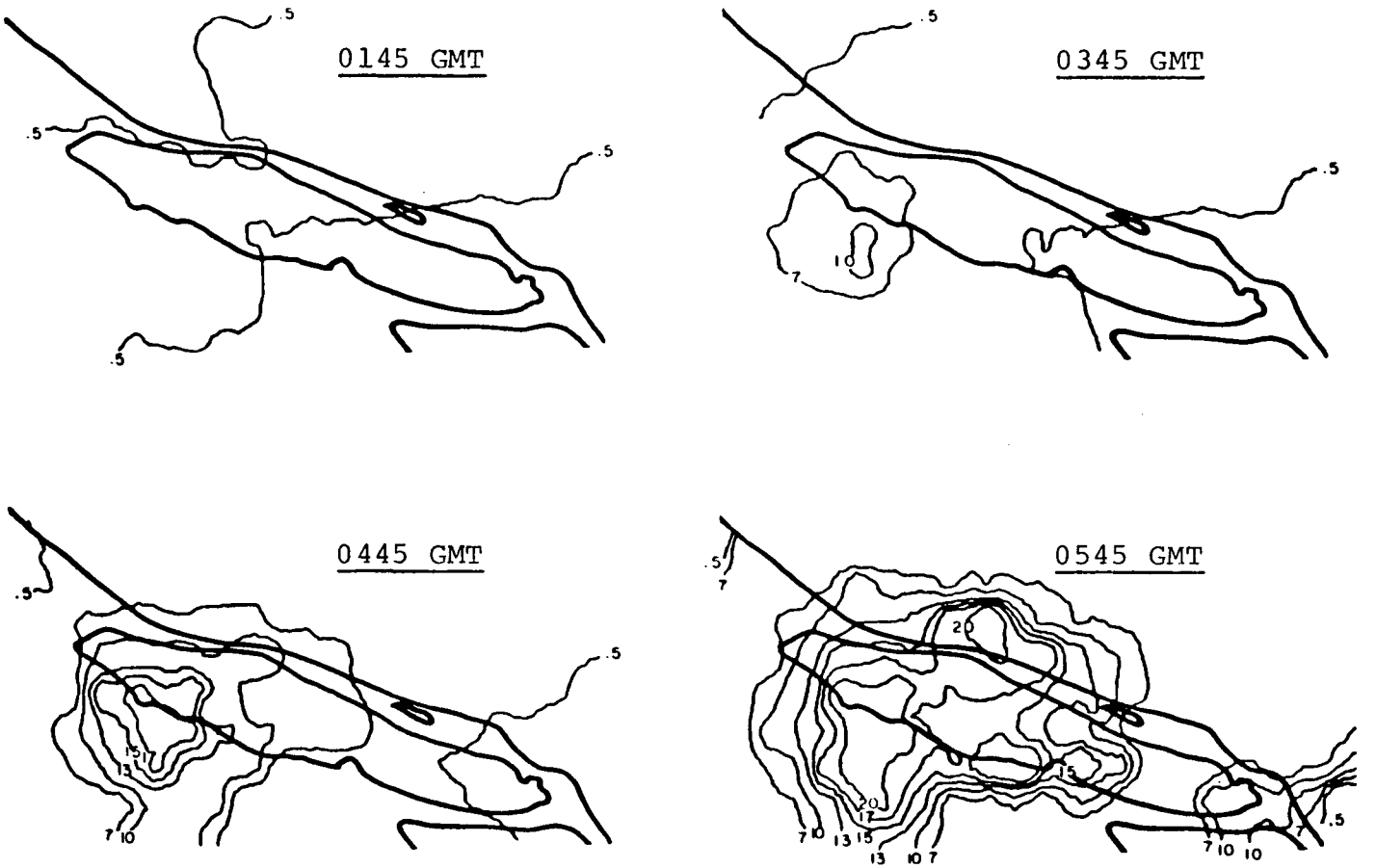

FIGURE 6.12

Evolution of Isohyets of Rainfall (mm) for the December 17, 1979 Storm Estimated for the Grid Points Shown in Figure 6.11.

The isohyets shown in Figure 6.5 by Schaefer (1980) were based on precipitation gauge data and Schaefer's knowledge of the terrain, while the isohyets in Figure 6.12 are derived entirely from satellite images. A visual comparison reveals subtle differences in the rainfall patterns. The isohyets derived from the satellite images show the short time variation in the spatial distribution of the rainfall due to changes in the vertical motions in the air mass that are reflected by changes in the tops of the clouds. Orographic effects on the rainfall distribution are implicitly included. The isohyets, determined from surface data for the entire seven day period of the storm, have had the effects of the topography explicitly incorporated into the rainfall pattern.

The advantage of using satellite images for rainfall estimation is that the distribution of rainfall over ungauged areas, for exmple, the ocean area to the west and the sparsely populated mountainous regions to the northeast of Vancouver Island can be determined. The evolution of the isohyets can be examined as often as every half-hour if necessary, whereas the precipitation gauge information is available less frequently. Ideally gauge data and satellite information should be combined - the gauge data

providing information on the small scale (<15 km) local variations in the rainfall, and the satellite images providing the meso- and macroscale spatial distribution of the rainfall.

6.4 The June 4, 1977 Rainfall Estimates

6.4.1 Storm Description

The June 4, 1977 storm was the first of three lesser storms analyzed to test the procedure for estimating rainfall from more typical events.

The storm was included to also test the procedure on a summer rainfall event for 7 stations in the interior of British Columbia. The station locations are shown in Figure 6.13. Rainfall came from a number of active cells along a weakening eastward moving frontal system and observed amounts were generally less than 10 mm, with a cell remaining over any one station for usually less than 2 hours. Figure 6.14 shows the cloud coverage for 0245 GMT as viewed from GOES-West. As well, film loops containing the 24-hour series of GOES infrared images were available allowing for a closer investigation of the development of the storm. The loops were provided on loan from NESS in Washington, D.C.

6.4.2 Results

Of the 27 available GOES images between 0115 and 2245 GMT, 10 were enhanced infrared images, 6 were unenhanced infrared images and 11 were visible images. The storm posed a special

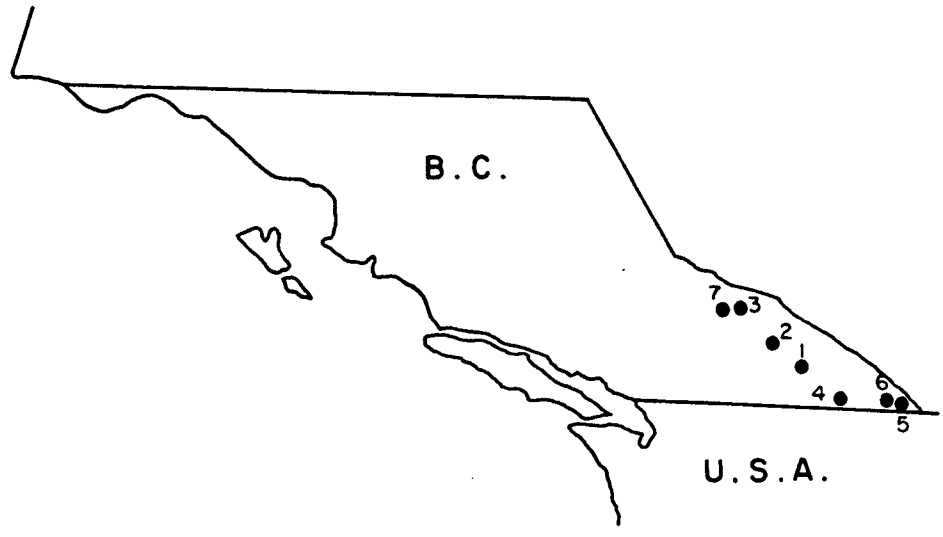

FIGURE 6.13

Location of Stations Used in the June 4, 1977 Storm Analysis

1 Duncan Lake Dam
2 Revelstoke Airport
3 Mica Dam
4 Castlegar Airport
5 Elko
6 Cranbrook Airport
7 Blue River

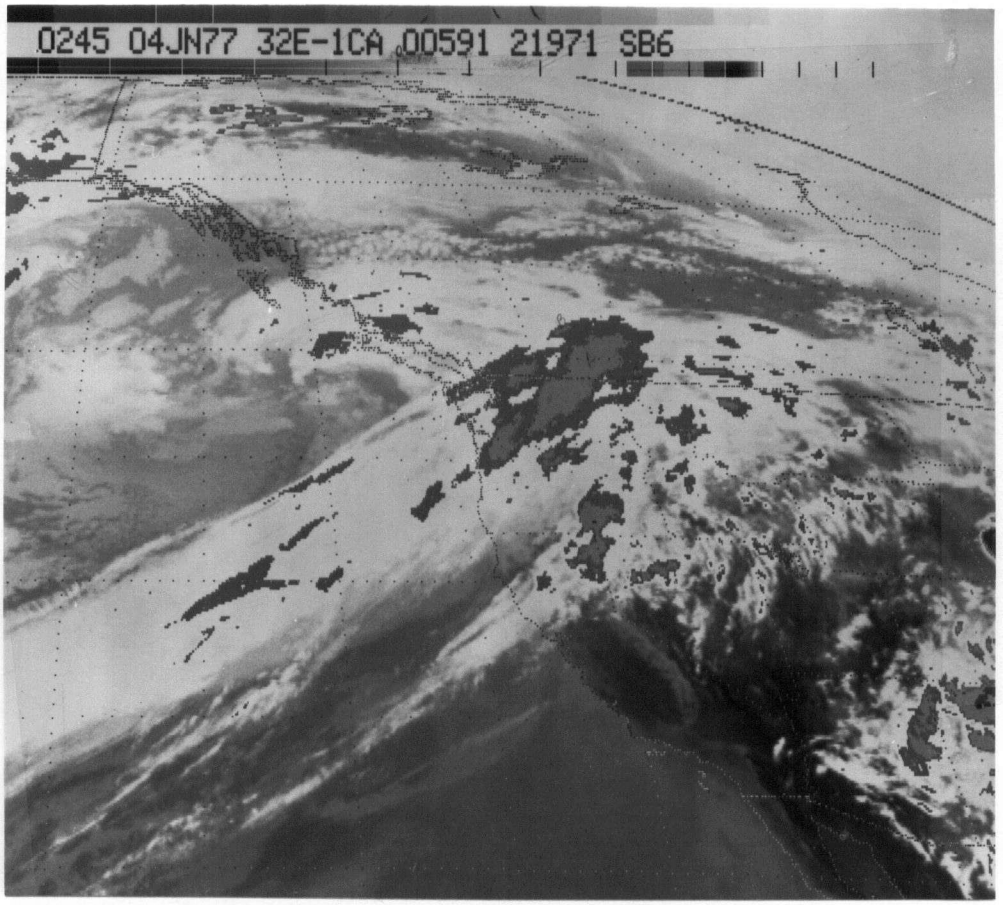

FIGURE 6.14

Areal Extent of June 4, 1977 Storm at 0245 GMT as Viewed from GOES-West.

problem in that two different enhancement schemes were employed: 7 of the enhanced infrared images had the "CA" enhancement scheme while the other 3 had the "EC" enhancement scheme. Consequently the 3 "EC" enhanced images along with the 6 unenhanced images were first analyzed with the video camera-special effects generator-video monitor system to find those contours that corresponded to the "CA" temperature contours, before rainfall estimates could be made.

For this storm, the model parameters efficiency e and water content wc were chosen from the literature such that the total observed and estimated rainfalls matched for Duncan Lake Dam. The lapse rate γ was set equal to the saturated adiabatic lapse rate $\gamma_s = 5^{o}C/1000m$. The values were assumed constant for the other stations which is reasonable given the small geographical area involved. Table 6.5 compares the observed and estimated storm rainfalls for the seven stations. The estimated rain totals are all within 40% or approximately 3 mm of the observed rain totals. Figure 6.15 shows a plot of the estimated and observed rain totals.

6.5 The November 20, 1979 Rainfall Estimates

6.5.1 Storm Description

The November 20, 1979 storm was an event suggested for analysis by the Pacific Weather Centre since it represented one of the usual widespread frontal rainfall events which occur over

TABLE 6.5 Comparison of Observed and Estimated Rainfall Totals for the Storm of June 4, 1977.

STATION	OBSERVED RAINFALL (mm)	ESTIMATED RAINFALL (mm)	DIFFERENCE (mm)	DIFFERENCE (%)	e	wc (g/m^3)	γ ($^oC/1000m$)
Calibration Station: Duncan Lake Dam	8.5	8.4	0.1	1	0.1	5	5
Revelstoke A.	3.3	2.2	1.1	33	0.1	5	5
Mica Dam	>1.7M	2.3	≈0.6	≈35	0.1	5	5
Castlegar A.	8.0	11.2	3.2	40	0.1	5	5
Elko	2.1	2.8	0.7	33	0.1	5	5
Cranbrook A.	2.1	2.8	0.7	33	0.1	5	5
Blue River	3.1	2.5	0.5	19	0.1	5	5

Key:
A. Airport
M Some data missing from observed record

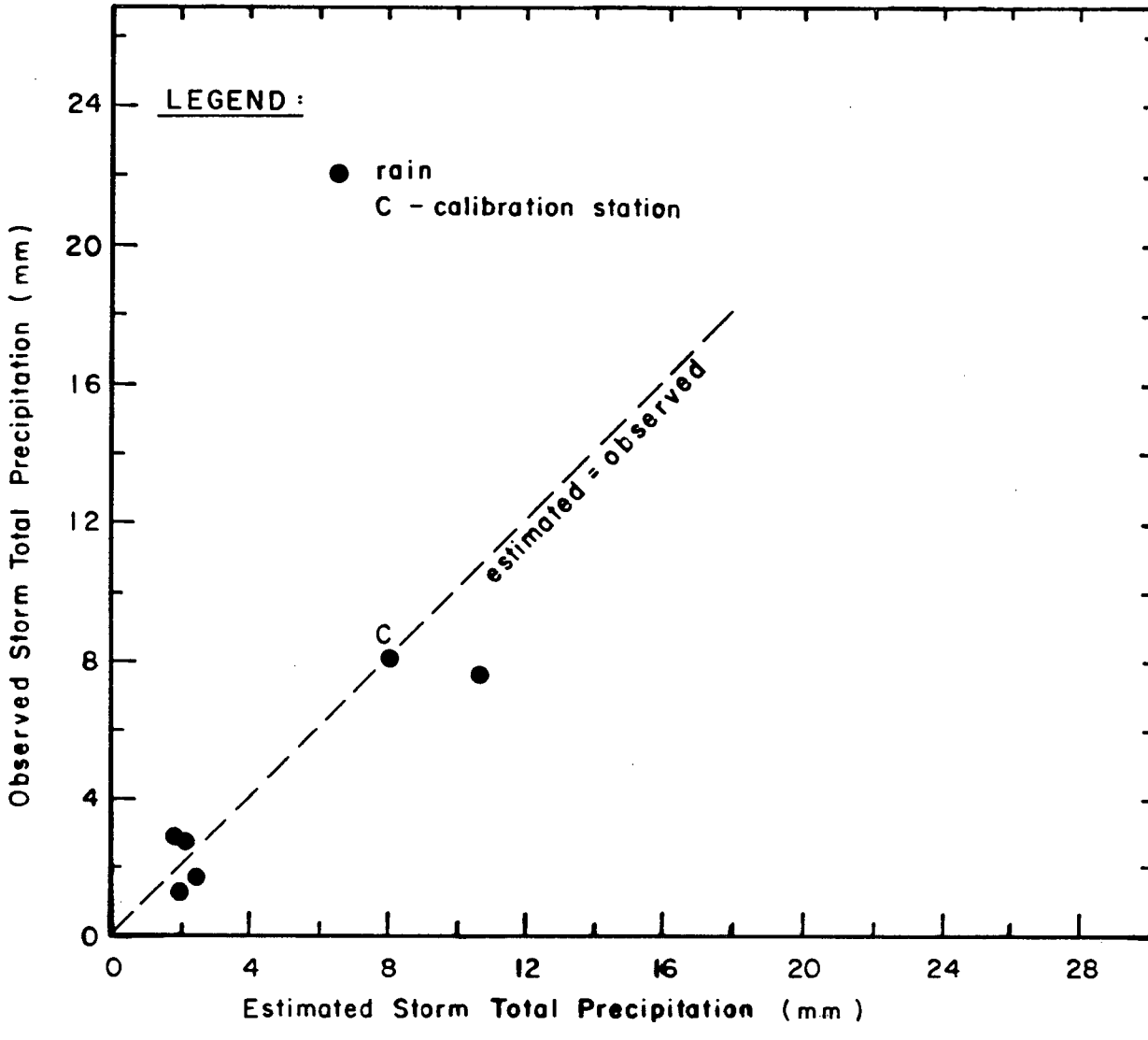

FIGURE 6.15

Estimated and Observed Precipitation for the June 4, 1977 Storm.

the Prince Rupert area of British Columbia. The Pacific Weather Centre was interested in determining whether or not the estimation procedure could distinguish differences in rainfall from this system at two adjacent stations: Prince Rupert and Terrace. Figure 6.16 shows the areal coverage of the storm at 1115 GMT as viewed from GOES-West. The storm provided an additional check of the procedure for the Terrace-Prince Rupert area under more normal conditions.

6.5.2 Results

Of the 26 possible GOES images in the rainfall period from 0145 to 1415 GMT, 12 were enhanced infrared images, 8 were unenhanced infrared images which had to first be processed through the video camera-special effects generator-video monitor system prior to analysis, and 6 were not available.

The water content was inferred from TIROS-N data and the lapse rate γ was set equal to the saturated adiabatic lapse rate $\gamma_s = 5^{\circ}C/1000m$. The efficiency e was determined from equation 4.35 using the first 6-hour observed total precipitation at Prince Rupert as the calibration. This value of e was assumed constant at Prince Rupert for the remainder of the storm, and was assumed to apply to Terrace for the entire storm. Table 6.6 compares the estimated and observed rainfall totals. The estimated rainfall was within 11% or 4 mm of the observed rainfall. The estimation procedure was able to distinguish the difference between the rainfall received at Prince Rupert on the coast and Terrace some 130 km inland.

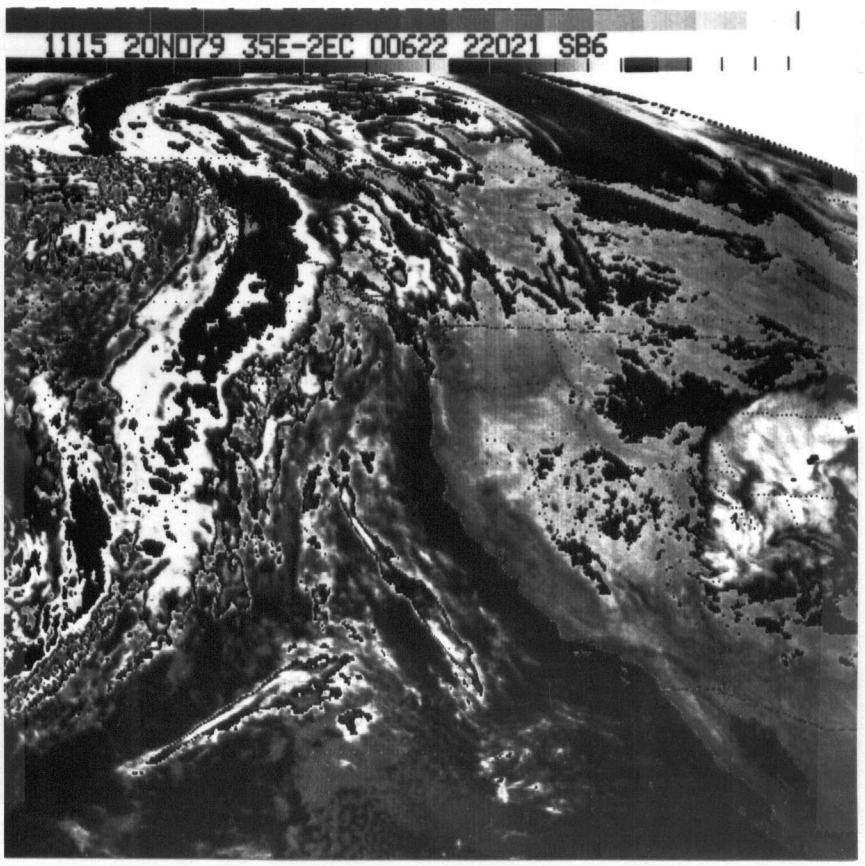

FIGURE 6.16

Areal Extent of November 20, 1979 Storm at 1115 GMT as Viewed from GOES-West.

TABLE 6.6 Comparison of Observed and Estimated Rainfall Totals for the Storm of November 20, 1979

STATION	OBSERVED RAINFALL (mm)	ESTIMATED RAINFALL (mm)	DIFFERENCE (mm)	DIFFERENCE (%)	e	wc (g/m^3)	γ ($^{o}C/1000m$)
Calibration Station: Prince Rupert A.	64.0	59.0	5.0	8	0.1	7	5
Terrace A.	36.4	40.2	3.8	10	0.1	7	5

Key:

A Airport

6.6 The December 5, 1979 Rainfall Estimates

6.6.1 Storm Description

The analysis of the December 5, 1979 storm was also suggested by the Pacific Weather Centre since they experienced less than normal accuracy in their forecast due to poor initialization of the numerical analyses they received. The forecast sunshine for the Lower Mainland of British Columbia was replaced by rain from a narrow band of cloud clearly visible on the satellite images. The observed precipitation ranged from a trace at Victoria International Airport to some 16 mm at New Westminster. Figure 6.17 shows the GOES-West satellite image for 1015 GMT on December 5, 1979.

The analysis provided an additional check of the procedure over a well-gauged area (such as Vancouver).

6.6.2 Results

Of the 46 possible GOES images for the period 0015 to 2315 GMT, 14 were enhanced infrared images, 14 were unenhanced infrared images which had to be first processed through the video camera-special effects generator-video monitor system, 4 were visible images and 14 were missing.

The water content wc was inferred from the TIROS-N data and the lapse rate γ was set equal to the saturated adiabatic

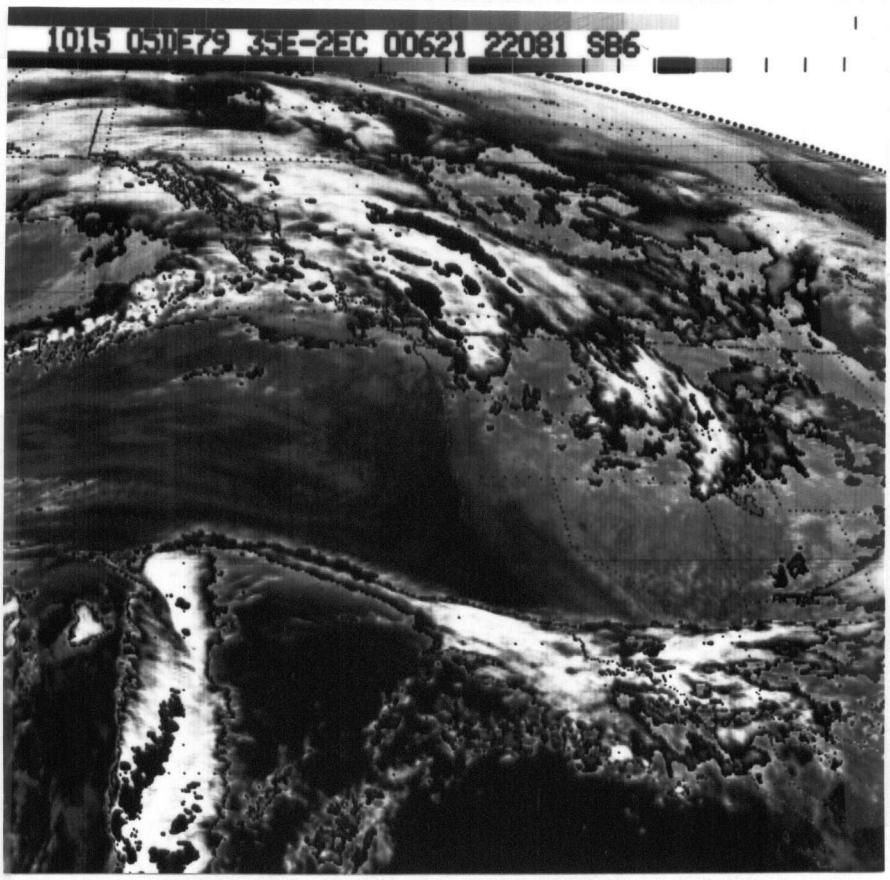

FIGURE 6.17

Areal Extent of December 5, 1979 Storm at 1015 GMT as Viewed from GOES-West.

lapse rate γ_s = 5°C/1000m. The efficiency e was determined from equation 4.35 using the first 6-hour observed total precipitation at Vancouver International Airport as calibration. This value for e was assumed constant at Vancouver International Airport for the remainder of the storm, and was assumed to apply at the other stations for the entire storm. Table 6.7 compares the observed and estimated rainfall totals for the stations analyzed. Except for the West Vancouver gauge, the comparison between observed and estimated rainfalls shows the estimated rainfall totals. For West Vancouver, the estimated rainfall is 73% (9.5 mm) below the observed rainfall. This may be due to the local orographic lifting and suggests the efficiency at West Vancouver was underestimated by using e determined from the Vancouver International Airport gauge. Figure 6.18 is a plot of the observed rainfall totals against the satellite estimated rainfall totals.

The analysis of the December 5, 1979 storm revealed another important aspect: satellite images often clearly define rainfall occurrences which are not suggested by the numerical analyses either because of the necessarily coarse grid used by the numerical models or because of problems in adequately and accurately initializing the models. It is true that the numerical models were designed for forecasting purposes and that forecasting from satellite images is still a difficult task; however, since the satellite images do record what cloud systems are actually present over an area, they are important for "nowcasting" the rainfall from these clouds.

TABLE 6.7 Comparison of Observed and Estimated Rainfall Totals for the Storm of December 5, 1979.

STATION	OBSERVED RAINFALL (mm)	ESTIMATED RAINFALL (mm)	DIFFERENCE (mm)	DIFFERENCE (%)	e	wc (g/m^3)	γ ($^{o}C/1000m$)
Calibration Station: Vancouver I.A.	3.6	3.5	0.1	3	0.1	10	5
Vancouver City	M	3.5	-	-	0.1	10	5
Vancouver Harbour	M	3.5	-	-	0.1	10	5
West Vancouver (Mathers Ave.)	13.0	3.5	9.5	73	0.1	10	5
New Westminster	16.4	12.2	4.2	26	0.1	10	5
Walley Forest Nursery	12.3	12.2	0.1	1	0.1	10	5
Victoria I.A.	T	O	-	-	0.1	10	5

Key:

I.A. International Airport
M observation missing
T trace

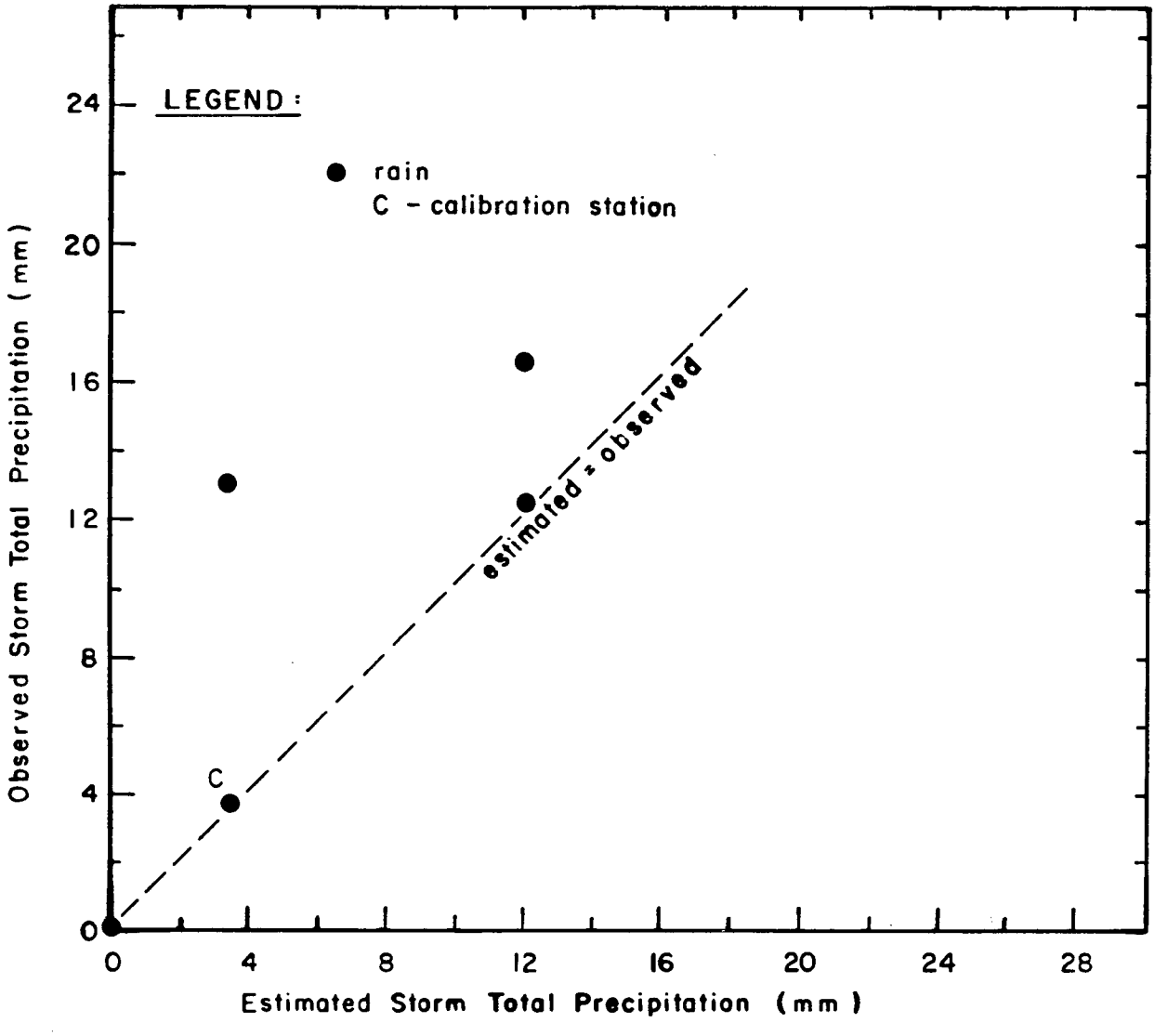

FIGURE 6.18

Estimated and Observed Precipitation for the December 5, 1979 Storm.

6.7 Comparison of Observed and Estimated Precipitation for All Storms

Figure 6.19 is a comparison of the observed and estimated storm total precipitations for all five test storms. The dashed curve represents a perfect match of the estimated storm total precipitation with the observed storm total precipitation. Although there is some scatter of the points about this line, it is evident from the results of the five test cases analyzed that the GOES satellite image rainfall estimation procedure generally performs well for both the low intensity typical rainfall events as well as the high intensity severe rainfall events over British Columbia.

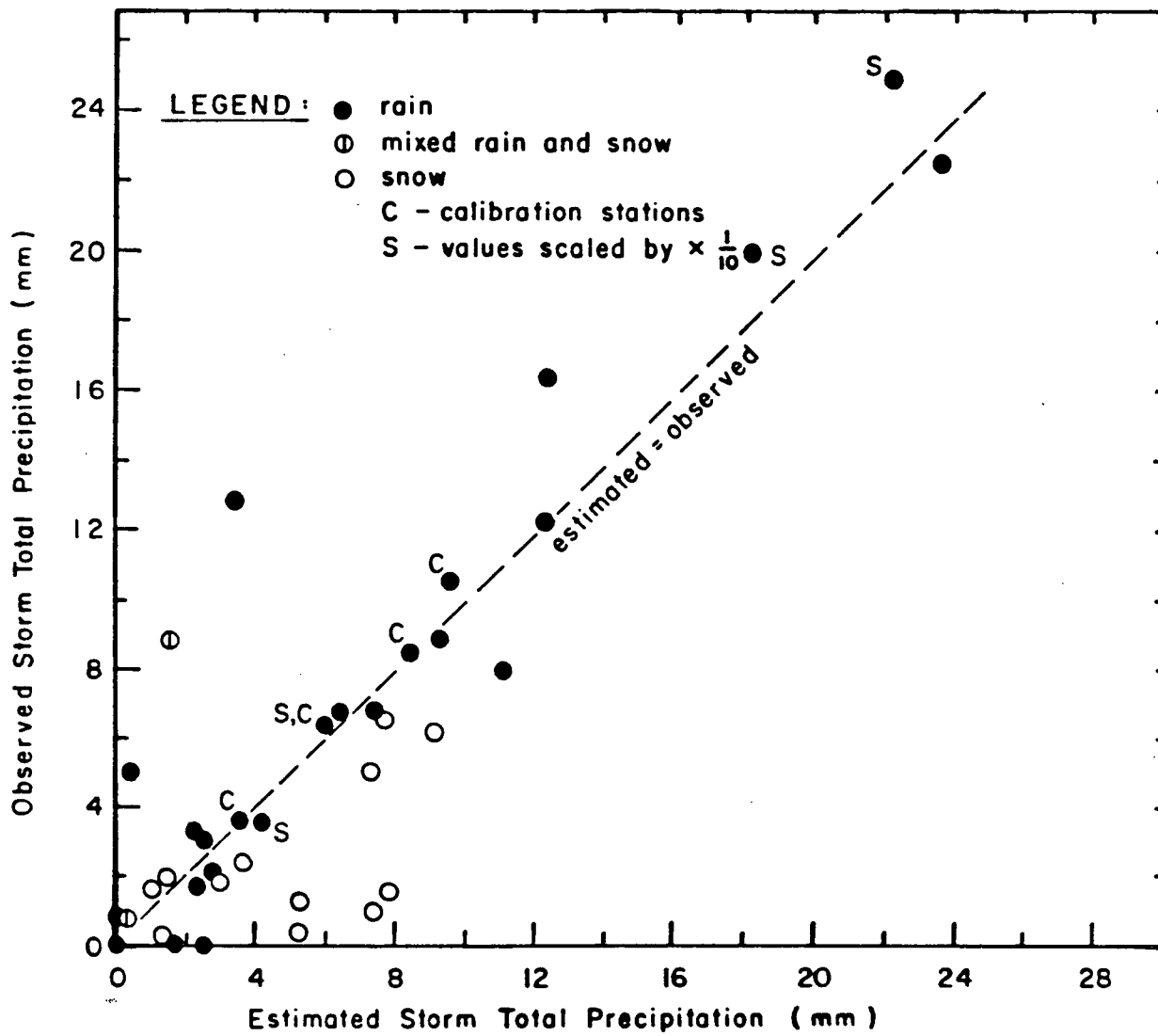

FIGURE 6.19

Estimated and Observed Precipitation for All Five Test Storms.

CHAPTER VII

AN UPDATING PROCEDURE USING OBSERVED DATA

The comparisons of observed and estimated rainfalls for the test storms discussed in Chapter VI show good agreement, although there is some uncertainty and inaccuracy in the satellite rainfall estimates which may be due to the form of the physical-conceptual model used to describe the rainfall process, to the determination of the parameters used in the model, and to the inherently random nature of the rainfall process itself. To a great extent this uncertainty has been acknowledged and accounted for in the empirical adjustment factor e. However, the satellite rainfall estimate can be further improved by incorporating the information contained in the observed rainfall data through the use of an updating procedure. In effect this means treating the series of satellite estimates as a "signal". There are many updating procedures available at various levels of sophistication. However, the more sophisticated methods, such as Kalman filtering (Kalman, 1960.), tend to have restrictive assumptions or require detailed information on error characteristics. For the present exploratory phase of the study, very simple procedures seemed most appropriate.

7.1 The Updating Model

On the assumption that the satellite rainfall estimates are reasonably representative of the true rainfall amounts (in-

spite of the uncertainties noted above) then one of the most straightforward procedures for updating such an estimated series in the light of observed data is to use a regression of the form

$$y=a+bx \tag{7.1}$$

where y is the "true" rainfall, assumed to be exactly represented by the observed rainfall, and x is the satellite estimate of that rain fall. At any point in time the unknown parameters, a and b, can be computed from the available date up to that time by the least squared method, that is,

$$a=\bar{y}-b\bar{x} \tag{7.2}$$

$$b=\frac{\sum_{i}^{n} x_i y_i - n\bar{x}\,\bar{y}}{\sum_{i}^{n} x_i^{2} - n(\bar{x})^{2}} \tag{7.3}$$

where $\bar{x}$ is the average of the estimated rainfall values x_i, ($\bar{x} = \sum_{i}^{n} x_i/n$), and $\bar{y}$ is the average of the observed (or "true") rainfall values y_i, ($\bar{y} = \sum_{i}^{n} y_i/n$). Values for a and b can be recalculated with the acquisition of each new pair of observed (y_i) and estimated (x_i) rainfalls. The redetermined values of a and b can then be used to update the satellite rainfall estimates until another observed and estimated rainfall pair of values is available.

For example, consider the following: Station A reports rainfall every 6 hours, and satellite images are used to make estimates of the rainfall at this station as well as for a number of other ungauged locations within the basin. With equation 7.1 the satellite estimates at Station A can be "corrected" or adjusted as the observed data is received. That is, the parameters a and b are recalculated once every 6 hours and do not change in value until the new observations are incorporated. In this way the estimates of precipitation do not drift far from the "true", observed precipitation because of the uncertainties in the estimation model.

The updating model in equation 7.1 gives equal emphasis to each pair of observed and estimated data used to determine the parameters a and b. This means that estimates and observations from the early part of the storm have as much effect on a and b as the latest ones. In practice, however, the most recent pairs should have the greatest influence.

By weighting the pairs by W_i, the emphasis of the updating model is shifted towards the latest pairs, with a and b now given by

$$a = \overline{Wy} - b\overline{Wx} \tag{7.4}$$

$$b = \frac{\sum_{i}^{n} W_i^2 x_i y_i - n\overline{Wx}\,\overline{Wy}}{\sum_{i}^{n} (W_i x_i)^2 - n(\overline{Wx})^2} \tag{7.5}$$

The weights must satisfy the condition:

$$W_i > W_{i-1} \tag{7.6}$$

There are a number of ways to choose W_i so that this is fulfilled. For example, weights of the form

$$W_i = W_1^{(n-i)} \tag{7.7}$$

satisfy 7.6, where W_1 is a user specified parameter chosen usually to reflect the actual interdependence of previous rainfalls on the present rainfall, n is the total number of observed-estimated rainfall pairs in this rainfall event up to the present, and i is the i-th consecutive one of these pairs. These weights are plotted for n=50 and various values of W_1 in Figure 7.1.

7.2 Comparison of Updated and Observed Rainfall

As a sample of what the updating can do, two of the five test storms analyzed in Chapter VI were chosen to be updated.

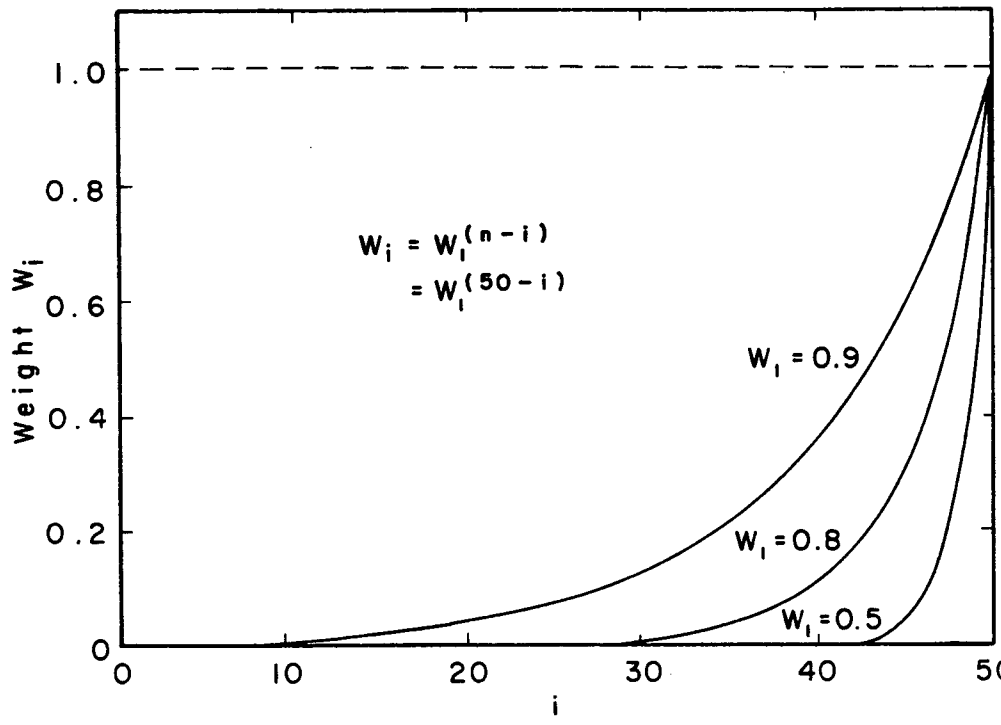

FIGURE 7.1

The Behaviour of the Weights $W_i = W_1^{(n-i)}$ for n=50 and 3 values of W_1.

These were the two major storms of October 31, 1978 and December 17, 1979. The first, October 31, 1978, was chosen because of the large number of observed-estimated pairs available and as such could serve as a test of the updating procedure on a long series. The second storm, December 17, 1979, was chosen as a test of the procedure for updating rainfall at a number of stations within a certain geographic area. The three lesser storms were not tested because their duration, in general, was too short to permit any meaningful determination of the updating model parameters, a and b.

7.2.1 Updated October 31, 1978 Rainfall Estimates

The satellite estimated rainfall values for Terrace and Gospel Point were updated using the weighted regression model with a and b defined by equations 7.4 and 7.5. The form of the weights was as given by equation 7.7, with W_1=0.8. This value for W_1 was chosen because as can be seen in Figure 7.1, the weights W_i drop off rapidly previous to W_{i-2}. In most of the storms examined the individual rain producing cells rarely lasted longer than 2 hours, except for the very largest ones and hence any effect of rainfall more than two hours previous on present rainfall is likely quite insignificant.

Since the GOES-West satellite images are received at 15 minutes to the hour and 15 minutes after the hour (that is, 0015, 0045, 0115, 0145 GMT, etc.), and the observed rainfall is reported on the hour, it was assumed that the rainfall esti-

mated for the one hour period ending with the satellite image which was received at 15 minutes past the hour corresponded to the observed rainfall reported for the hour ending 15 minutes earlier. This is not believed to cause a significant discrepency in the updating procedure, and is the only means of performing the updating using the GOES-West images. This time shift is not a problem with the GOES-East images received on the east coast of the continent, since they are received on the hour and half-hour(that is, 0000, 0030, 0100 GMT, etc.).

The estimated rainfalls were updated sequentially and then summed to arrive at the accumulated updated rainfall estimates shown in Figure 7.2. The updating procedure does improve the fit of the satellite estimated rainfall to the observed rainfall. The variation of the parameters a and b is given in Table 7.1. The change in a and b may indicate that some or all of the rainfall estimation model parameters (efficiency e, water content wc., and the lapse rate γ) vary in time as the cloud system evolves and moves. Whether or not this is so remains a problem to be investigated.

The ability to update sequences has another use besides improving the fit of estimated rainfall for stations with observed data. Since the satellite images allow rainfall to be estimated for a grid of positions throughout a basin, then it

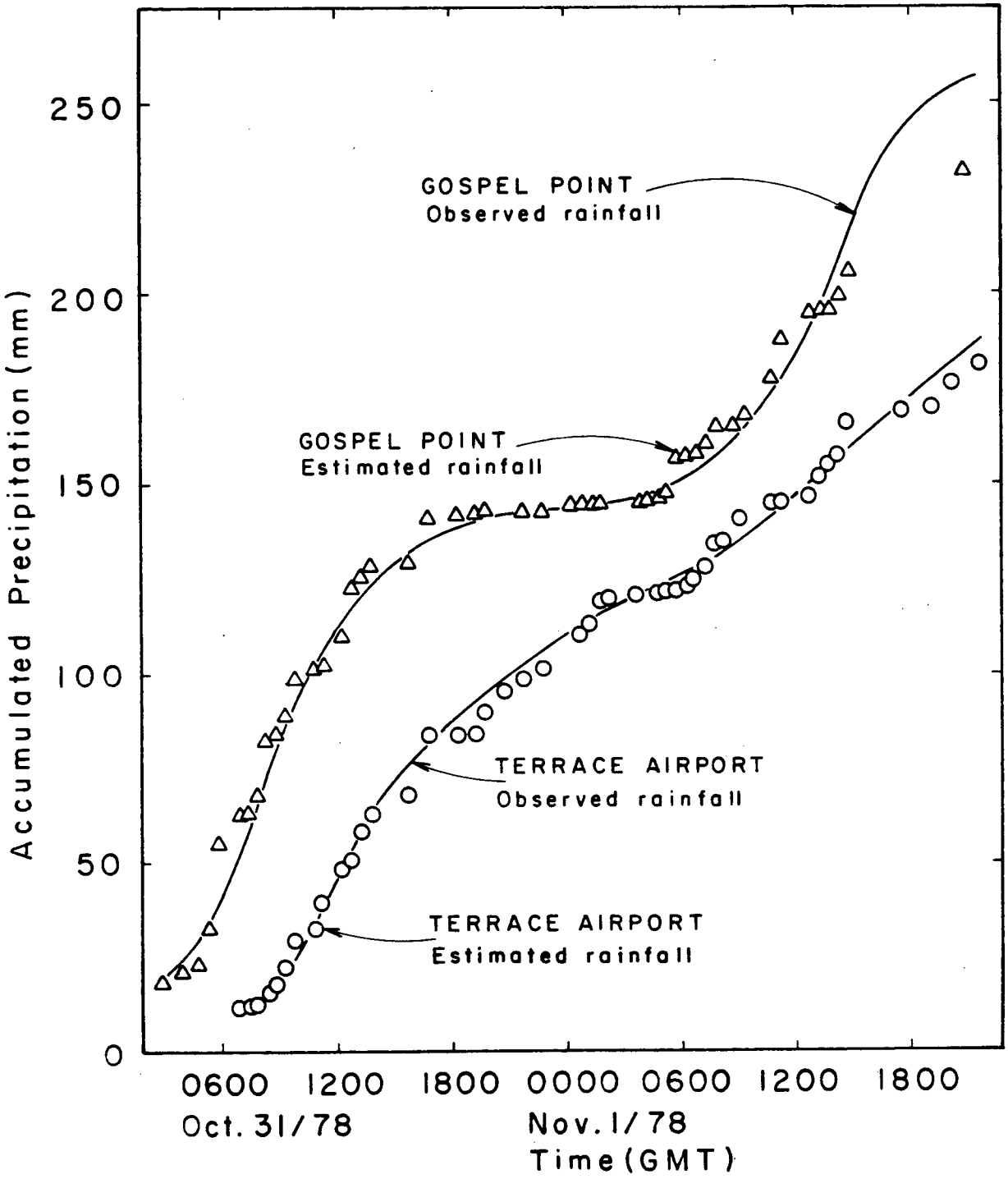

FIGURE 7.2

Comparison of Updated Satellite Estimated Rainfall and Observed Rainfall for Gospel Point and Terrace Airport. Typical Values for a,b for Each Station are Given in Table 7.1. (W_1 = 0.8).

TABLE 7.1 Variation of a and b for Terrace Airport and Gospel Point as the last 25 Pairs of Observed and Estimated Rainfalls are Added Sequentially to the Updating Procedure

Number of Pairs i	Terrace Airport a	b	Gospel Point a	b
⋮	⋮	⋮	⋮	⋮
26	0.29	1.07	0.00	1.27
27	0.28	1.02	-0.01	1.23
28	0.16	1.02	-0.01	1.19
29	0.04	1.03	0.001	1.15
30	-0.02	1.04	0.002	1.15
31	0.01	1.04	0.00	1.14
32	-0.01	1.04	-0.001	1.14
33	0.10	1.00	-0.002	1.15
34	0.03	1.01	-0.001	1.15
35	0.15	0.96	-0.01	1.13
36	0.12	0.94	-0.03	1.08
37	0.07	0.94	-0.02	1.02
38	-0.001	0.95	-0.01	0.97
39	0.05	0.94	-0.01	0.94
40	-0.05	0.96	-0.004	0.92
41	-0.11	0.99	-0.001	0.91
42	-0.01	0.98	-0.004	0.91
43	0.03	0.96	-0.002	0.90
44	-0.10	1.01	-0.003	0.89
45	-0.09	1.02	-0.002	0.89
46	-0.15	1.06	-0.003	0.89
47	-0.15	1.09	-0.004	0.91
48	-0.09	1.10	-0.01	0.94
49	-0.10	1.12	-0.02	1.03
50	-0.17	1.17	-0.01	1.03

is reasonable that the estimates at these points can be updated by using the values of the updating model parameters a and b as determined from the observed data. Figure 7.3 shows a hypothetical case. The same approach was used to update the rainfall for Gospel Point during the October 31, 1979 storm, and for the Vancouver area during the December 17, 1979 storm discussed in the next section. The values of a and b for Terrace Airport, given in Table 7.1, were used to update the Gospel Point satellite estimates shown plotted along with the "true" (observed) rainfall in Figure 7.4. The effect of the updating is as satisfactory as updating Gospel Point satellite estimates with Gospel Point observed data. This suggests that for the October 31, 1979 storm, the transferring of the updating parameters a and b from Terrace Airport to Gospel Point is both feasible and worthwhile.

7.2.2. The Updated December 17, 1979 Rainfall Estimates

The satellite estimated rainfall values for Vancouver International Airport and Victoria International Airport were updated using the model (equation 7.1) with a and b defined by equations 7.4 and 7.5. Again the form of the weights was that given by equation 7.7 with $W_1=0.8$. As for the October 31, 1978 storm, the estimated rainfalls were updated sequentially and then summed to yield cumulative updated satellite rainfall estimates.

Since the purpose of using the December 17, 1979 storm was to test the procedure for updating estimated rainfall at a

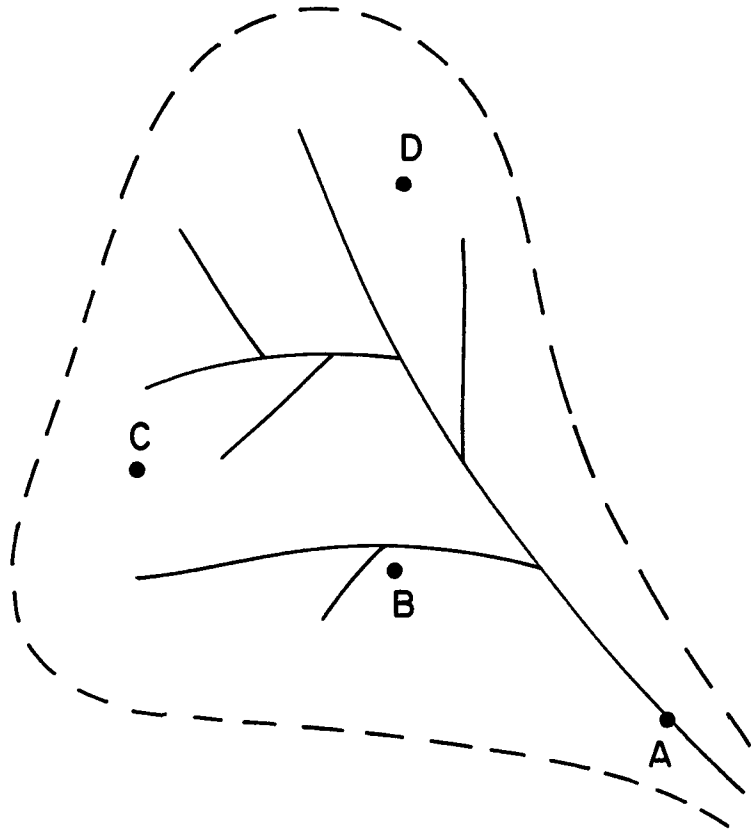

FIGURE 7.3

Schematic of a river basin with 4 stations (A,B,C,D) where the areal rainfall distribution is of interest but where only one of the stations (A) has a raingauge. Satellite estimates of rainfall are available for all 4 stations throughout the duration of the storm. By updating the estimated series for A with the observed data measured there, values of a and b can be determined for each time interval. These values of a and b can be used to update the estimated rainfall at the other ungauged stations (B, C, D).

number of stations and grid points shown in Figure 6.8, most of which lack hourly observations but some of which do have 6-hour precipitation totals, the parameters a and b for the two stations with hourly observations (Vancouver and Victoria) were compared in Table 7.2 to ascertain to what extent they were different. Subjectively there was little difference; therefore, the updating model parameters a,b, for Vancouver International Airport were assumed to be representative over the entire area and were used to update the other stations in the area as well as the 150 grid points used to construct the isohyets in Figure 6.12. The evolution of the updated isohyets is shown in Figure 7.5.

7.3 Limitations on Transferring a And b

The updating model parameters a and b may very depending on station location, terrain, and type of storm. Although it is beyond the scope of this research to investigate the nature of this variability, some guidelines for transferring a and b from a gauged location to an ungauged one for updating purposes are mentioned. The parameters a and b can be transferred if the ungauged station is receiving rainfall from the same cloud system as the gauged station, if both gauged and ungauged stations lie within the same meteorological and topographical region, or if from professional experience, the gauged and ungauged stations are believed to behave similarly given identical conditions even though they may be in different regions or be receiving rainfall from different cloud systems. If it is found from investigating

TABLE 7.2 Comparison of a and b for Vancouver International Airport and Victoria International Airport for the Storm of December 17, 1979

No of pairs i	a		b	
	Vancouver I.A.	Victoria I.A.	Vancouver I.A.	Victoria I.A.
1	0.00	-0.03	1.06	1.11
2	0.00	-0.03	1.07	1.08
3	0.05	-0.01	1.12	1.13
4	0.16	0.09	1.37	1.24
5	0.09	0.06	1.36	1.27
6	-0.03	-0.01	1.28	1.27

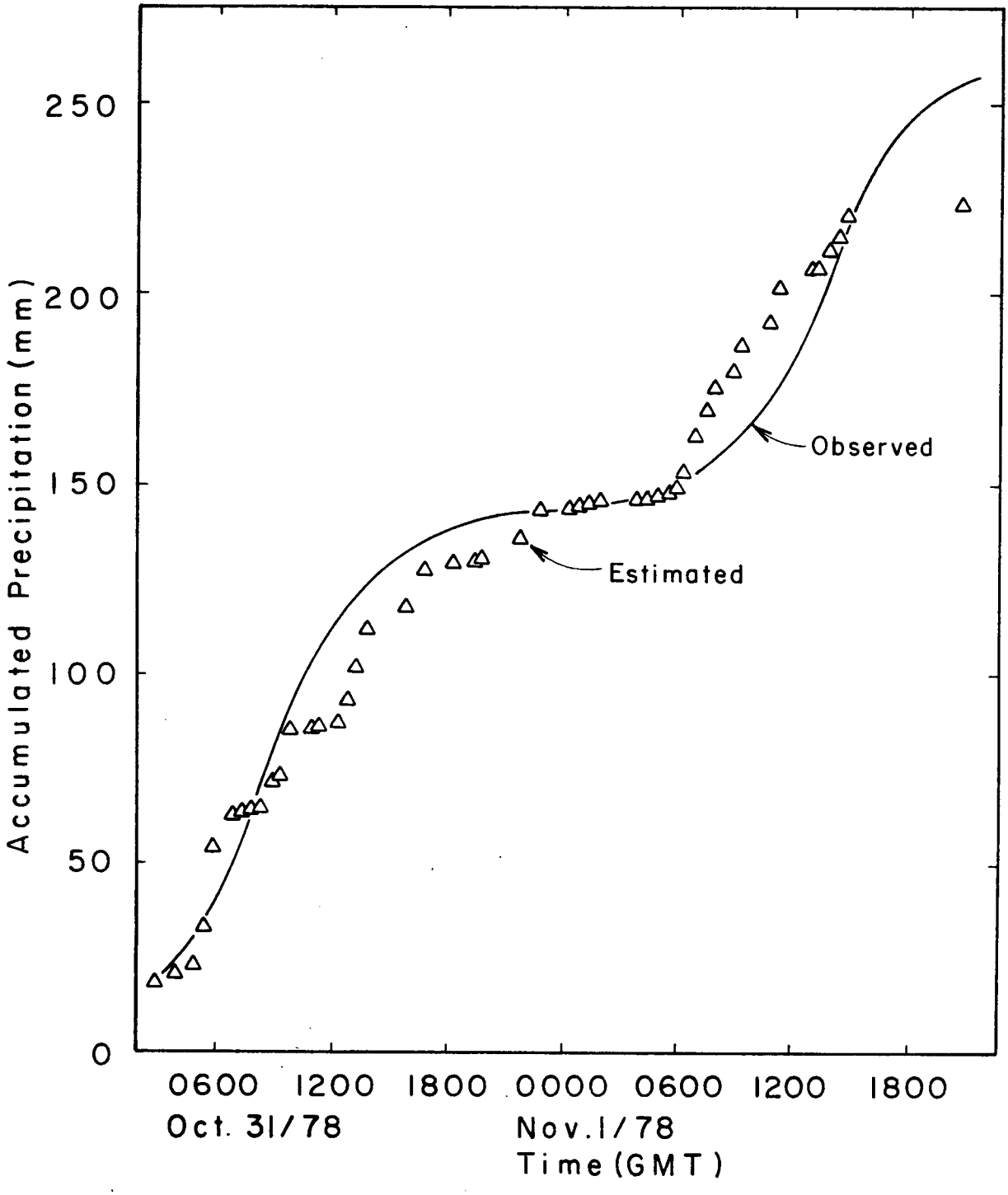

FIGURE 7.4

Comparison of Updated Satellite Estimated Rainfall and Observed Rainfall for Gospel Point. This is similar to Figure 7.2 except that in this case the satellite estimated rainfalls for Gospel Point were updated using the a and b values determined at Terrace Airport.

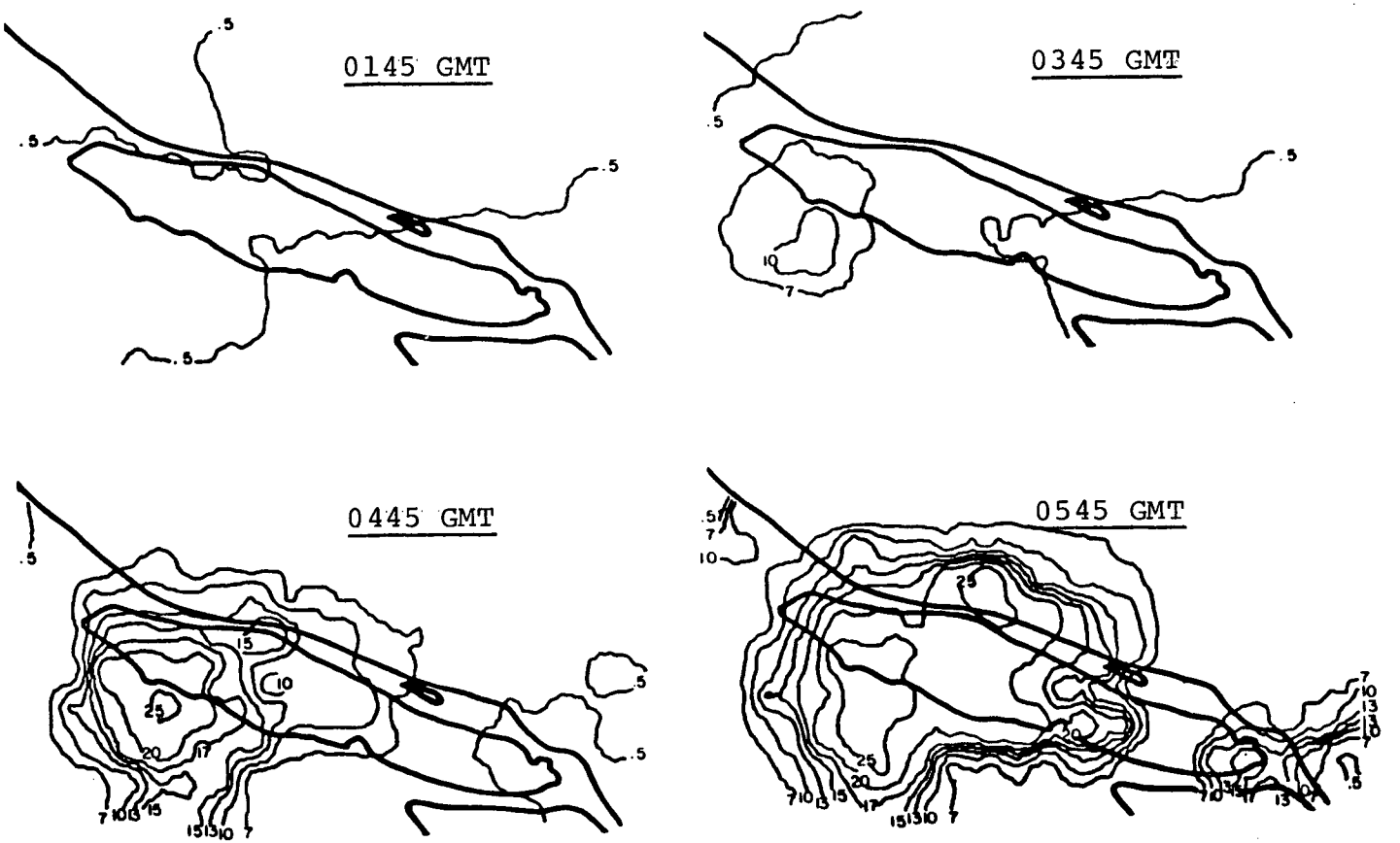

FIGURE 7.5

Evolution of Isohyets (mm) Constructed for the December 17, 1979 Storm Updated Satellite Rainfall Estimates for the Grid Point Shown in Figure 6.11.

a and b that they are fairly constant from storm to storm for a particular region then updating short duration (0.5 to 2 hour) rainfall events over that region would be greatly facilitated, as well as updating half-hourly rainfall estimates for gauged locations in that region which report on a less frequent basis, say once every 6 or 12 hours.

7.4 Summary

The need for a method for incorporating observed data into the satellite estimate of rainfall was discussed and a very simple weighted regression type model, requiring only one parameter W_1 to be provided by the user, was presented. The model was used to successfully update the estimated rainfalls for the October 31, 1978 and December 17, 1979 storms.

CHAPTER VIII

SUMMARY AND CONCLUSIONS

The development and managementof water resources requires the exploitation of modern technological achievements, such as the geostationary meteorological satellites, GOES, which promise to provide more, inexpensive data on an areal scale and frequency of coverage which can never be achieved by groundbased data collection systems. The successful work of previous investigators (Scofield and Oliver, 1977a; Griffith *et al.*, 1978; and Stout *et al.*, 1979), relating the growth of convective cloud tops as seen in the GOES satellite images to the rainfall in tropical and semi-tropical areas, suggested a similar approach to estimating rainfall from other types of storms in northern latitudes. However, it was necessary to develop a physical explanation for the relationship between the rate of growth of the cloud top to the rate of precipitation from the cloud. Before the concept could be extended to the estimation of rainfall from the types of storms commonly occurring in the higher latitudes, something which had not previously been attempted.

A model for estimating precipitation from GOES satellite images was developed and tested on a number of major and minor frontal storms which passed over British Columbia. Considering the quality and consistency of the GOES-West images received by

the Pacific Weather Centre, the results were remarkable and indicated the feasibility of the approach as an operational tool. Further tests showed that the accuracy of the precipitation estimates could be improved through the use of an updating procedure which incorporated the information obtained from ground measurements. To facilitate the application of the model, computer routines were developed to perform the numerous accounting steps and calculations involved in estimating and updating rainfall from satellite images.

The quality of satellite precipitation estimates could be much better if the user had access to a dedicated GOES satellite receiving station (such as the one proposed for the Vancouver area in 1981), with the appropriate computer software to choose his own enhancement scheme, one which distinguishes the temperature gradients at the tops of warmer cloud tops. This capability would be particularly useful in analyzing those weather systems over British Columbia which are not sufficiently well developed vertically to be apparent on the enhanced infrared images presently received and yet which result in steady, low intensity precipitation.

Further use of this technique on an operational basis by both hydrologists and meteorologists is needed to fully assess its benefits and limitations, however, this study revealed that GOES satellite images are well-suited as an alternate or supplementary source of information, particularly on the spatial dis-

tribution of rainfall. Its advantages over more conventional data sources, for example radar or raingauges, are its frequency of coverage (day and night), its large areal coverage, and its cost in comparison with ground networks. Its limitations are few: the resolution of the VISSR (1 km in the visible and 8 km in the infrared at the satellite sub-point) means that individual cloud elements smaller than the resolution of the sensor cannot be distinguished. But it is worth noting that cloud systems of this small a scale rarely produce major rains over a basin, and that even estimates of rainfall from only the large (>8 km) systems in remote areas is better than no information at all about the rainfall distribution there.

This study has shown that the GOES satellite infrared images, when used with a sound physically based rainfall estimation procedure, can provide acceptable estimates of the spatial precipitation from cloud systems of a non-tropical nature. Such a capability is invaluable for providing economical and frequent estimates of rainfall in higher latitudes. In areas where the conventional raingauge networks are sparse it provides area-depth-duration information vital to water resources design and management activities which would be otherwise unobtainable.

8.1 Future Directions

In theory, the transition from using this procedure with hardcopy images to using it with digital images ought to be

straightforward and result in a fully-automated rainfall estimation procedure. The major difficulty would be the problem of recognition, identification and tracking of the many individual cells which make up a particular storm. It is more likely that a semi-automatic procedure will be used in practice, with the recognition and identification of individual cells performed by the user, until suitable pattern recognition procedures become available.

For the development and initial testing of the satellite rainfall estimation procedure, it was necessary to use the hard-copy images because of their availability and for their visual impact as a series of "snap-shots" of weather conditions. This was an acceptable approach during the research phase. However, current computer digital image display systems, such as the Comtal Vision I system, in operation at the University of British Columbia, already are capable of displaying the image on a screen, enhancing the infrared images in colour, as well as, automatically extracting the area information for each temperature contour directly from the digital image data after the storm cell of interest has been visually identified and located by the user. This information could then be fed directly to the rainfall estimation routines developed during the course of this study thus eliminating the time required for the user to digitize each contour.

In the immediate future the procedure developed here holds the promise of improving short-term forecasts of severe weather

events over the province. Since satellite images record the movement of a storm as well as its rate and stage of development, timing the approximate arrival of the storm over a particular region can be immediately estimated from successive images. With experience in the behaviour and life expectancy of storm cells, gained by analyzing satellite images for rainfall, it should be possible to predict in the short-term (on the order of a few hours) the probable rainfall that might be received from a particular system. Proposed use of a version of this procedure by the Pacific Weather Centre to aid in the identification and delineation of rainfall areas over the ocean is seen as the first step towards this end, and a necessary one given the inevitable phasing out of Ocean Station Papa and the increasing reliance on weather satellite observations. The importance of this is reflected in the Atmospheric Environment's five year $10 million proposal to conduct further research and development into the operational use and dissemination of meteorological satellite data (Department of Communications, 1980). Further study and modelling of the internal structure of cyclonic systems, in conjunction with satellite images, would improve this predictive capability.

BIBLIOGRAPHY

Adler, R.F., and D.D. Fenn 1979a "Thunderstorm Intensity As Determined From Satellite Data", J. Appl. Met., Vol. 18, April, 502-517

———— and ———— 1979b "Thunderstorm Vertical Velocities Estimated From Satellite Data", J. Atmos. Sci, Vol. 36, Sept., 1747-1754

Anderson, E.K., and N.F. Veltischchev 1973 "The Use Of Satellite Pictures In Weather Analysis And Forecasting", WMO Tech. Note 124 (WMO No. 333)

Barrett, E.C. 1970 "The Estimation Of Monthly Rainfall From Satellite Data", Mon. Wea. Rev. 98, 322-327

Beebe, R.G. and F.C. Bates 1955 "A Mechanism For Assisting In The Release Of Conventive Instability", Mon. Wea. Rev. 83, 1-10

Bjerknes, J. 1918 "On The Structure Of Moving Cyclones", Geophysiske Publikationer 1, No. 2

————, and H. Solberg 1922 "Life Cycles Of Cyclones And The Polar Front Theory Of Atmospheric Circulation", Geophysiske Publikationer 3, No. 1, 3-18

Browning, K.A., M.E. Hardman, T.W. Harrold, and C.W. Pardoe 1973 "The Structure Of Rainbands Within A Mid-Latitude Depression", Quart. J. Roy. Met. Soc. Vol. 99, No. 420, 215-231

Byers, H.R., and R.R. Braham, Jr. 1948 "Thunderstorm Structure And Circulation", J. of Meteorology Vol. 5, No. 3, 71-86

Cheng, N. and D. Rodenhius 1977 "An Intercomparison Of Satellite Images And Radar Rainfall Rates", 11-th AMS Tech. Conf. on Hurricanes and Tropical Meteorology, Dec. 13-16, 1977 Miami Beach, 224-226

Chinook 1979 "The Halloween Deluge, B.C.", Chinook Vol. 1, No. 2, January, 25

Clark, J.D., A.J. Lindner, R. Borneman, and R.E. Bell 1980 "Satellite Observed Cloud Patterns Associated With Excessive Precipitation Outbreaks", Preprints 8-th AMS Conf. on Weather Forecasting and Analysis, Denver, 463-473

Corbell, R.P., C.J. Callahan and W.J. Kotsch (eds.) 1977 "The GOES/SMS User's Guide, NCAA, NESS, NASA

Cressman, G.P. 1954 "An Approximate Method Of Divergence Measurement", J. of Meteorology Vol. 11, No. 2, 83-90

Danard, M. 1975 "24-Hr Rainfall Amounts For Various Return Periods Over Southwestern British Columbia", Report No. 17 for Water Investigation Branch, Water Resources Service, Province of British Columbia, 37p.

———— 1978 "24-Hr Rainfall Amounts For Various Return Periods For South-Central And Southeastern British Columbia", Report No. 21 for Water Resources Service, Province of British Columbia, 25p.

Davis, N.E. 1980 "METEOSAT Looks At The General Circulation: Some Remarks", Weather, Vol. 35, 64-68

Davis, P.A., and S.M. Serebreny 1972 "Precipitation Estimates From Meteorological Data", Distribution of Precipitation In Mountainous Areas - Geilo's Symposium, Norway, 31 July - 5 August, Vol. II, WMO No. 326, 474-483

Department of Communications 1980 "The Canadian Space Program: Five-Year Plan (80/81 - 84/85)", Government of Canada, Serial No. DOC-6-79DP, Discussion Paper, January 80.

Farley, A.L. 1980 Personal Communication, Dept. of Geography, University of British Columbia

Fleagle, R.G., 1946 "A Study Of The Effects Of Divergence And Advection On Lapse Rate", J. of Met. Vol. 3(1), March, 9-13

Fletcher, N.H. 1962 The Physics Of Rainclouds, Cambridge University Press

Follansbee, W.A. 1973 "Estimation Of Average Rainfall From Satellite Cloud Photographs", NOAA Techn. Memo, NESS 44, 39p.

————, and V.J. Oliver 1975 "A Comparison Of Infrared And Video Pictures In The Estimation Of Daily Rainfall From Satellite Data", NOAA Tech. Memo, NESS 62, 14p.

Fordyce, D.V., R.J. Wirth and W.E. Shenk 1974 "The Synchronous Meteorological Satellite SMS System", 6-th Conf. on Aerospace and Aeronautical Meteorology, 158-164

Fortuna, J.J., and L.N. Hambrick 1974 "The Operation Of The NOAA Polar Satellite System", NOAA Tech. Memo, NESS 60, 127p.

Gantry, R.G., E. Rodgers, W.E. Shenk and V. Oliver 1976 "Deriving Winds For Hurricanes Using Short Interval Satellite Imagery", 7-th Conf. on Aerospace and Aeronautical Meteorology and Symp. on Remote Sensing from Satellites, 115-118

Gerrish, H.O. 1970 "Satellite And Radar Analysis Of Mesoscle Features In The Tropics", Semiannual Report, Research and Development Tech. Rep. ECOM-0205-20, U.S. Army Electronics Command, Ft. Monmouth, N.J., 39p.

Griffith, C.G., W.L. Woodley, S. Browner, J. Teijeiro, M. Maier, D.W. Martin, J. Stout, and D.N. Sikdar 1976 "Rainfall Estimation From Geisynchronous Satellites Imagery During Daylight Hours", NOAA Tech. Rep. ERL-356-WMPO-7, 106p.

————, ————, P.G. Grube, D.W. Martin, J. Stout, and D.N. Sikdar 1978 "Rain Estimation From Satellite Imagery - Visible and Infrared Studies", Mon, Wea. Rev. Vol. 106, Aug., 1153-1171

Gurka, J.J. 1976 "Satellite And Surface Observations Of Strong Wind Zones Accompanying Thunderstorms", 6-th AMS Conf. on Weather Forecasting and Analysis, 252-256

Haering, P. 1978 "A Glossary Of Terms And Concepts Used In Satellite Imagery Interpretation", Pacific Weather Centre (Personal Communication)

Hammond, B. 1978 "The Halloween Deluge - Terrace 1978", Pacific Region Tech. Notes No. 78-041, Pacific Weather Centre, Vancouver, B.C.

Hare, F.K. 1963 The Restless Atmosphere, An Introduction To Climatology, Addison Wesley Pub. Co.

Harrold, T.W. 1973 "Mechanisms Influencing The Distribution Of Precipitation Within Baroclinic Disturbances," Quart. J. Roy. Met. Soc. 99, 232-251

Hetherington, E.D. 1976 "Investigation of Orographic Rainfall In South Central Mountains Of British Columbia", Ph.D. Thesis Univ. Of British Columbia, Forestry Department

Hobbs, P.V., and J.D. Locatelli 1978 "Rainbands, Precipitation Cores And Generating Cells In A Cyclonic Storm", J. Atmos. Sci Vol. 35, 230-241

Holton, J.R. 1972 An Introduction To Dynamic Meteorology, Academic Press

House, D.C. 1968 "Air Mass Modification And Upper Divergence", Bull. Amer. Met. Soc. 39, 137-143

Houze, R.A., P.V. Hobbs, K.R. Biswas, and W.M. Davis 1976 "Mesoscale Structure Of Rainfall In Occluded Cyclones", 6-th AMS Conf. of Weather Forecasting and Analysis, Albany, 310-317

Hussey, W.J. 1977 "TIROS-N Polar-Orbitting Environmental Satellite", 10th Session ESCAP/WMO Typhoon Committee, Tokyo; NESS, NOAA, Washington, D.C., 29p.

Ingraham, D.V., J. Amorocho, M. Guilarte and M. Escalona 1977 "Preliminary Rainfall Estimates In Venezuela And Columbia From GOES Satellite Images", 2-nd AMS Conf. on Hydrometeorology, Toronto, 316-323

Kalman, R.E. 1960 "A New Approach To Linear Filtering And Prediction Theory", Trans. ASME J. Of Basic Engineering Series D, Vol. 82, March, 35-45

Kendrew, W.G., and D. Kerr 1955 The Climate Of British Columbia And The Yukon Territory, Queen's Printer, Ottawa

Knox, J. 1978 Geography 312 Lecture Notes - Fall Term, University of British Columbia

Kodaira, N., and N. Murayama 1976 "Development of Geostationary Meteorological Satellite Systems", 7-th AMS Conf. on Aerospace and Aeronautical Meteorology and Symp. on Remote Sensing from Satellites, 249-252

Leigh, J.L., and T. Duke 1978 "UBC Facilities", Computing Centre, University of British Columbia

Lethbridge, M. 1967 "Precipitation Probability And Satellite Radiation Data", Mon. Wea. Rev. 95, 487-490

Lienesch, J.H., B.P. Bauer and B.B. Goddard 1965 "SMS Infrared Observations: Their Accuracy And Calibration". Proc. 10-th International Symp. on Remote Sensing of the Environment, Vol. 1, 149-158

Lintz, J. and D.S. Simonett 1976 Remote Sensing of Environment, Addison Wesley Pub. Co. (See Chapter 2)

Lovejoy, S. 1978 "The Relationship Between Coarse Resolution Satellite Data And Area Of Rain", 4-th AMS Symp. on Meteorological Observations and Instrumentation, 239-242

_____, and G.L. Austin 1979 " The Delineation Of Rain Areas From Visible And Infrared Data For Gate And Mid-Latitudes", Atmosphere-Ocean 17(1), 77-92

Maddox, R.A. 1980 "A Satellite-Based Study Of Mid-Latitude, Mesoscale Convective Complexes", Preprints 8-th AMS Conf. on Weather Forecasting and Analysis, Denver, June, 329-338

Mair, S. 1978a "UBC IG - The Integrated Graphics System", Computing Centre, University of British Columbia

_____, 1978b "UBC Surface-Surface Visualization Routines", Computing Centre, University of British Columbia

Martin, D. W., and W.D. Scherer 1973 "Review of Satellite Rainfall Estimation Methods", Bull. Amer. Met Soc., No. 29, Jul. 661-674

_____, and V.E. Suomi 1971 "A Satellite Study Of Cloud Clusters Over The Tropical North Atlantic Ocean", Final Report Of Tropical Cloud Organization Studies, Task Order No. 3 To STAG, Contract E-127-69-(N) Space Science And Engineering Center, Madison, Wisconsin, 80p.

————, and ———— 1972 "A Satellite Study Of Cloud Clusters Over The Tropical North Atlantic Ocean", Bull. Amer. Met. Soc., No. 53, 135-156

Mason, B.J. 1971 The Physics Of Clouds, 2-nd Edition, Clarendon Press, Oxford, 671p.

———— 1975 Clouds, Rain, and Rainmaking, 2-nd Edition, Cambridge University Press

Matejka, T.J., R.A. Houze, and P.V. Hobbs 1980 "Microphysics And Dynamics Of Clouds Associated With Mesoscale Rainbands In Extra-tropical Cyclones", Quart. J. Roy. Met. Soc. 106, 29-56

McGinnis, D.F., R.A. Scofield, S.R. Schneider, and C.P. Berg 1980 "Satellites As Aid To Water Resource Managers", J. Of Water Resources And Management Div., ASCE, Vol. 106, NoWRI, 1-20

McIntosh, D.H., and A.S. Thom 1973 Essentials of Meteorology, Wykeham Pub.,(London) Ltd.

McKowan, P.L. 1977 "VISSR Data Processing Plan For Synchronous Meteorological And Geostationary Operational Environmental Satellites (SMS/GOES)", Goddard Space Flight Center, Maryland.

McNulty, R.P. 1977 "On The Relationship Of Wind Maxima To Severe Weather And Its Operational Application", 10-th AMS Conf., On Severe Local Storms

MDA 1977 "Remote Sensing Data Systems", report by MacDonald, Dettweiler, And Associates, Consultants, Vancouver, B.C.

Miers, B.T. 1976 "Application Of Meteorological Satellite Observations To Weather Sensitive Army Operations", 7-th AMS Conf. On Aerospace And Aeronautical Meteorology And Symp. On Remote Sensing From Satellites, 125-230

NOAA 1979 "The View From Space", NOAA Magazine October, P56-57

NESS 1976 "Satellite Activities of NOAA 1975", NOAA S/T 76-2185, April

Oliver, V.J., and R.A. Scofield 1976 "Estimation Of Rainfall From Satellite Imagery", Proc. 6-th AMS Conf. On Weather Forecasting and Analysis, May, 242-245

Popham, R., and E. Rich 1975 "A Direct Readout SMS/GOES VISSR Ground Station Configuration", NESS, Preliminary Note, Washington D.C.

Purdom, J.F.W. 1976 "Some Uses Of High Resolution GOES Imagery In Mesoscale Forecasting Of Convection And Its Behaviour", Proc. 6-th AMS Conf. on Weather Forecasting and Analysis, May, 260-267

Rogers, R.R. 1976 A Short Course In Cloud Physics Pergammon Press

Schaefer, D.G. 1979a "Meteorological Development Contributing To The Terrace Area Flood Of Early November 1978", Scientific Services Unpublished Report, AES, Vancouver

———————— 1979b "The Multi-Day Rainstorm Of October-November 1978, On The Queen Charlotte Islands", Scientific Services Unpublished Report, AES, Vancouver

———————— 1980 "The Rainstorm Of December 13-18, 1979 Over Southwestern British Columbia", Report To Inland Waters Directorate Of Environment Canada, May.

Schaefer, J.T. 1977 "On The Applicability Of The Divergence Equation To Severe Storm Forecasting", 10-th AMS Conf. On Severe Local Storms, Omaha, Oct. 18-21, 358-363

Scherer, W.D., and M.D. Hudlow 1971 "A Technique For Assessing Probable Distributions Of Tropical Precipitation Echo Lengths For X-Band Radar From NIMBUS 3 HRIR Data", BOMEX Bull. No. 10 BOMAP office, NOAA, Rockville, Maryland, 63-68

Scofield, R.A. 1976a "Nowcasting: Fine Tuning The Local Forecast", Proc. 6-th AMS Conf. on Weather Forecasting and Analysis, May, 268-272

———————— 1976b "Satellite Pictures Used For Locating The Rainfall Associated With A Convective Storm Over Texas", SAIN 76/18

———————— 1978a "Using Satellite Imagery To Estimate Rainfall During The Johnstown Rainstorm", Proc. AMS Conf. on Flash Floods: Hydrometeorological Aspects, May, 181-189

———————— 1978b "Using Satellite Imagery To Detect And Estimate Rainfall From Flash-Flood Producing Thunderstorms", Proc. AMS Conf. on Weather Forecasting and Analysis and Aviation Meteorology, Oct., 132-141

———————— and V.J. Oliver 1975 "The Synchronous Meteorological Satellite (SMS): Its Advantages And Applications", Proc. 10-th International Symp. on Remote Sensing of the Environment, Vol. 1, 159-162

———————— and ———————— 1977a "A Scheme For Estimating Convective Rainfall From Satellite Imagery", NOAA Tech. Memo, NESS 86, April, 47p.

———————— and ———————— 1977b "Using Satellite Imagery To Estimate Rainfall From Two Types Of Convective Systems", 11-th AMS Tech. Conf. on Hurricanes and Tropical Meteorology, Dec. 13-16, 204-211

———————— and ———————— 1980 "Some Improvements To The Scofield/Oliver Technique", 2-nd AMS Conf. on Flash Floods, Atlanta, Mar. 18-20, 115-122

———————— and ————————, and L. Spayd 1980 "Estimating Rainfall From Thunderstorms With Warm Tops In The Infrared Imagery", Preprints 8-th AMS Conf. on Weather Forecasting and Analysis, Denver, June, 85-92

————————, and C.E. Weiss 1976 "Applications Of Synchronous Meteorological Satellite (SMS) Products And Other Data For Short-Range Forecasting In The Chesapeake Bay Region", Proc. 6-th AMS Conf. on Weather Forecasting and Analysis, May, 67-73

Seymour, D.W., D.S. Sloan, and N.W. Bowker 1977 "A Low-Cost System For Reception, Processing And Distribution Of Line Scan Data From Environmental Satellites", The American Institute Of Aeronautics And Astronautics Satellite Application To Marine Operations Conf., Louisiana, Nov.

Sikdar, D.N. 1972 "ATS-3 Observed Cloud Brightness Field Related To A Meso- To Sub-synoptic Scale Rainfall Patterns", TELLUS, 24,5 400-413

————————, and V.E. Suomi 1971 "Time Variation Of Tropical Energetics As Viewed From A Geostationary Altitude", J. of Atmos. Sci. 28, 170-180

Spaceflight 1980 "Space Affairs", Spaceflight, Vol.22(5), May 1980 P222

Spangler, M.J. 1974 "The DMSP primary Data Sensor", 6-th AMS Conf. on Aerospace and Aeronautical Meteorology, 150-157

Stout, J., D.W. Martin, and D.N. Sikdar 1977 "Rainfall Estimation From Geostationary Satellite Images Over The GATE Area", 11-th AMS Conf. on Hurricanes and Tropical Meteorology, Miami Beach, Dec. 13-16, 212-215

————————, ———————— and ———————— 1979 "Estimating GATE Rainfall From Geosynchrous Satellite Images", Mon. Wea. Rev. Vol. 107, May, 585-598

UBC Computing Centre 1979 "XPAND.S" Preliminary note, Computing Centre, University of British Columbia

Vesely, C.J., and W.B. Botzong 1974 "Defense Meteorological Satellite Program", Proc. 6-th AMS Conf. on Aerospace and Aeronautical Meteorology, 146-149

Viezee, W., P.A. Davis and D.E. Wolf 1978 "Technique To Use Satellite Microwave Spectrometer Data In Moisture Budget Studies Of Cyclones", Mon. Wea. Rev. Vol. 106, Nov., 1627-1633

Wallace, J.M. and P.O. Hobbs 1977 Atmospheric Science, Academic Press

Waters III, M.P., C.G. Griffith and W.L. Woodley 1977 "Use Of Digital Geostationary Imagery For Real-time Estimation Of Hurricane Rain Potential In Landfalling Storms", 11-th AMS Tech. Conf. on Hurricanes and Tropical Meteorology, Miami Beach, Dec. 13-16, 198-203

Woodley, W., and B. Sancho 1971 "A First Step Towards Rainfall Estimation From Satellite Cloud Photographs", Weather, 26, 279-289

———————, ———————, and A.H. Miller 1972 "Rainfall Estimation From Satellite Cloud Photographs", Noaa Tech. Memo., ERL OD-11, 43p.

WMO 1976 "Informal Planning Meeting On The Satellite Applications In Hydrology", Final Report, Geneva, Oct.

APPENDIX A

For a divergence function of the form

$$\frac{1}{A(T,t)} \frac{dA(T,t)}{dt} = f_1 + f_2 T^n \qquad A.1$$

the average divergence between the level of non-divergence T_2 and the coldest contour level T_3 can be determined as follows:

$$\overline{\frac{1}{A(T,t)} \frac{dA(T,t)}{dt}} = \overline{f_1 + f_2 T^n} \qquad A.2$$

$$= \frac{1}{(T_3-T_2)} \int_{T_2}^{T_3} f_1 + f_2 T^n \, dT \qquad A.3$$

$$= \frac{1}{(T_3-T_2)} \left\{ f_1 (T_3-T_2) + f_2 \frac{(T_3^{n+1}-T_2^{n+1})}{(n+1)} \right\} \qquad A.4$$

The values of the two constants f_1 and f_2 can be found from the two boundary conditions. For $T=T_2$ (the level of non-divergence)

$$f_1 + f_2 T_2^n = 0 \qquad A.5$$

so that

$$f_1 = -f_2 T_2^n \qquad A.6$$

For $T=T_3$ (the coldest contour level)

$$f_1 + f_2 T_3^n = K \qquad A.7$$

where K is the divergence of the coldest contour. Using A.6 to substitute for f_1 gives

$$f_2 = \frac{K}{T_3^n - T_2^n} \qquad \text{A.9}$$

Substituting A.9 back into A.6 yields

$$f_1 = \frac{-KT_2^n}{T_3^n - T_2^n} \qquad \text{A.10}$$

Using A.9 and A.10 in the expression for the average divergence A.4 results in

$$\overline{\frac{1}{A(T,t)} \frac{dA(T,t)}{dt}} =$$

$$\frac{1}{(T_3-T_2)} \left\{ \frac{-KT_2^n(T_3-T_2)}{T_3^n - T_2^n} + \frac{K}{T_3^n - T_2^n} \frac{(T_3^{n+1} - T_2^{n+1})}{n+1} \right\} \qquad \text{A.11}$$

which can be rewritten as

$$K \frac{1}{(T_3-T_2)} \frac{1}{(n+1)} \left\{ \frac{T_3^{n+1} - (n+1)T_2^n T_3 + nT_2^{n+1}}{T_3^n - T_2^n} \right\} \qquad \text{A.12}$$

APPENDIX B

Sensitivity analysis using a typical cell and the expression for the amount of rainfall given by equation 4.32):

$$\Delta P = \frac{-e \cdot wc}{\gamma} \Delta T \ln \left\{ \frac{A(T_3, t+\Delta t)}{A(T_3, t)} \right\} \qquad B.1$$

B.1 The Control

The values of the parameters used in the control are:

$e = 0.2$

$wc = 10 \text{ gm m}^{-3}$

$\gamma = 5^{\circ}C/1000m$

$A(T_3, t+\Delta t) = 65.0113$ area units

$A(T_3, t) = 25.8830$ area units

$\Delta T = T_3 - T_2 = -30^{\circ}C$

$T_3 = -60^{\circ}C$

$T_2 = -30^{\circ}C$

which give a rainfall of

$$\Delta P = 11.05 \times 10^{3} \text{ gm m}^{-2} = 11.05 \text{ mm}$$

B.2 Variation of ΔP with e

A ±10% variation in the empirical adjustment factor e, holding the other parameters at their control values gives

1) for a +10% change in e, e=0.22

$\Delta P = 12.16$ mm

which is a 1.11 mm or 10% increase in the estimated rainfall.

2) for a -10% change in e, e=0.18

ΔP = 9.95 mm

which is a 1.11 mm or 10% decrease in the estimated rainfall.

B.3 Variation of ΔP with wc

A ±10% variation in the water content wc, holding the other parameters at their control values gives:

1) for a +10% change in wc, wc=11 gm m^{-3}

ΔP = 12.16 mm

which is a 1.11 mm or 10% increase in the estimated rainfall.

2) for a -10% change in wc, wc=9 gm m^{-3}

ΔP = 9.95 mm

which is a 1.11 mm or 10% decrease in the estimated rainfall.

B.4 Variation of ΔP with γ

A ±10% variation in the lapse rate γ, holding the other paramters at their control values gives:

1) for a +10% change in γ , γ=5.5°C/1000m

ΔP = 10.05 mm

which is a 1 mm or 9.1% decrease in the estimated rainfall.

2) for a -10% change in γ , γ=4.5°C/1000m

ΔP = 12.28 mm

which is a 1.23 mm or 11.1% increase in the estimated rainfall.

B.5 Variation of ΔP with $A(T_3, t+\Delta t)$

A ±10% variation in the area of the coldest temperature (T_3) contour at time ($t+\Delta t$), $A(T_3, t+\Delta t)$, holding the other parameters at their control values gives:

1) for a +10% change in $A(T_3, t+\Delta t)$, $A(T_3, t+\Delta t)=71.5124$

$\Delta P = 12.20$ mm

which is a 1.15 mm or 10.4% increase in the estimated rainfall.

2) for a -10% change in $A(T_3, t+\Delta t)$, $A(T_3, t+\Delta t)=58.5102$

$\Delta P = 9.79$ mm

which is a 1.26 mm or 11.4% decrease in the estimated rainfall.

B.6 Variation of ΔP with $A(T_3, t)$

A ±10% change in the area of the coldest temperature (T_3) contour at time (t), $A(T_3, t)$, holding the other parameters at their control values gives:

1) for a +10% change in $A(T_3, t)$, $A(T_3, t)=28.47$

$\Delta P = 9.91$ mm

which is a 1.14 mm or 10.4% decrease in the estimated rainfall.

2) for a -10% change in $A(T_3, t)$, $A(T_3, t)=23.29$

$\Delta P = 12.32$ mm

which is a 1.26 mm or 11.4% increase in the estimated rainfall.

B.7 Variation of ΔP with ΔT

A ±10% change in the temperature thickness, ΔT, holding the other parameters at their control values gives:

1) for a +10% change in the temperature thickness ΔT,

$\Delta T = -33^{o}C$

ΔP = 12.16 mm

which is a 1.11 mm or 10% increase in the estimated rainfall.

2) for a -10% change in the temperature thickness ΔT,

$\Delta T = -27^{o}C$

ΔP = 9.95 mm

which is a 1.11 mm or 10% decrease in the estimated rainfall.

B.8 Variation of ΔP with T_3 and T_2

The radiance temperatures recorded on the satellite infrared images are based on the assumption that clouds radiate as black bodies. In other words the emissivity ε is assumed to equal unity in the Stefan-Boltzman relation $E=\varepsilon\sigma T^4$, in which E is the energy radiated (W m^{-2}), σ = 5.669×10^{-8} W $m^{-2}K^{-4}$, and T is the temperature (K). Cloud emissivities, however, change throughout the development of the cloud.

Suppose that the emissivity were in reality less than 1, say 10% less, ε=0.9, then the actual temperature (T_{3a}) of the coldest contour on the satellite image is given by

$$E = \varepsilon\sigma T_{3a}^4 = \sigma T_3^4$$

or

$$T_{3a} = T_3(\varepsilon)^{-.25}$$
$$= T_3(0.9)^{-.25}$$

For $T_3 = -60^oC = (273.15-60)K = 213.15K$, $T_{3a} = -54.31^oC$. The temperature thickness ΔT would then be

$$\Delta T = -54.31-(-30) = -24.31^oC$$

Keeping the other parameters at their control values, then

$$\Delta P = 8.96 \text{ mm}$$

which is a 2.14 mm or 19% decrease in the estimated rainfall.

A similar calculation can be performed for the temperature at the level of non-divergence T_2. A 10% decrease in the emissivity at this level would result in the actual temperature T_{2a} being

$$T_{2a} = T_2(\varepsilon)^{-.25}$$
$$= T_2(0.9)^{-.25}$$

For $T_2 = -30^oC = (273.15-30)K = 243.15K$, $T_{2a} = -23.51^oC$. The temperature thickness ΔT would then be

$$\Delta T = -60-(-23.41) = -36.49^oC$$

Keeping the other parameters at their control values, then

$$\Delta P = 13.44 \text{ mm}$$

which is a 2.39 mm or 21.6% increase in the estimated rainfall.

B.9 Summary

A ±10% variation in the individual values of the parameters in the expression for rainfall (equation B.1) generally results in a ±10% variation in the estimated rainfall. A 10% decrease in the emissivity assumed at a particular cloud level results in a 20% change in the estimated rainfall; however, this is considered as a "worst case" example of the actual variations in cloud emissivity.

One interesting facet of this analysis is that the uncertainties in the parameters may act to cancel each other out in the estimation procedure. For example, if areas of the coldest contours at both times were each 10% larger than they actually were, then the net effect yields P = 11.05 mm which is the same rainfall estimate as using the control values of the areas.

PUBLICATIONS:

Loucks, R.H., D.J. Lawrence, D. Ingraham and B. Fleming, "A Technique for Estimating Extreme Ocean Current Vectors", Bedford Institute of Oceanography Rep. Series BI-R-73-5, 1973.

Ingraham, D., B. Fleming, D.J. Lawrence and R.H. Loucks, "Statistics and Extremes of Currents on the Scotian Shelf", Bedford Institute of Oceanography Rep. Series BI-R-73-10, 1973.

Loucks, R.H., D.J. Lawrence, and D.V. Ingraham, "Summary of Physical, Biological, Socio-Economic and Other Factors Relevant to Potential Oil Spills in the Passamaquoddy Region of the Bay of Fundy, Section 2. Dispersion of Spilled Oil", Fisheries Research Board of Canada, Technical Report No. 428, pp. 215-228, 1973.

Loucks, R.H., and D.V. Ingraham, "Summary of Physical, Biological, Socio-Economic and Other Factors Relevant to Potential Oil Spills in the Passamaquoddy Region of the Bay of Fundy, Section 9. The Influence of Environmental Conditions on the Operations of Oil Terminals", Fisheries Research Board of Canada, Technical Report No. 428, PP. 215-228, 1973.

McGonigal, D., R.H. Loucks and D.V. Ingraham, "Halifax Narrow Sample Current Meter Data", Bedford Institute of Oceanography Data Series BI-D-14-5, 1974.

Loucks, R.H., D.J. Lawrence and D.V. Ingraham, "Note on the Estimation of Plume and Patch Dispersion Scales", Proceedings of the International Conference of Applied Statistics as Dalhousie University, Halifax, May 2-4, 1974.

Adams, E.E., C.W. Almquist, D.V. Ingraham and K.D. Stolzenbach, "Waste Heat Disposal from Offshore Nuclear Power Plants", Proceedings of A.S.C.E. Specialty Conference Ocean Engineering III, University of Delaware, Newark, 1975.

Ingraham, D.V., K.D. Stolzenbach and E.E. Adams, "Phase II Final Report - Forecasting Power Plant Effects on the Coastal Zone, Section 6.5" for E.G. & G. Environmental Consultants of Waltham, Mass. 1975.

Ingraham, D.V., "The Stochastic Simulation of Ocean Currents", S.M. Thesis of Civil Engineering at the Massachusetts Institute of Technology, 1976.

Ingraham, D.V., J. Amorocho, M. Guilarte and M. Escalona, "Preliminary Rainfall Estimates in Venezuela and Colombia from GOES Satellite Images", Second Conference on Hydrometeorology, Atmospheric Environment Service, Toronto, Oct. 1977.

Ingraham, D.V., "Satellite Image and Airphoto Interpretation - Casamance River" Report to R.H. Loucks Oceanology, July, 1978.

Ingraham, D.V., and S.O. Russell "Estimating Precipitation from Satellite Photographs" Submitted for publication in Water Resources Research 1980.